Through Lignin Biodegradation to Lignin-based Plastics

A DISSERTATION
SUBMITTED TO THE FACULTY OF THE GRADUATE SCHOOL
OF THE UNIVERSITY OF MINNESOTA
BY

Yun-Yan Wang

IN PARTIAL FULFILLMENT OF THE REQUIREMENTS
FOR THE DEGREE OF
DOCTOR OF PHILOSOPHY

Advisor: Simo Sarkanen

January 2015

ACKNOWLEDEGMENTS

The author recognizes the following with gratitude:

Professor Simo Sarkanen, her adviser, whose advice, analyses, evaluation and interpretation of experimental results were invaluable throughout this research.

Dr. Yi-ru Chen, whose identification of salicylate-hydroxylase-like enzymes as lignin depolymerases and estimates of stabilization energies for interacting lignin substructures were of central importance to the conceptual basis of this research. Dr. Chen also made major contributions to the light-scattering studies and produced many materials for the lignin-based plastics formulations.

The members of the thesis committee (Professors Mrinal Bhattacharya, Steve Gantt and Jonathan Schilling) whose input was particularly useful: it included recommendations about the comparative assessment of mechanical properties that appears in the Appendix, the compilation of a more complete verdict from the literature about functional lignin depolymerases, and suggestions about the development of viable career paths in the future.

Support for these studies from the U.S. Department of Energy Bioenergy Science Center, U.S. Department of Agriculture National Institute of Food and Agriculture Sustainable Bioenergy program, and the Northwest Advanced Renewables Alliance is gratefully acknowledged. Parts of this work were carried out in the Characterization Facility, University of Minnesota, which receives partial support from NSF through the MRSEC program.

Finally, the author would like to thank her parents for their understanding and support during her graduate research.

ABSTRACT

The consequences of strong noncovalent intermolecular interactions between oligomeric and/or polymeric lignin components are encountered during enzyme-catalyzed lignin degradation and in the properties of lignin-based plastics.

A new chapter in the 30-year quest for functional lignin-depolymerizing enzymes has been opened. The lignin-degrading capacity of the flavin-dependent monooxygenase, salicylate hydroxylase acting as a putative lignin depolymerase, has been characterized using a water-soluble native softwood lignin substrate under mildly acidic aqueous conditions. When macromolecular lignins undergo lignin-depolymerase catalyzed degradation, the cleaved components tend to associate with one another, or with nearby associated lignin complexes, through processes mediated by the enzyme acting in a non-catalytic capacity. As a result, the radius of gyration (R_g) falls rapidly to approximately constant values, while the weight-average molecular weight (M_w) of the substrate rises more slowly to an extent dependent on enzyme concentration. Xylanase, when employed in an auxiliary capacity, is able to facilitate dissociation of the foregoing complexes through its interactions with the lignin depolymerase.

The flavin-dependent lignin depolymerase must be reduced before reaction with oxygen can occur to form the hydroperoxy intermediate that hydroxylates the lignin substrate prior to cleavage. In the absence of the cofactor, NADH, the necessary reducing power can be provided (albeit more slowly) by the lignin substrate itself. Under such conditions, a simultaneous decrease in R_g and M_w is initially observed during the enzymatic process through which the lignin is cleaved.

The partially degraded product-lignins arising from lignin depolymerase activity can be readily converted into polymeric materials with mechanical properties that supersede those of polystyrene. Methylation and blending of ball-milled softwood lignins with miscible low-T_g polymers, or simple low-molecular-weight compounds, readily produce plastics with 80-100% lignin contents that exhibit >60 MPa tensile strengths and >10% elongations at break. X-ray powder diffraction analyses reveal that these materials are largely composed of associated lignin complexes. During casting, continuity between the macromolecular species is established through conformational changes in the peripheral components of the associated complexes that make up the plastics. Such a working hypothesis is supported by atomic force microscopy of surfaces created by ultramicrotomy of these new lignin-based polymeric materials.

TABLE OF CONTENTS

LIST OF TABLES

LIST OF FIGURES

Chapter 1

Objectives

1.1 Functional Ligninolytic Enzymes

"After 30 years of lignin biodegradation research, we still don't know how lignins are biodegraded" This assertion was made during the final panel summary at the 2007 10th International Conference on Biotechnology in the Pulp and Paper Industry; it is as true in 2014 as it was seven years before.

White-rot basidiomycetes are well known to be able to break down lignins rapidly and completely to carbon dioxide and water. They invade the lumens of plant cells whereupon lignin can be degraded at some distance from the hyphae (although not always) and is removed progressively from the lumens towards the middle lamella [Blanchette et al., 1997; Nicole *et al.*, 1995]. In 1983, an enzyme (that later came to be called lignin peroxidase) present in extracellular *Phanerochaete chrysosporium* culture solution was claimed to be the first one detected that is capable of degrading lignins [Tien and Kirk, 1983]. Since then, more extracellular white-rot fungal enzymes including manganese peroxidase, versatile peroxidase and laccase were proved to be capable of cleaving carbon-carbon bonds in dimeric lignin model compounds through oxidative mechanisms, and yet there has been little evidence that they actually engender net cleavage of lignin macromolecules. In fact, the consequences of peroxidase activity have been typically poised between depolymerization and (re)polymerization. The latter process originates

from phenoxy radical coupling that can occur after peroxidase-catalyzed oxidative cleavage of nonphenolic substructures in the macromolecular lignin substrate.

In 2008, particular flavin-dependent monooxygenases were identified, on a mechanistic basis, as candidates for functional lignin depolymerases by comparison of secretome models among three white-rot fungi and one brown-rot fungus (Yi-ru Chen, unpublished). Such enzymes are proposed to cleave polymeric lignin chains through a mechanism different from traditional lignolytic peroxidases and laccases, therefore re-polymerization resulting from phenoxy radical coupling will no longer be a concern during enzyme-catalyzed lignolytic processes.

One of the objectives of my Ph.D. research was to characterize the lignin-depolymerase activity exhibited by the flavin-dependent monooxygenase, salicylate hydroxylase (*Pseudomonas* sp.), towards a soluble native polymeric lignin preparation in aqueous solutions. One straightforward method is to monitor the variations in M_w and R_g of the macromolecular lignin substrate during its depolymerization catalyzed by the putative lignin depolymerase. However, the changes in the two parameters exhibited opposing trends because of the powerful noncovalent intermolecular forces (enzyme-mediated in part) between substructures in lignin components. This research has been focused on developing a coherent working hypothesis that accounts for the effects of the lignin depolymerase on the native lignin substrate under a full range of conditions.

1.2 Lignin-based Polymeric Materials

As efficiencies in the overall saccharification and fermentation processes are facilitated by future enzyme discovery and improvement, less co-product lignin will be required as solid fuel to generate heat in biorefinery unit operations. One prospective result could be the conversion of lignin derivatives that are close in configuration to the native biopolymer into economically profitable polymeric materials.

At a molecular level, the strong noncovalent interactions between individual lignin components must have a profound impact on the mechanical properties of any lignin-containing polymeric material. Taking such fundamental physicochemical effects into consideration, the first successful formulations for genuine lignin-based thermoplastics with 85% kraft-lignin contents far exceeded the low 40% lignin-incorporation limit for conventional lignin-containing polymeric materials [Li *et al.*, 1997]. The second generation of true lignin-based thermoplastics confirmed the feasibility of plasticizing simple alkylated lignin-based polymeric materials (as brittle as polystyrene at a 100% lignin-derivative content) with miscible low-T_g polymers [Li and Sarkanen, 2002; 2005]. Methylated kraft lignin-based thermoplastic foams were created for the first time very recently [Sarkanen and Wang, unpublished results] and their densities are within a factor of 2–3 of those of polystyrene foams.

Here, it was our intention to formulate plastics from biorefinery co-product lignins as a basis for improving the economic viability of producing liquid biofuels from lignocellulosic materials. The ball-milled softwood lignins chosen for this work were expected to be reasonable representatives of the lignin preparations that would be formed

through the enzyme-catalyzed depolymerization of native lignins, when such a process becomes an integral part of lignocellulose pretreatment in the biorefinery.

Therefore, the second objective for my thesis has been to develop new formulations for thermoplastics containing more than 80% methylated native softwood lignin. Plastic deformation and strength in uniaxial extension have been the criteria in testing whether the selected blend components are capable of improving the resulting formulations mechanically to an extent that is comparable with traditional engineering plastics. The morphology of the ensuing amorphous lignin-based materials has been investigated by using wide-angle x-ray diffraction and atomic force microscopy.

Chapter 2

Introduction

2.1 Lignins in Plant Cell Walls

As the second most abundant renewable biopolymeric material in nature, lignins represent 15-35% (w/w) of plant lignocellulose. They embody more solar energy than any other group of biopolymers. Electron microscopic studies [Goring *et al.*, 1979] imply that lignin, which is connected to hemicelluloses, is arranged in 2-dimensional lamellae (~2 nm) connected through about 3% their monomer units to hemicelluloses [Balakshin *et al.*, 2007]; the lignin-hemicellulose matrix forms the most recalcitrant part in plant cell walls to provide drought-resistance and a protective barrier against attack by microorganisms.

2.2 Building Blocks of Macromolecular Lignins

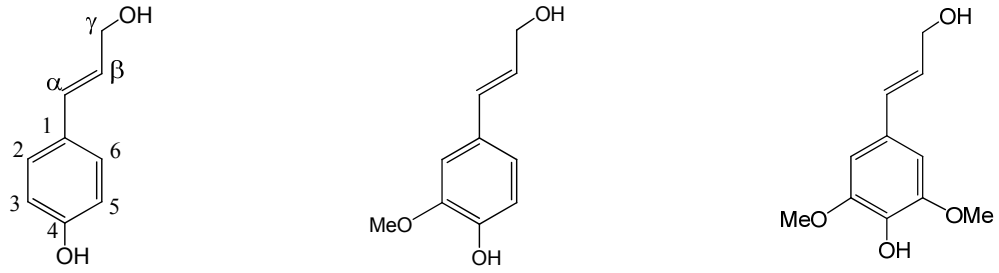

(1) (2) (3)

Figure 2.1 Primary monolignols: (1) *p*-coumaryl alcohol, (2) coniferyl alcohol and (3) sinapyl alcohol.

During lignin biosynthesis, macromolecular lignins are assembled through dehydrogenative coupling of as many as three primary monolignols (Fig. 2.1), coniferyl alcohol, sinapyl alcohol and *p*-coumaryl alcohol in various proportions. Softwood lignin is mainly composed of coniferyl alcohol. Hardwood lignin is formed from mixtures of sinapyl alcohol and coniferyl alcohol. Both of them contain a small amount of coumaryl alcohol. In grass lignin, these three monomers can be found in approximately equal amounts. A single electron is transferred from the monolignol precursor to an oxidized enzyme, such as peroxidase, as a result of which the remaining unpaired electron is delocalized over the 4–*O*, C3, C5, C1, and C*β* atoms. New bonds are formed through radical coupling and the macromolecule is extended by coupling with a monomer on the end of a growing polymer chain. Fig. 2.2 depicts the six predominant inter-unit linkages in softwood lignin: *β*–*O*–4, *β*–5, *β*–1, 5–5, 4–*O*–5 and *β*–*β*, among which the *β*–*O*–4 ether linkage is the most frequent and readily degradable.

2.3 Prevailing Paradigm about Lignin Primary Structure

In the 1980's, lignins were depicted as macromolecules with frequent long-chain branches based upon the analysis of products from hydrolysis in aqueous dioxane and catalytic hydrogenolysis [Sakakibara, 1980]. During the past 30 years, the prevailing view on lignin primary structure has changed dramatically. A new lignin structural model (Fig. 2.3, adapted from Brunow *et al.* (1998)) with a lower frequency of long-chain branches was published in 1998. It incorporates the six predominant substructures (Fig. 2.2)

including the 5-5-*O*-4 dibenzodioxocin and β-1 spiro-dienone discovered by 2D NMR spectroscopy [Karhunen *et al.*, 1995].

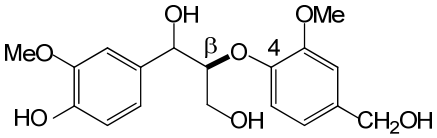

β–*O*–4 linked alkyl aryl ether

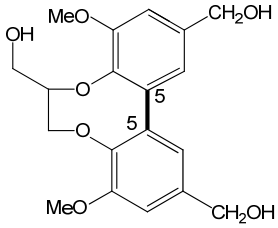

5–5 linked dibenzodioxocin

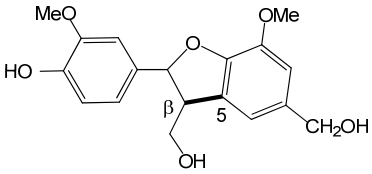

β–5 linked phenylcoumaran

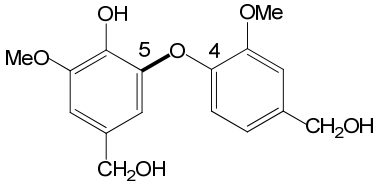

4–*O*–5 linked diaryl ether

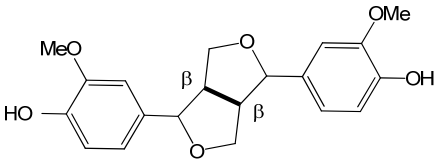

β–*β* linked pinoresinol

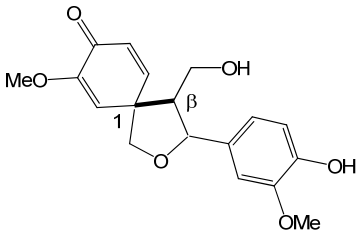

β –1 linked tetrahydrofuran-3-*spiro*-4-cyclohexadienone

Figure 2.2 Predominant substructures in softwood lignins depicted as dilignols [Zhang and Gellerstedt, 2000].

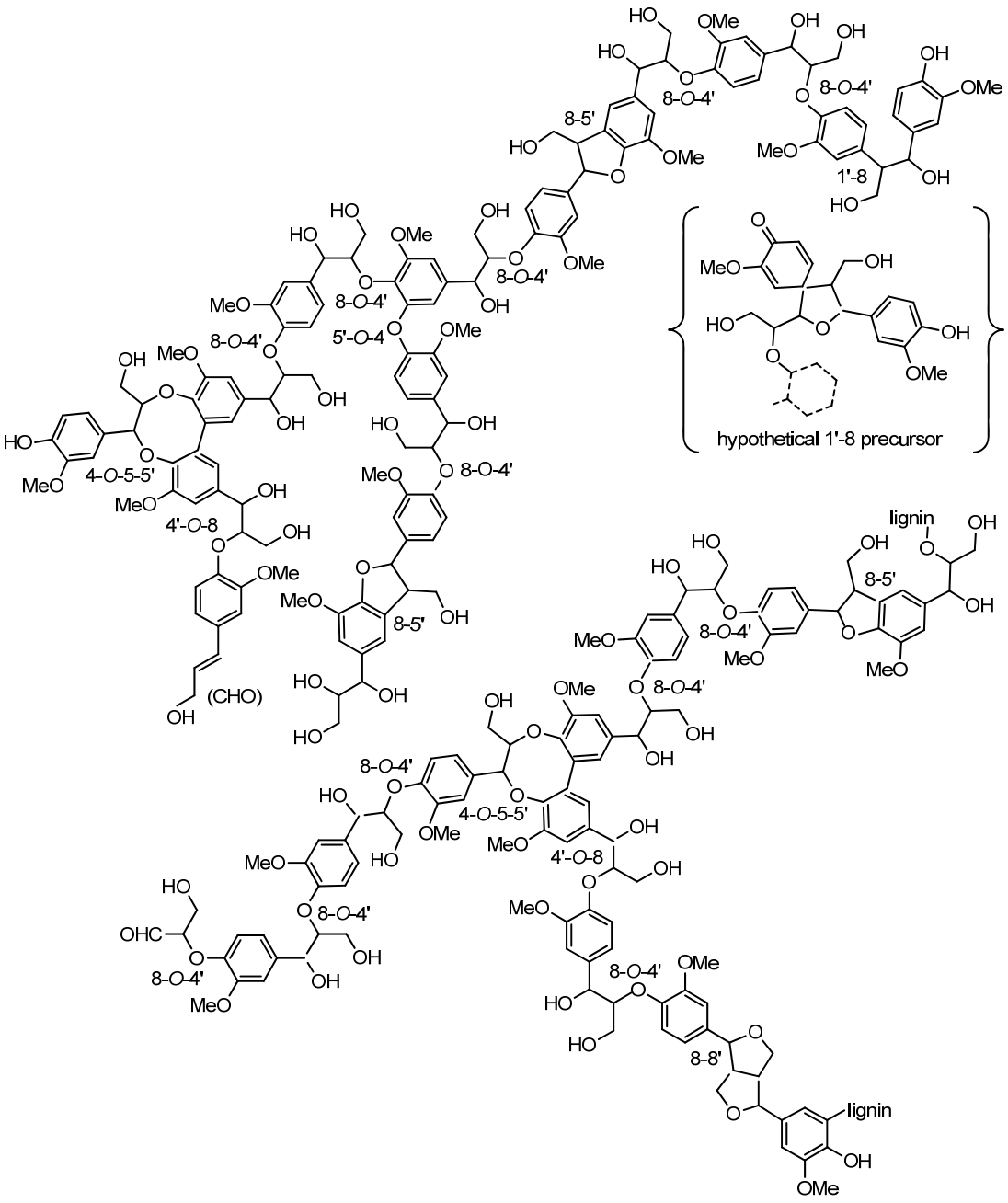

Figure 2.3 Structural model of softwood lignins depicted by Chen and Sarkanen (2003) in an adaptation from Brunow *et al.* (1998).

2.4 Spruce Lignin-Carbohydrate Complexes with Two Distinct Configurations

Five years ago, an important discovery in the identification of two different lignin-carbohydrate complexes (LCCs) with two distinct configurations drew both attention and confusion in lignin research [Lawoko *et al.*, 2005; 2006]. The LCCs were separated through consecutive treatments with aqueous 8M urea, alkaline borate and/or barium hydroxide. As a result, 90% of the total lignin in partially endoglucanase-treated spruce wood meal was recovered in two homogeneous fractions, *i.e*. xylan-lignin and glucomannan-lignin complexes (Fig. 2.4). The molecular weight distributions of lignin derivatives from thioacidolysis, in which the *β–O–*4 inter-unit linkage in lignin is preferentially cleaved, reveals the fact that macromolecular lignin chains (40% of the total lignin in spruce wood) in xylan-rich LCCs are composed almost exclusively of *β–O–*4 alkyl aryl ether substructures. On the other hand, lignins (48% of the total lignin in spruce wood) in glucomannan-rich LCCs possess all the inter-unit linkages present in softwood lignins. Such a striking result is clearly inconsistent with a random or combinatorial radical coupling mechanism during lignin biosynthesis [Ralph *et al.*, 2004].

2.5 Biofuels from Lignocellulose

In the U.S., approximately 200 million dry tons of lignocellulose can be harvested sustainably each year that could be converted biologically into liquid fuels to replace about 30% of current U.S. petroleum consumption (Biomass as Feedstock for a Bioenergy and Bioproducts Industry: The Technical Feasibility of a Billion-Ton Annual Supply, USDA, 2005, 4).

In an industrial biofuel refinery, lignocellulose is processed through four major unit operations: pretreatment, saccharification, fermentation, and product separation/purification. Most potential substrates for lignocellulose bioconversion are heavily lignified as they are designed by nature to be resistant to degradation, thus effective and economically viable procedures are required to remove or modify lignin. During pretreatment, the barriers formed by lignin and hemicelluloses are broken down and the crystalline domains of cellulose are exposed. However, pretreatment has been viewed as the most expensive step during the conversion of lignocellulose to fermentable sugar [Mosier *et al.*, 2005]. Delignification is therefore one of the techno-economic challenges in current pretreatment research. Modification of lignin in plant cell walls has been viewed as a means of reducing the cost of pretreatment. Decreasing the lignin content in alfalfa stems up to 40% by down-regulating genes in lignin biosynthesis pathways led to a two-fold increase of saccharification efficiency [Chen and Dixon, 2007]. As a result, stunted plant development, reduction in biomass production and enhanced susceptibility to pathogen attack were observed among transgenic alfalfa plants with lower lignin levels [Shadle *et al.*, 2007]. The growing interest in economic production of biofuel from vascular plants cells prompted reconsideration of ligninolytic enzymes as an alternative approach to overcoming the bottleneck in the efficient digestion of lignocellulosic materials.

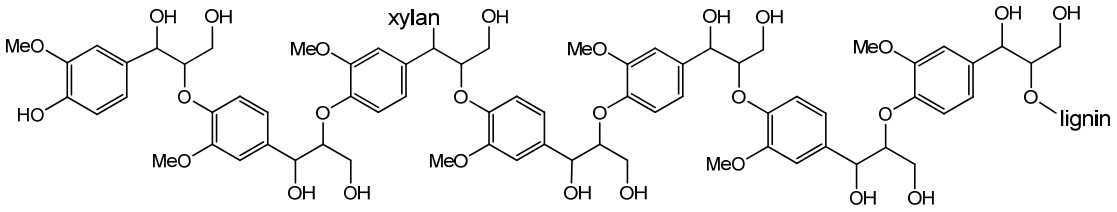

xylan-lignin

high proportion of β-*O*-4 ethers
(40% of the lignin in wood)

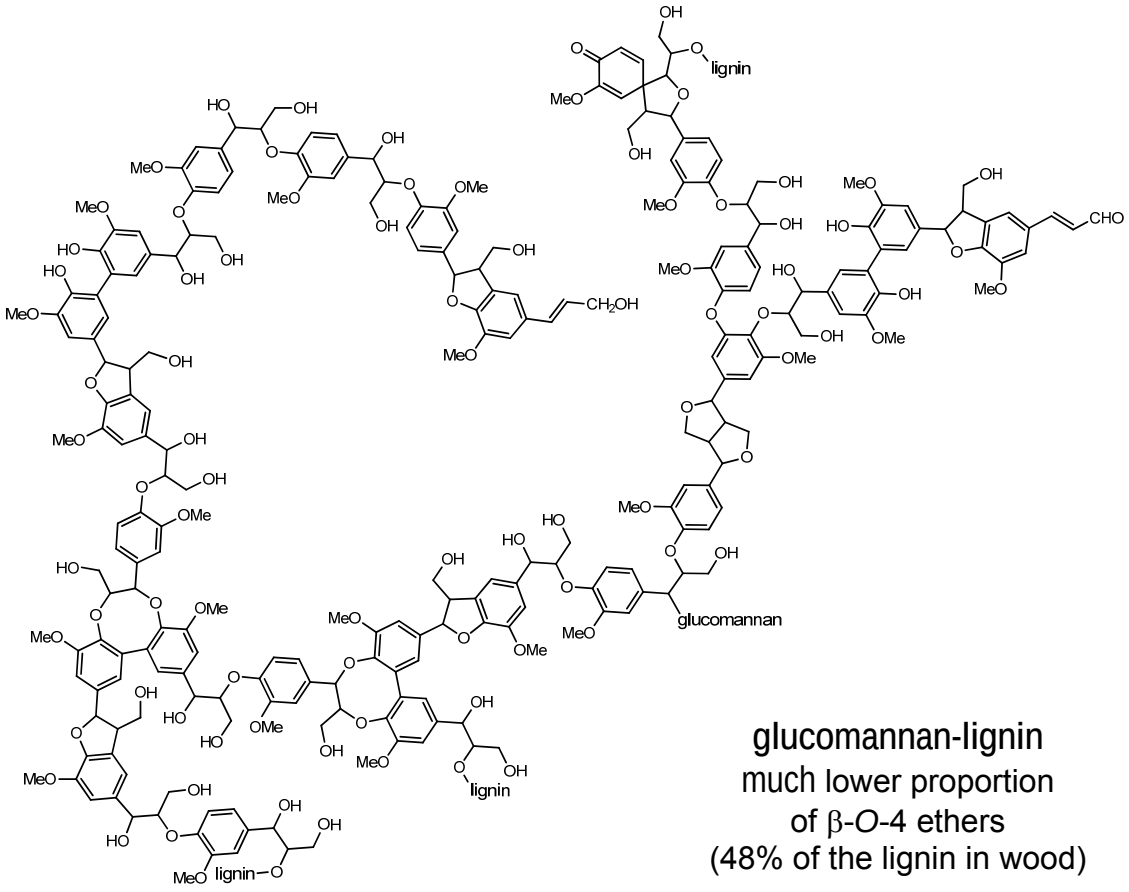

glucomannan-lignin

much lower proportion
of β-*O*-4 ethers
(48% of the lignin in wood)

Figure 2.4 Lignin-carbohydrate complexes isolated by successively fractionating endo-glucanase-treated spruce wood meal with aqueous 8 M urea, alkaline borate and/or $Ba(OH)_2$ [Chen and Sarkanen (2010) adapted from Gellerstedt (2007)]

Chapter 3

Literature Review

3.1 Enzymatic Lignin Degradation

3.1.1 Discovery of lignin peroxidase

In 1983, the detection of lignin peroxidase activity in *P. chrysosporium* extracellular culture solution in the presence of H_2O_2 brought attention to enzymatic lignin degradation for the first time [Tien and Kirk, 1983; Glenn *et al.*, 1983]. In the early reports, lignin peroxidase seemed to be capable of degrading two quite different kinds of lignin preparation. About 22% of a ^{14}C-methylated aqueous acetone extract from spruce wood appeared to undergo depolymerization after 1 h incubation at 37°C in a concentrated extracellular *P. chrysosporium* culture fluid with H_2O_2 at pH 3. The enzyme activity was confirmed by the release of veratraldehyde from the spruce wood extract [Tien and Kirk, 1983]. In the other case, a ^{14}C-labeled synthetic lignin was partially (~10%) degraded in the extracellular medium of *P. chrysosporium* with glucose oxidase/glucose/O_2 as the H_2O_2-producing system [Glenn *et al.*, 1983].

There are two problems with this putative lignin-degrading enzyme activity. First, neither the methylated aqueous acetone wood extract nor the synthetic lignin was actually a native polymeric lignin preparation. Second, owing to the formation of substrate-derived phenoxy radical intermediates, lignin peroxidase and other lignin degrading enzymes of a peroxidase type isolated afterwards tend to be poised in their effects between polymerization and depolymerization of lignin. In fact, three years after the discovery of

lignin peroxidase, it was disclosed that the oxidation of 1 mg/ml milled wood lignin by 0.8 units/ml crude or purified lignin peroxidase from a carbon-limited extracellular *P. chrysosporium* culture medium in the presence of 0.54 μM H_2O_2 at pH 4.0 mainly leads to more polymerized lignins, a process comparable to the oxidation of lignin by 1 mg/ml hoseradish peroxidase at pH 4.5, and the polymerization was enhanced by the addition of 1.2 μM veratryl alcohol [Haemmerli *et al.*, 1986]. Moreover, it was demonstrated that lignin peroxidase was able to catalyze the synthesis from coniferyl alcohol of lignin-like dehydropolymerizates which are structurally similar to those obtained with a horseradish/H_2O_2 system [Sarkanen *et al.*, 1991].

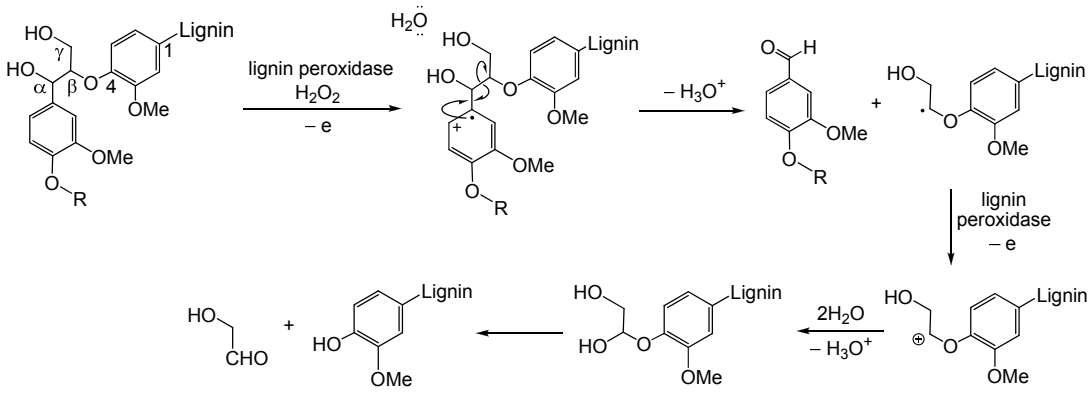

Figure 3.1 Lignin peroxidase catalyzed homolytic C_α–C_β cleavage of nonphenolic *β–O–*4 linked arylglycerol β–aryl ether lignin substructure [Lundell *et al.*, 1993]

Lignin peroxidase is known for its high redox potential (1.4-1.5 V), thus it is capable of oxidizing a wide range of aromatic compounds including veratryl alcohol, methoxybenzenes [Kersten *et al.*, 1985] and nonphenolic *β–O–*4 linked arylglycerol *β–*aryl ethers [Lundell *et al.*, 1993]. For example (Fig. 3.1), lignin peroxidase catalyzes homolytic C_α–C_β cleavage of nonphenolic alkyl aryl *β–O–*4 linked lignin model

compounds, and as a result a free phenolic group is formed when the C_β–O bond is subsequently broken [Lundell *et al.*, 1993]. Coupling between the ensuing phenoxy radicals tends to polymerize the substrate and thus counteracts the initial degradative effects. Even though limitingly low substrate concentrations have been employed to minimize such phenoxy radical coupling, net polymerization was inevitable [Hammel *et al.*, 1993]. It appears that lignin peroxidase oxidizes phenolic lignin model compounds much more easily than the corresponding nonphenolic ones [Lundell *et al.*, 1993], and the catalytic efficiency of the enzyme tends to decrease as the size of the oligomeric substrates increases [Baciocchi *et al.*, 2003]. Consequently, neither guaiacylglycerol *β*–guaiacyl ether nor guaiacylglycerol *β*–syringyl ether were actually degraded by lignin peroxidase/H_2O_2 at pH 3.0 [Yokota *et al.*, 1991]. Similar results were observed in the oxidation of a tetrameric nonphenolic *β–O–*4 linked lignin model compound by lignin peroxidase: the respective phenol-terminal trimeric, dimeric and monomeric degradation products were not detected owing (presumably) to 5–5' linked biphenyl oligomer formation [Mester *et al.*, 2001]. The marked preference for phenolic lignin units is responsible for the tendency of lignin peroxidase to polymerize [Haemmerli *et al.*, 1986] rather than depolymerize lignin preparations *in vitro* (Fig. 3.2).

Some provisional roles of lignin peroxidase have been proposed [Sarkanen, 1991]. First and most likely, lignin peroxidase could, through polymerization, detoxify the lower molecular weight phenolic compounds released during lignin biodegradation. Second, lignin peroxidase, as it oxidizes non-phenolic units in lignins, may introduce new benzylic

carbonyl groups into the structure so that the macromolecule becomes more susceptible towards subsequent degradation by another enzyme.

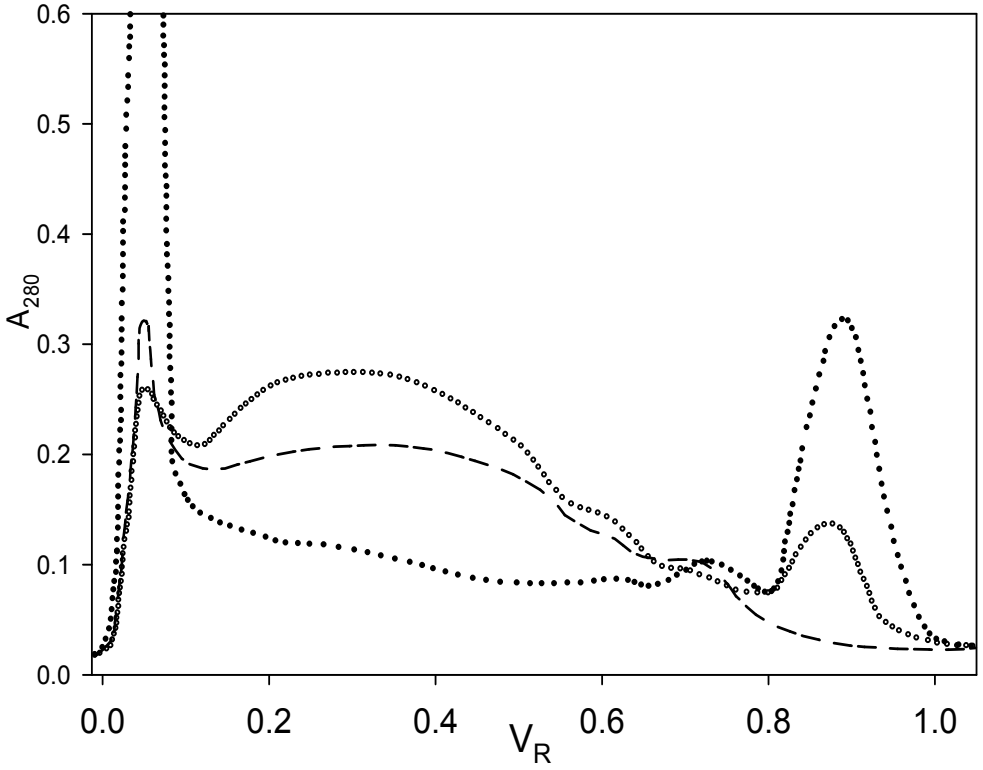

Figure 3.2 Polymerization of 1 mg mL^{-1} alkali-isolated straw lignin (dash-dotted line) by 0.8 units mL^{-1} lignin peroxidase (in concentrated extracellular *P. chrysosporium* culture solution) at pH 4.0 with (dotted line) and without (dashed line) 1.2 μmole mL^{-1} veratryl alcohol in the presence of 0.54 μmole H_2O_2 added at 2 hourly intervals. (Sephadex G75/aqueous 0.5% (w/v) NaOH elution profiles after 24 h [Haemmerli *et al.*, 1986]).

3.1.2 Manganese peroxidase

When cultured under ligninolytic conditions, the white-rot basidiomycete *P. chrysosporium* produces two different kinds of heme peroxidase, lignin peroxidase and manganese peroxidase [Kuwahara *et al.*, 1984]. Manganase peroxidase oxidizes Mn^{2+} to Mn^{3+} which is stabilized by a variety of bidentate chelating agents, such as lactate,

malonate or oxalate. Chelated Mn^{3+} can oxidize phenolic lignin model compounds and various phenols leading to phenoxy radical formation [Hammel *et al.*, 1993; de la Rubia *et al.*, 2002], but not veratryl alcohol [Hammel *et al.*, 1993] or nonphenolic lignin substructures [Hammel and Cullen, 2008].

Manganese peroxidase catalyzes the one-electron oxidation of a phenolic arylglycerol *β*–aryl ether lignin model compound to generate a phenoxy radical, unlike lignin peroxidase that can oxidize the aromatic ring of a nonphenolic model compound directly to a cation radical. The C_α–oxo dimer obtained from C_α-oxidation of the phenoxy radical can be further oxidized by chelated Mn^{3+} and then undergo C_α–C_β cleavage or more favorably C_α-arene cleavage. Findings from *P. chrysosporium* cultures indicated that degradation of the phenolic *β*–*O*–4 dimer *in vivo* was proceeding primarily via C_α-oxidation. [Tuor *et al.*, 1992]

Inevitably, like lignin peroxidase, manganese peroxidase also depolymerizes and polymerizes lignin *in vitro*, and polymerization predominated as it did with lignin peroxidase when synthetic lignins were employed as substrates [Hammel *et al.*, 1993; Wariishi *et al.*, 1991].

3.1.3 Versatile peroxidase

Versatile peroxidase was first isolated from *Pleurotus eryngii* that had been reported to remove lignin selectively while maintaining a high cellulose content from lignocellulosic substrates [Camarero *et al.*, 1998]. It possesses a hybrid molecular structure (with multiple oxidation sites) that supports both of the oxidative reactions characteristic

of *P. chrysosporium* lignin peroxidase and manganese peroxidase. For example, the versatile peroxidase from *P. eryngii* liquid culture is capable of degrading both phenolic and nonphenolic *β–O–*4 lignin model dimers. In a pH 4.5 solution containing 0.1 mM H_2O_2, 65% of 0.25 mM guaiacylglycerol *β*–guaiacyl ether was degraded by ~0.5 U/mL enzyme within 70 min. The process was accelerated 1.5-fold in the presence of 0.1 mM Mn^{2+} [Caramelo *et al.*, 1999]. Moreover, this enzyme is able to directly oxidize high redox-potential compounds, *e.g.* the dye Reactive Black 5, which lignin peroxidase can oxidize only in the presence of redox mediators such as veratryl alcohol [Heinfing *et al.*, 1998].

3.1.4 *β*–Etherase

An extracellular 65 kDa *β*–etherase has been isolated from an ascomycete believed to be a member of the genus *Chaetomium*. It catalyzes the cleavage of the *β*–aryl ether bond in the quinone methide intermediate derived from the phenolic *β*–O–4 lignin model dimer, guaiacylglycerol *β*-guaiacyl ether. In its mechanism, *α*– and 4–hydroxyl groups are required for activity of the *β*–etherase. This is consistent with the experimentally observed cleavage of terminal *β*–aryl ether bonds in a synthetic lignin with *α*– and 4–hydroxyl groups on its peripheral dimeric fragments [Otsuka *et al.*, 2003].

3.1.5 Laccase

Laccases are polyphenol oxidases with four copper ions of three different types in their active sites. The type 1 copper (in the T1 site) is suggested to be involved in the reaction with the substrate. It has a strong absorption band around 600 nm which gives the

enzyme its characteristic blue color. The type 2 and the two type 3 copper ions form a trinuclear cluster (in the T2/T3 site) where O_2 is reduced to water. The T2 copper does not show visible absorbance, while the T3 coppers can be identified by an absorption band at 330 nm [Giardina *et al.*, 2010].

Due to their relatively low redox potentials (0.42-0.79 V, based on that of the T1 site), laccases can only oxidize phenolic lignin model compounds directly [Kawai *et al.*, 1993]. However, the presence of a suitable mediator, *e.g.* ABTS which can be slowly oxidized by laccase, enables the degradation of nonphenolic lignin moieties by the enzyme [Bourbonnais *et al.*, 1998]. The overall process occurs spontaneously, even though the redox potential of the laccase has not been altered, because the oxidized nonphenolic lignin substructures undergo irreversible transformations once they are formed. An aminophenol, 3-hydroxyanthranilic acid (3-HAA), had been proposed as a natural mediator for the laccase secreted by the white-rot fungus, *Pycnoporus cinnabarinus* (which was initially thought to lack genes for lignin peroxidase, manganese peroxidase and versatile peroxidase). However, it was proved that 3-HAA is not necessary for the fungus to efficiently degrade lignin, while laccase alone is not able to oxidize non-phenolic substructures of lignin, and thus it was concluded that laccase is not the essential enzyme for lignin biodegradation by *P. cinnabarinus* [Li *et al.*, 2001].

On the other hand, the genome of *P. cinnabarinus* does actually embody genes encoding four lignin peroxidases, three manganese peroxidases and one versatile peroxidase, but none of these class II peroxidases have been detected as extracellular proteins in solid-state fermentation cultures containing micronized birchwood. In contrast,

four GMC-oxidoreductase-like proteins (including three identified as aryl alcohol oxidases) were detected in the *P. cinnabarinus* cultures with birchwood [Levasseur *et al.* 2014].

3.1.6 Lignin degradation by reactive oxygen species

In 1980, it appeared that reactive oxygen species might be responsible for the initial depolymerization of lignins in white-rot fungal cultures [Hall, 1980]. Two years later, ligninolytic activity was found to be correlated to the production of H_2O_2 in *Phanerochaete chrysosporium* cell extracts [Forney *et al.*, 1982]. In the same year, it was reported that synthetic lignin, a dehydropolymerizate from sidechain [2-^{14}C] coniferyl alcohol, was degraded almost completely in the (Fenton's reagent) hydroxyl radical generating system, 1 M H_2O_2/10 mM $FeSO_4$ [Gold *et al.*, 1983], moreover, lignin degradation by *P. chrysosporium* was inhibited by hydroxyl radical scavengers such as mannitol [Forney *et al.*, 1982] and benzoate [Faison and Kirk, 1983].

The discovery of lignin peroxidase and subsequently the other three enzymes, manganese peroxides, versatile peroxidase and laccase, quickly diverted attention from the hydroxyl radical as a likely agent for lignin depolymerization. Yet, those lignocellulolytic enzymes are too large to penetrate through undecayed wood cell walls [Blanchette *et al.*, 1997; Srebotnik *et al.*, 1988]. It was suggested that low molecular weight reactive oxygen species including hydroxyl radicals (HO·) as well as less reactive peroxyl (ROO·) and hydroperoxyl (HOO·) radicals generated at a distance from white-rot [Hammel *et al.*, 2002] or brown-rot [Wei *et al.*, 2010] fungal hyphae could be responsible for initiating decay

within lignocellulosic cell wall domains. Alternatively, instead of those oxidants, electron transfer between closely spaced aromatic rings in interacting lignin chains [Chen and Sarkanen, 2010] induced by enzymatic oxidation of substructures at the lumen surface could be a prelude to the cleavage of lignin macromolecules.

3.2 A Brief History of Lignin-containing Polymeric Materials

3.2.1 Traditional lignin-containing polymeric materials

During the latter half of the 1950's and throughout the 1960's, the structures of lignin macromolecules were depicted as three-dimensionally crosslinked networks formed mostly from lignin-lignin covalent bonds. Their viscosimetric, sedimentation and diffusion behavior confirmed that soluble lignin derivatives are compact spherical fragments hewn out of a three-dimensional structure [Goring, 1971]. Under the impact of a fundamental misperception of polymeric lignin as a "3-dimensionally branched network" [Hsu and Glasser, 1976], lignin's structural rigidity needed to be softened by incorporating a linear chain polymer [Hsu and Glasser, 1975]. Thus, lignins were covalently linked into commercial polymeric materials to bring about a combination of high modulus and strength "by crosslinking or reinforcing a soft segment matrix with hard segment domains" [Saraf *et al.*, 1985]. Attempts have also been made to introduce lignin derivatives into compatible multiphase polymer blends. Such a goal has resulted in 40 years of trial and error. Numerous efforts have been made to optimize these lignin-containing polymeric materials, yet the outcomes were quite disappointing: in general, the lignin contents of the traditional

lignin-containing polymeric materials are limited to 30–40%, beyond which the resulting materials were extremely brittle.

3.2.2 Crosslinked lignin-containing polymeric materials

In the past 30 years, due to their macromolecular and multifunctional nature, isolated lignins and their derivatives were thought to be ideal components for incorporation into thermosetting resins such as polyurethanes [Saraf and Glasser, 1984; Yoshida *et al.*, 1990], epoxies [Hofmann and Glasser 1993], phenol-formaldehyde resins [Muller *et al.*, 1984], and acrylics [Glasser and Wang, 1989]. The strategy for producing homogeneous lignin-containing polymer networks was predicated on delaying phase separation during the curing process until crosslinking had progressed to the point where individual molecules could no longer demix [Glasser, 1989]. For example, a series of five lignin-derived polyurethanes, synthesized from hexamethylene diisocyanate and hydroxypropyl kraft lignin, embodied lignin contents between 26% and 44% (corresponding to reactant isocyanate/hydroxyl group ratios between 4.7 and 0.9) [Saraf and Glasser, 1984]. The Young's modulus rose perceptibly as kraft lignin content increased; meanwhile, a systematic reduction from ~15% to 1% was observed in the ultimate strain over the same range of lignin content. When the kraft lignin content reached 44%, the tensile strength fell abruptly to 14.8 MPa, compared to roughly 77 MPa at kraft lignin levels between 26% and 38%. These observations were opposite to the theoretical prediction that higher crosslinking density as a result of higher isocyanate/hydroxyl group ratio should give rise to a more rigid material [Saraf and Glasser, 1984]. One possible explanation for the

unexpected rigidity in the face of fewer crosslinks in these kraft lignin-derived polyurethanes can be found in the effects of the strong non-bonded orbital interactions between aromatic rings in lignin derivatives [Sarkanen and Chen, 2005]. Such non-covalent interactions arising from dynamical electron correlation are computed to be stronger than the stabilization energies for GC/CG base pairs in DNA double-helices [Chen and Sarkanen, 2010]. An improvement in mechanical properties was achieved by the addition of 18% polyethylene glycol ($\overline{M}_n$ = 400) as soft-segments into the hydroxypropyl-kraft-lignin-containing polyurethane network [Saraf *et al.*, 1985]. At the expense of lowering the kraft lignin content 1.3-fold to 28%, the flexiblizing complementation contributed by linear polyethylene glycol brought about a ~4-fold reduction in Young's modulus, a ~3-fold decrease in tensile strength and a ~6-fold increase in the ultimate strain. In general, crosslinked polymeric materials with high lignin contents are inevitably extremely brittle.

The impact of the molecular weight of lignin components on homogeneous crosslinked lignin-containing polymeric materials was revealed with a series of kraft lignin–polyether triol–polymeric MDI polyurethanes [Yoshida *et al.*, 1990]. Four kraft lignin fractions of different number average molecular weight ($\overline{M}_n$) were applied as crosslinking agents in the three-component MDI system with a constant NCO/OH ratio. The tensile strength of the polyurethane containing the highest molecular weight fraction ($\overline{M}_n$ = 3800) reached its maximum at a 10% lignin content, compared to 25% ~30% for the other three fractions ($\overline{M}_n$ = 1710, 900, 450). When the kraft lignin content was increased

above 30%, regardless of the molecular weight of the lignin components, the polyurethanes obtained were glassy and rigid whatever the NCO/OH ratio employed in the formulation.

In a study of lignin-containing epoxy resins [Hofmann and Glasser, 1993], epichlorohydrin endcapped alkoxylated lignins were crosslinked with m-phenylenediamine. The stiffest network was produced from an unfractionated ethyoxylated organosolv lignin at 57% lignin content that exhibited a Young's modulus of 1.0 GPa, tensile strength of 42 MPa and ultimate strain of 6%. This was one of the few cases in the past 30 years that demonstrated the possibility of producing lignin-based crosslinked polymeric material by covalent incorporation of a lignin derivative.

3.2.3 Multiphase lignin-containing polymer blends

As an alternative approach to developing useful lignin-containing polymeric materials, multiphase blends composed of lignin and other commercially available polymers were brought into the picture. Disappointingly, the introduction of lignin derivatives hardly improved the mechanical properties of the composite overall. Multiphase blends of hydroxypropyl kraft lignin with poly(methyl methacrylate) were expected to show mechanical compatibility originating from good interfacial adhesion between the phases of the blend components. In fact, as the proportion of lignin rose to 20%, an increase in Young's modulus but decreases in tensile strength and ultimate strain were observed. [Ciemniecki and Glasser, 1988]. Besides the immiscible blends between lignin and poly(methyl methacrylate), cellulose acetate butyrate was blended with lignin esters with different ester substitutents, acetate, butyrate, hexanoate and laurate, to produce

multiphase composites. At a 50% incorporation level of lignin esters, the tensile strength decreased sharply to 5~15% of the original value, and increasing the lignin content up to 20% led to a more than 4-fold reduction in the ultimate strain [Ghosh *et al.*, 1999]. The idea of lignin-containing interpenetrating polymer networks was brought up in the late 1980's in the expectation that a synergistic interaction between the polymeric components could enhance the system mechanically. However, the situation was not fundamentally improved in interpenetrating composites of lignin-containing polyurethanes and poly(methyl methacrylate). On the one hand, when the lignin content in the lignin-containing polyurethane was fixed at 30%, both Young's modulus and tensile strength decreased dramatically as the proportion of poly(methyl methacrylate) decreased [Kelley *et al.*, 1990]. On the other hand, when the proportion of crosslinked poly(methyl methacrylate) was held at 50% and the true lignin contents were increased from 13% to 28%, the ultimate strain decreased; Young's modulus and the tensile strength both increased conspicuously with lignin content, although their value did not reach those characteristic of poly(methyl methacrylate) itself (3200 MPa Young's modulus, 35 MPa tensile strength [Kelly *et al.*, 1989; 1990]).

With few exceptions, whether the lignin preparations were incorporated covalently or noncovalently, the findings described above share a common deficiency in that the lignin contents were limited to 30–45% (w/w) levels beyond which the resulting polymeric materials became fatally brittle. Considering the total amount of lignin byproducts to be generated from the future mass production of bio-fuels, one could ask whether a simple

lignin derivative could act as an active principal component in any potentially useful polymeric material.

3.2.4 The first true lignin-based thermoplastics

In the late 1990's, a major step forward was realized by the advent of the first true lignin-based thermoplastics formulated by blending 85% (w/w) kraft lignin with 12.6% poly(vinyl acetate) in the presence of 1.6% diethyleneglycol dibenzoate and 0.8% indene [Li *et al.*, 1997]. Despite the fact that they were partially soluble in aqueous alkaline solution, they proved the feasibility of fabricating homogeneous polymer blends with very high lignin contents. Their mechanical properties were very sensitive to the degree of association between the kraft lignin components. Interestingly, removal of the individual lignin components which were not incorporated into supramacromolecular complexes led to exceptionally weak materials. Thus, it was concluded that these individual lignin components were responsible for promoting compatibility between the associated lignin complexes and poly(vinyl acetate) [Li and Sarkanen, 2003].

3.2.5 Simple alkylated kraft lignin-based thermoplastics

Despite the fact that the 85% kraft lignin-based thermoplastics tended to be soluble to a limited extent in aqueous alkaline solution, they proved the feasibility of fabricating homogeneous polymer blends with very high lignin contents. It was then discovered that the tensile behavior of alkylated 100% kraft lignin-based polymeric materials was very similar to that of polystyrene, which itself is fairly brittle but can be plasticized easily [Li

and Sarkanen, 1999]. In contrast to the underivatized kraft lignin, alkylated kraft lignin derivatives are readily plasticized by blending with miscible low-T_g polymers such as aliphatic main-chain polyesters with methylene/carboxylate group (CH_2/COO) ratios of 2.0-4.0 [Li and Sarkanen, 2002].

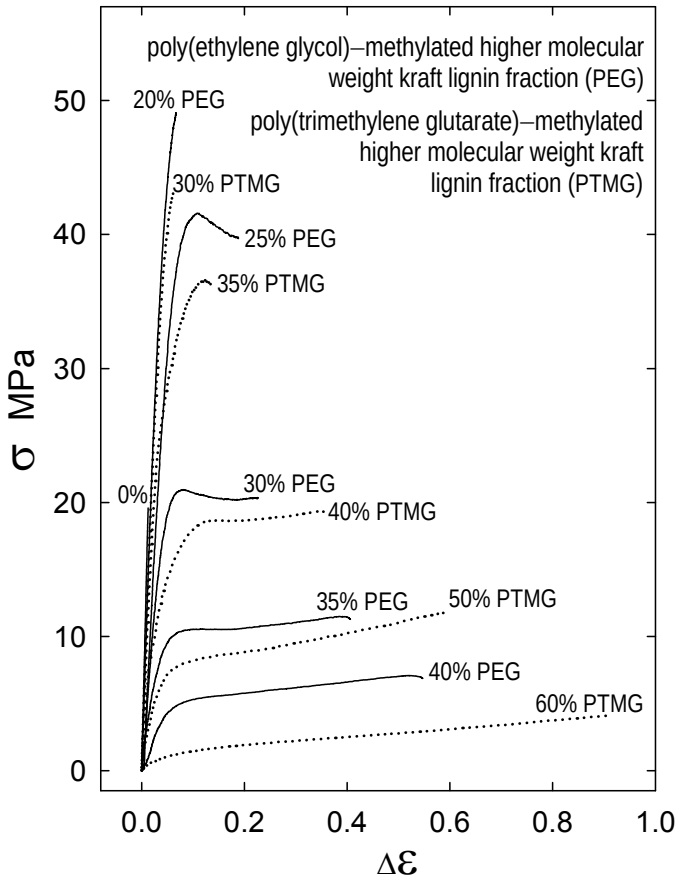

Figure 3.3 Progressive plasticization of methylated polydisperse higher molecular weight kraft lignin fraction ($\overline{M}_w$ = 23.0 x 10^3, $\overline{M}_n$ = 8.8 x 10^3) in blends with poly(ethylene glycol) and poly(trimethylene glutarate). Data from [Li and Sarkanen, 2002; 2005].

Fig. 3.3 depicts the plasticization of a methylated kraft lignin fraction with progressive incorporation of poly(ethylene glycol) (PEG) or poly(trimethylene glutarate) (PTMG) into the blend [Li and Sarkanen, 2002; 2005]. The methylated sample was derived

from a polydisperse kraft lignin fraction ($\overline{M}_w$ = 10,100) obtained by ultrafiltration in aqueous 0.10 M NaOH [Li and Sarkanen, 2002]. Compared with PTMG (35%), less than 25% of the PEG was required to reach the plasticization threshold for the same methylated kraft lignin fraction.

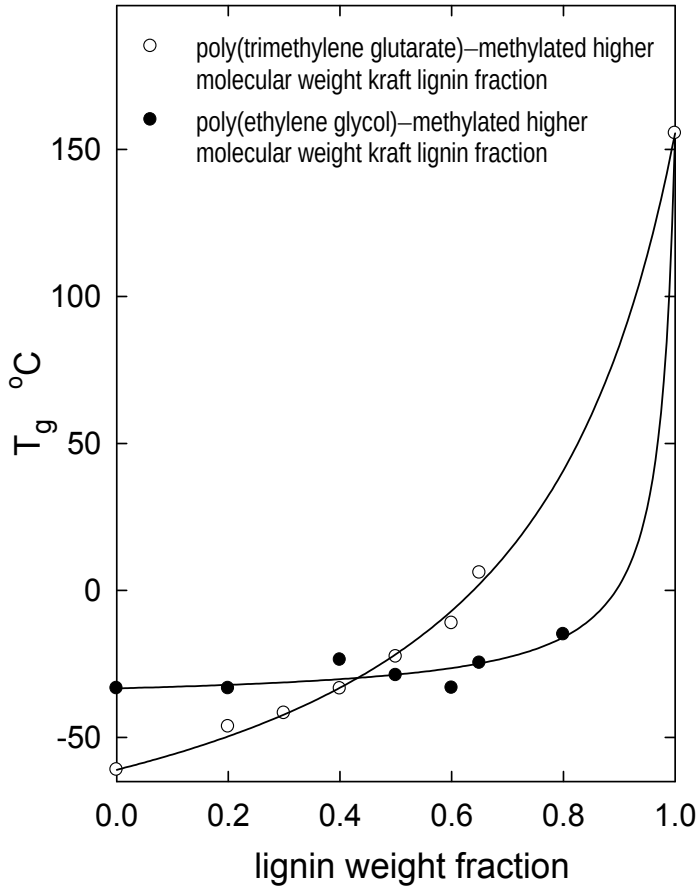

Figure 3.4 Variation of T_g with composition for blends of methylated polydisperse higher molecular weight kraft lignin fraction ($\overline{M}_w$ = 23.0 x 10^3, $\overline{M}_n$ = 8.8 x 10^3) in blends with poly(trimethylene glutarate) and poly(ethylene glycol). Data from [Li and Sarkanen, 2002; 2005].

The relative magnitudes of the interactions between polymeric plasticizer and the lignin components can be reflected in the concavity of the T_g–composition curves for the corresponding blends. As the content of the methylated kraft lignin fraction increases from 0 to 65%, the change in T_g of the PTMG blends is much more dramatic than the corresponding blends with PEG (Fig. 3.4) [Li and Sarkanen, 2005]. Indeed, an efficacious plasticizer should interact with associated lignin complexes strongly enough to form a miscible blend. However, a low-T_g polymer that interacts more weakly with the lignin components will dissociate the supramacromolecular complexes to a smaller extent, and therefore less of this low-T_g polymer will be required in the blends to reach the plasticization threshold. For main-chain polyesters, the least efficacious plasticization occurs when the CH_2/COO ratio lies between 2.5 and 3.0, where the intermolecular interactions between the blend components are most favorable [Li and Sarkanen, 2002; 2005].

3.3 Non-covalent Interactions between Individual Lignin Macromolecules

It was assumed that the chain stiffness in lignin-containing polymeric materials arises from the presence of aromatic rings in the macromolecular chains [Yoshida *et al.*, 1987], however this alone could not result in brittleness that exceeds that of polystyrene. The most prominent physicochemical characteristic of lignin components is their pronounced tendency to associate with one another. The strong interactions between the individual lignin macromolecules will have a profound impact on the mechanical properties of any lignin-containing polymeric materials. A telling result is depicted in Fig.

3.5 [Li and Sarkanen, 2003] which demonstrates how extensively lignin components associate. The effect is evident in the apparent molecular weight distributions of a series of acetylated methylated kraft lignin preparations that differ only in their degree of association [Li and Sarkanen, 2003]. Before derivatization, the degree of association between individual components was varied by incubation at different concentrations in aqueous 0.4 M NaOH. The interconvertibility between the multimodally distributed supramacromolecular complexes composed of ~10^3 – 10^4 individual components, reveals that the associative processes are non-random, and their rates are thought to be controlled by conformational changes in the individual molecular components [Sarkanen *et al.*, 1984; Dutta *et al.*, 1989; Garver *et al.*, 1989].

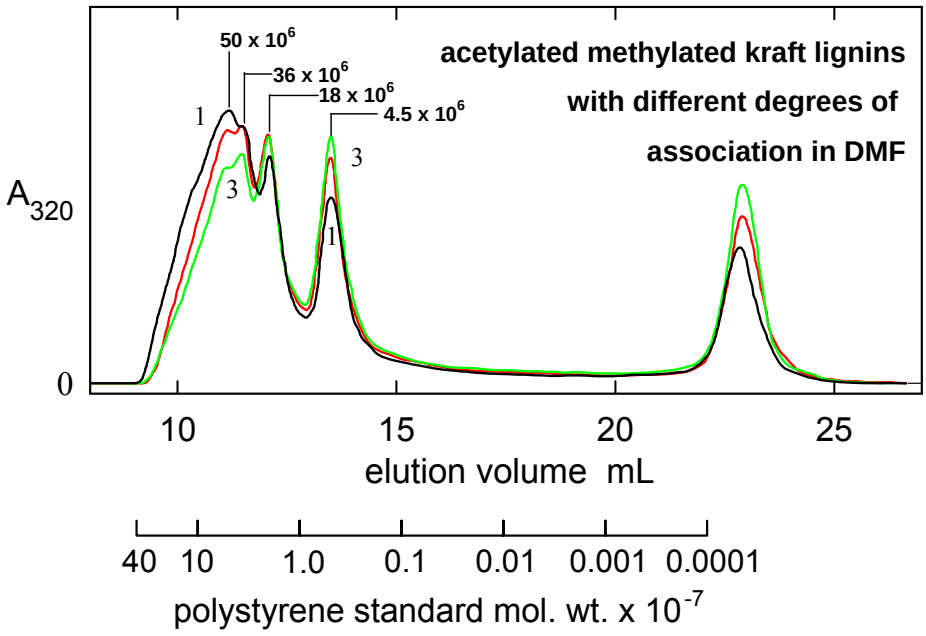

Figure 3.5 Molecular weight distributions of acetylated methylated kraft lignins in DMF. Before derivatization, these samples had been fractionated through Sephadex LH20 in aqueous 35% dioxane after association at 195 g/L for (1) 6740 h, (2) 3910 h and (3) 1630 h in aqueous 1.0 M ionic strength 0.40 M NaOH [Li and Sarkanen, 2003].

In 1997, the first lignin-like dehydropolymerisates were synthesized from the monolignol, coniferyl alcohol, through single-electron oxidation by horseradish peroxidase in the presence of pre-existing lignin macromolecules acting as templates [Guan *et al.*, 1997]. Whether lignin configuration is preserved in regard to its primary structure through a template polymerization mechanism was not established at that time.

One step toward an answer to this important question was facilitated by the development of the M05-2X hybrid meta exchange-correlation functional which made it possible to locate geometry optimizations for stacked complexes of nucleobases or aromatic amino acids using density functional theory (DFT) [Zhao *et al.*, 2006]. The stabilization energies of lignol radicals interacting noncovalently with monomeric closed-shell lignin units have been calculated at the M05-2X/6-31+G(d,p) level of DFT [Chen and Sarkanen, 2010]. As summarized in Fig. 3.6, the cofacial head-to-tail configurations (Fig. 3.6 b,c) of complexes between coniferyl alcohol radical and veratryl alcohol are more stable than the edge-on head-to-head (Fig. 3.6 a) or the cofacial head-to-head (Fig. 3.6 d) configuration.

It was concluded that dynamical electron correlation in the π-obitals is primarily responsible for the strong intermolecular attraction for two reasons: 1) there is no intermolecular hydrogen bonding in any of the complexes; 2) although the 3.4 Å separation between the cofacial aromatic rings could allow significant π-orbital overlap, hardly any unpaired electron density from the coniferyl alcohol radical is delocalized over the atomic centers in the veratryl alcohol. The calculated non-covalent stabilization energies of ~9 kcal/mol that arise from dynamical electron correlation are significantly stronger than those

engendered by the hydrogen bonds and aromatic stacking interactions in the GC/CG base pairs of DNA double helices in aqueous solution [Every and Russu, 2007]. This finding implies that, during monolignol template dehydropolymerization *in vitro* or lignin biosynthesis in plant cell walls, each daughter strand is likely to be topologically complementary to the parent chain from which it is derived [Chen and Sarkanen, 2010]. Such effects provide important insights into the origins of the strong associative interactions between individual lignin macromolecules that lead to the formation of supramacromolecular lignin complexes.

(**a**) edge-on head-to-head *anti* coniferyl alcohol radical at **4.9 Å** ring-center distance from ring plane of veratryl alcohol;

5.1 kcal/mol
stabilization energy

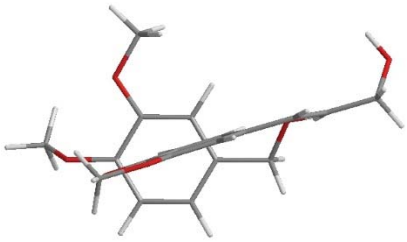

(**b**) cofacial head-to-tail *anti* coniferyl alcohol radical at **3.3 Å** interplanar separation from ~parallel veratryl alcohol;

8.9 kcal/mol
stabilization energy

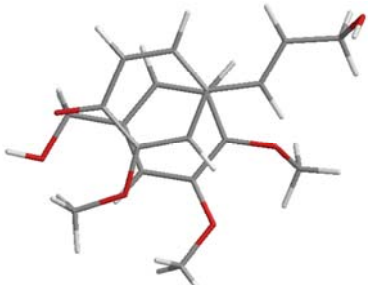

(**c**) cofacial head-to-tail *syn* coniferyl alcohol radical at **3.4 Å** interplanar separation from~parallel veratryl alcohol;

9.1 kcal/mol
stabilization energy

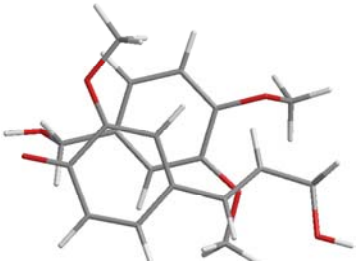

(**d**) cofacial head-to-head *anti* coniferyl alcohol radical at **3.4 Å** interplanar separation from ~parallel veratryl alcohol;

6.2 kcal/mol
stabilization energy

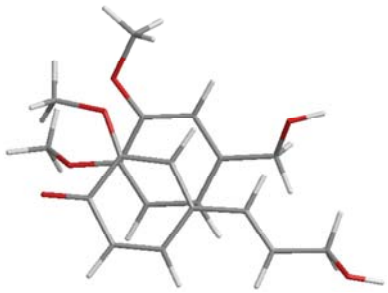

Figure 3.6 Monolignol radical complexes with veratryl alcohol [Chen and Sarkanen, 2010], as a model for a closed-shell lignin monomer unit, in component conformations that preclude intermolecular hydrogen bonds (ChemBio3D depictions of M05-2X/6-31+G(d,p) geometry-optimized structures). Half of the counterpoise correction has been applied to each stabilization energy because of basis set superposition error [Kim *et al.*, 2000].

Chapter 4

Experimental Section

4.1 Ball-milled Lignin Isolation and Purification [Lundquist, 1992]

The Jack pine sapwood chips were ground in a Wiley mill (40 mesh particle size). The harvested wood meal was Soxhlet-extracted with acetone for 48 h. The dry extractive-free wood meal was milled in a vibratory ball mill (with two 0.3 L stainless steel jacketed grinding vessels, purchased from Siebtechnik GmbH, Germany) under N_2 for 48 h. Each jar was loaded with ~6 g of the wood meal and stainless steel balls to about 80% of the jar volume. 40 g ball-milled wood powder was suspended in 400 mL of dioxane–water (96:4, v/v) with stirring for 24 h. The extraction was then repeated with 300 mL of fresh dioxane/water (96:4, v/v) for 24 h and then with 200 mL for 48 h. The extracts were centrifuged to remove any particles (3000 rpm, 30 min) and the solvent mixture was removed by means of rotary evaporation.

1 g crude product was dissolved in 28 mL pyridine–acetic acid–water (9:1:4 v/v/v), and then the mixture was extracted with 36 mL chloroform in a separatory funnel. The mixture was centrifuged at 3000 rpm until the organic layer was clear. After careful removal of the aqueous layer and the precipitates located in between the organic and aqueous layers, the clear organic layer was combined with another 28 mL pyridine–acetic acid–water (9:1:4 v/v/v), and then again extracted with 36 mL chloroform. The clear organic extract was collected by repeating the preceding steps. The solvents were removed through rotary evaporation; the last trace of pyridine was evaporated by adding and

evaporatively removing ethanol repeatedly. In order to minimize possible chemical modifications, rotary evaporation in this section of the work has to be carried out at a temperature below 35 °C. The glossy residue was redissolved in 10 mL dichloroethane–ethanol (2:1 v/v). The mixture was added dropwise to 250 mL ether with vigorous stirring; the precipitates formed through this process were collected by centrifugation at 3000 rpm and then washed with 200 mL ether three times. The purified ball-milled lignin was dried in a desiccator under mild vacuum.

4.2 Preparation of Water Soluble Ball-milled Lignin Fractions

1 g of the parent ball-milled lignin was dissolved in 200 mL carbonate-free 0.10 M NaOH and added to a solvent-resistant stirred cell (accommodating a 76 mm diameter membrane, Millipore Corp., Billerica, MA). The solution was ultrafiltered exhaustively in aqueous 0.10 M NaOH (carbonate-free) in turn through 30,000, 10,000 and 5,000 or 1,000 nominal molecular weight cutoff membranes (Amicon YM30, YM10 and PLCC or PLAC respectively; Millipore Corp., Billerica, MA). In each case, the time-course for ultrafiltration was extended to allow dissociation of the retained macromolecular lignin complexes to occur so that the individual components released may have the opportunity of passing through the membrane. When the permeate from ultrafiltration in 0.10 M NaOH became colorless, the retentate was subjected to washing by continuing the ultrafiltration processing with distilled water to pH 8.0, and then triply-distilled water until the pH reached ~7.0. The carbonate-free retentate solution (150 mL) was centrifuged (3000 rpm) to remove any small quantity of precipitate, and the supernatant containing polymeric

native lignin substrate was stored in a Teflon bottle under N_2. Each ball-milled lignin (BML) fraction was named after the nominal molecular weight cutoff of the corresponding retentate membrane, such as BML 30k, BML 10k and BML 5k or BML 1k.

4. 3 Size Exclusion Chromatography (SEC)

4.3.1 Column preparation

26 g Sephadex G-100 gel was allowed to swell in 1100 mL 0.10 M NaOH for 3 days. After proper degassing under reduced pressure with ultrasonication, the swollen gel mixture was slowly poured down a long glass rod into a 2.5 x 100 cm column which had been 1/3 filled with 0.10 M NaOH in such a way that all bubbles would be simultaneously removed from below the nylon gauze of the lower endplate. After standing for 3 days, the excess gel was removed from the packing reservoir attached to the top of the column. The packing reservoir was removed and the column was carefully closed with an upper endplate that was connected to a carboy containing carbonate-free 0.10 M NaOH as the eluent. The column was conditioned by running for consecutive 12 h periods at flow rates of 5, 15, 20, 30 and 35 mL/h followed by alternately running at 45 mL/h for 15 min and 32 mL/h for 30 min 3 times altogether.

4.3.2 Sample preparation for enzymatic lignin degradation studies

The assay solutions of water-soluble native lignin with the presence or absence of enzymes were prepared in 25 mM phosphate buffer. After incubation in buffer, the assay

solutions were diluted with water and 1.0 M NaOH to make a sample solution equivalent to 0.10 M NaOH. 2mL sample solution (~0.75 mg of lignin) was loaded on top of the gel followed by 2.0 mL 0.10 M NaOH twice after lowering the respective solution volumes into the gel bed. The column was run at a flow rate of ~32 mL/h. The elution was monitored by an ISCO V^4 absorbance detector set at 280 nm.

4.3.3 Elution profiles

The elution profiles were scanned and then digitized by the Engauge Digitizer (software version 2.15, developed by Mark Mitchell). The relative retention volume, V_R, is the ratio of the retention volume, V_t, to the void volumn, V_0 (Eq. 4.3.3-1). V_0 was determined for the profile with blue dextran. The scale of V_R for sample profile was correlated with an assignment of 0.8 as the standard value for the peak-maximum of blue dextran. All the profiles were normalized on the basis of their areas. In Eq. 4.3.3-2 and 4.3.3-3, t represents the time; f_1 and f_2 are the flow rates measured after running the column for 2 h and before stopping the column at the end respectively; the experimental flow rates (f_1 and f_2) are plotted against t assuming that the flow rate changes linearly with time, the intercept on the y-axis is defined as f_0 and a denotes the slope of the fitted line. The chart speed of the recorder was set at 0.05 mm/min.

$$V_R = \frac{V_t}{V_0} \tag{4.3.3-1}$$

$$V_t = f_0 t - \frac{at^2}{2} \tag{4.3.3-2}$$

$$a = \frac{f_1 - f_2}{t_1 - t_2} \tag{4.3.3-3}$$

4.4 Detection of Lignin Depolymerase Activities by Rayleigh Light Scattering

4.4.1 Debye fitting for molecular weight and radius of gyration

Light scattering is an important experimental technique for characterizing polymers and biopolymers. In practice, it can be used to determine the absolute weight-average molecular weight, M_w, and z-average radius of gyration, R_g; it also provides polymer scientists with information about polymer-polymer and polymer-solvent interactions through the second virial coefficient, A_2.

In this study, M_w and R_g for lignins have been determined by using a multi-angle laser light scattering photometer (Dawn HELEOS, Wyatt Technology) equipped with a polarized 780 nm laser light source. The intensity of the scattered light at angle θ is proportional to the weight concentration, c, and molecular weight, M of the sample as described in Eq. 4.4.1-1 [Zimm, 1948]:

$$\frac{R_\theta}{Kc} = MP(\theta) - 2A_2cM^2P^2(\theta) \qquad (4.4.1\text{-}1)$$

where $P(\theta) = 1 - \frac{16\pi^2 n_0^2}{3\lambda_0^2}\sin^2\left(\frac{\theta}{2}\right)R_g^2$ is the form factor.

and $K = 4\pi^2 n_0^2 (dn/dc)^2 \lambda_0^{-4} N_A^{-1}$ is the optical constant.

R_θ is the excess Rayleigh ratio; n_0 is the solvent refractive index in the absence of polymer; N_A is Avogadro's number, and λ_0 is the vacuum wavelength of the incident light. The refractive index increment, dn/dc, can be determined at 780 nm with an Optilab rEX instrument (Wyatt Technology).

When the sample solution containing substrate and enzymes is passed (with a syringe pump) through the HELEOS flow cell, the scattered intensity at each angle changes

not only as a function of concentration (which allows extrapolation ideally to zero concentration), but also as a function of time due to enzyme-catalyzed physicochemical changes in the macromolecular lignin chains. Such effects would compromise the traditional Zimm-plot analysis of the data. This matter can better handled through the Debye formalism, where R_θ/Kc is plotted against $\sin^2(\theta/2)$ (Fig. 4.1). As $\theta \rightarrow 0$, $P(\theta) \rightarrow 1$. The intercept at zero angle, R_0/Kc, will be given by:

$$\frac{R_0}{Kc} = M - 2A_2cM^2 \qquad (4.4.1\text{-}2)$$

As a result of plotting R_0/Kc versus c, the weight concentration of the lignin preparation (as shown in Fig. 4.2), the absolute value of M at $c \rightarrow 0$ can be determined from the intercept on the y-axis.

Subsequently, the values of the apparent R_g for different concentration slices can be calculated based on

$$R_g^2 = \frac{-3m_0\lambda^2}{16\pi^2M(1 - 4A_2Mc)} \qquad (4.4.1\text{-}3)$$

where $m_0 \equiv d[R_\theta/Kc]/d[\sin^2(\theta/2)]_{\theta \rightarrow 0}$ is the slope at zero angle of the Debye plot. For a well behaved polymer, m_0 is generally negative. The absolute values of R_g were determined by extrapolation to c = 0 through a process for which each apparent value of A_2 was calculated using Eq. 4.4.1-2 (Fig. 4.3). Note that in Eq. 4.4.1-3, the reciprocals of $(dn/dc)^2$ in the reciprocals of K for determining both m_0 and M cancel one another at c = 0, and therefore dn/dc should not affect the accuracy of R_g as much as it does the molecular weight.

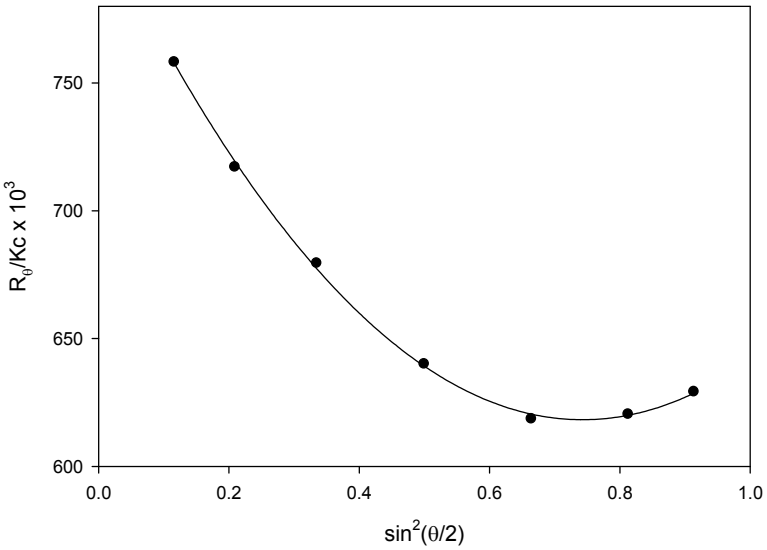

Figure 4.1 An example of a Debye plot (only odd-numbered detectors with interference filters are used in the plot). Assay conditions: 1.42 g/L soluble native polymeric lignin preparation incubated with 1 μM lignin depolymerase for 3 h in 25 mM phosphate buffer, pH 6.3.

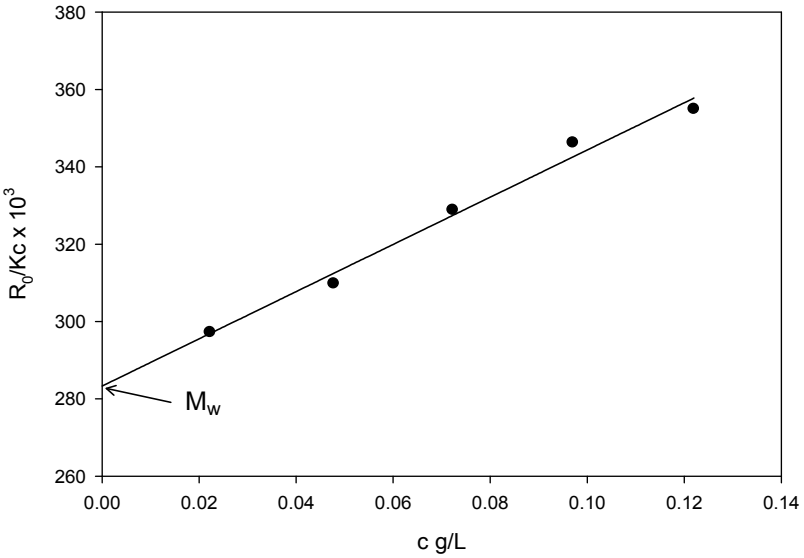

Figure 4.2 Determination of M_w for native lignin substrate from light-scattering measurements. Extrapolation of R_0/Kc to c = 0. Assay conditions: 0.95 g/L soluble native polymeric lignin preparation incubated with 4 μM lignin depolymerase for 8.5 h in 25 mM phosphate buffer, pH 7.1. (Standard error of intercept is 1.16%)

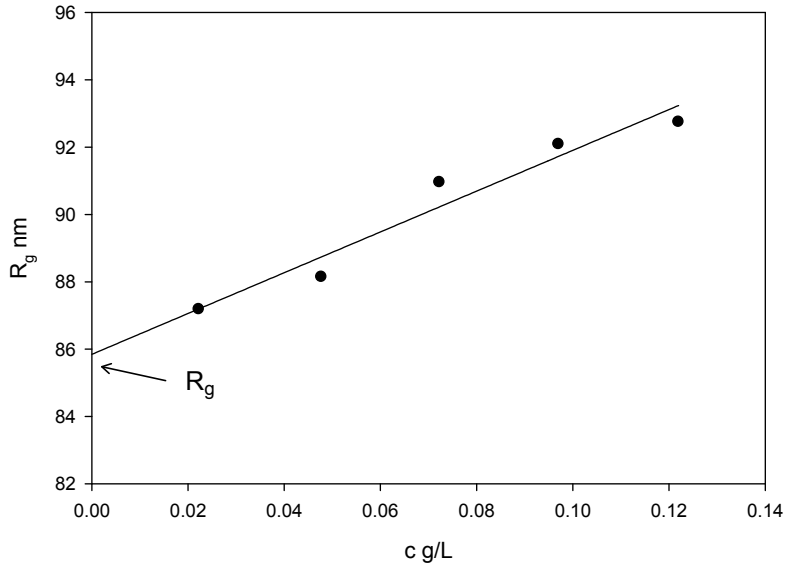

Figure 4.3 Determination of R_g for native lignin substrate from light-scattering measurements. Extrapolation of apparent R_g to c = 0. R_g is deduced from the set of Debye plots used to generate molecular weight data in Fig. 4.2. (Standard error of intercept is 0.77%)

4.4.2 Sample preparation and data collection

The lignin depolymerase, salicylate hydroxylase from *Pseudomonas* sp. (Sigma-Aldrich S2907), was dissolved in 50 mM phosphate buffer in the presence or absence of the NADH cofactor depending on the experimental conditions. The enzyme solution was pre-filtered through a 0.2 μm PTFE membrane (TF-200 13 mm, Pall, Ann Arbor, Michigan). The filtrate was mixed with an equal volume of substrate solution containing a native polymeric lignin fraction (BML10k) to perform an assay in 25 mM phosphate buffer. The assay solution was further diluted to a series of 5 concentrations for determining M_w, R_g and dn/dc.

Batch modes were employed in this work. Each sample solution was loaded in two 5 mL Hamilton syringes and then injected into the Dawn HELEOS and Optilab rEX simultaneously at 7.63 mL/h by RAZEL syringe pumps (model R-99). To guard against flow-cell blockage, sample solutions were filtered through 1 μm PTFE membranes (TF-1000 13 mm, Pall, Ann Arbor, Michigan) prior to injection; on the other hand, the blank aqueous buffer was filtered through an Acrodic CR 13 mm syringe filter (0.45 μm PTFE membrane, Pall, Ann Arbor, Michigan). A fresh filter membrane was employed for each concentration.

When the changes of detector voltage (Dawn HELEOS) and differential refractive index (Optilab rEX) with time had reached their respective plateaus (Fig. 4.4 and 4.5), 1 mL samples of the two solutions were collected from the outlets of the Dawn HELEOS and the Optilab rEX separately so that their actual concentrations in the flow cells (recognizing possible adsorptive losses of the solutes) could be determined on the basis of UV absorbance at 280 nm.

4.4.3 Data processing

The ASTRA software (Wyatt Technology) was responsible for data collection and processing for the Dawn HELEOS and Optilab rEX. However, the experimental data from the Dawn HELEOS had to be re-evaulated manually for the following reasons: 1) the ASTRA software did not provide users with the opportunity of making an absorbance correction; 2) the data clusters at the bottom of the envelope on the plateau (Fig. 4.4) are more representative of the scattered intensity from the sample macromolecules.

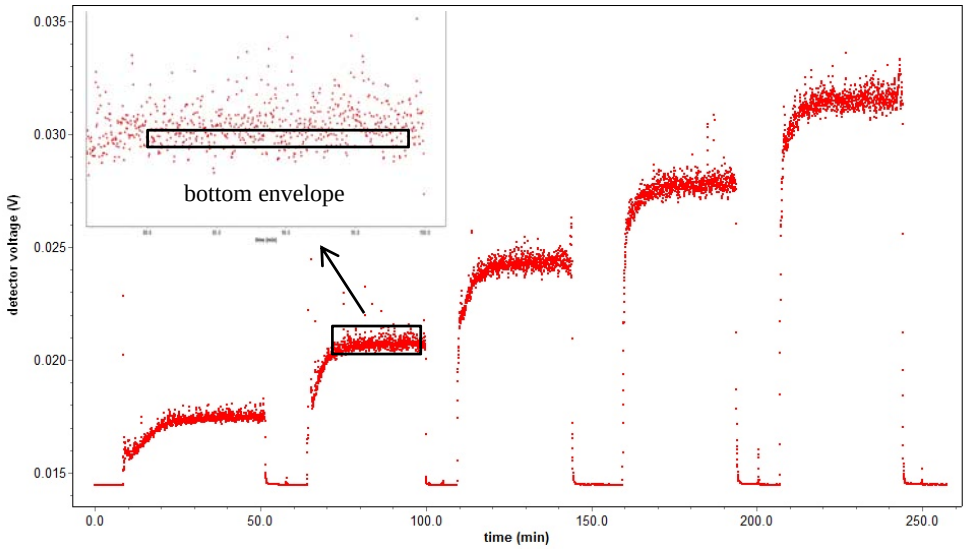

Figure 4.4 HELEOS data collection for 90º detector (LS 11) voltage changing with time and sample concentration. Each peak represents one sample concentration and baselines in between peaks represent blank phosphate buffer. The concentration of lignin in the sample solution varies from 0.012 to 0.066 g/L.

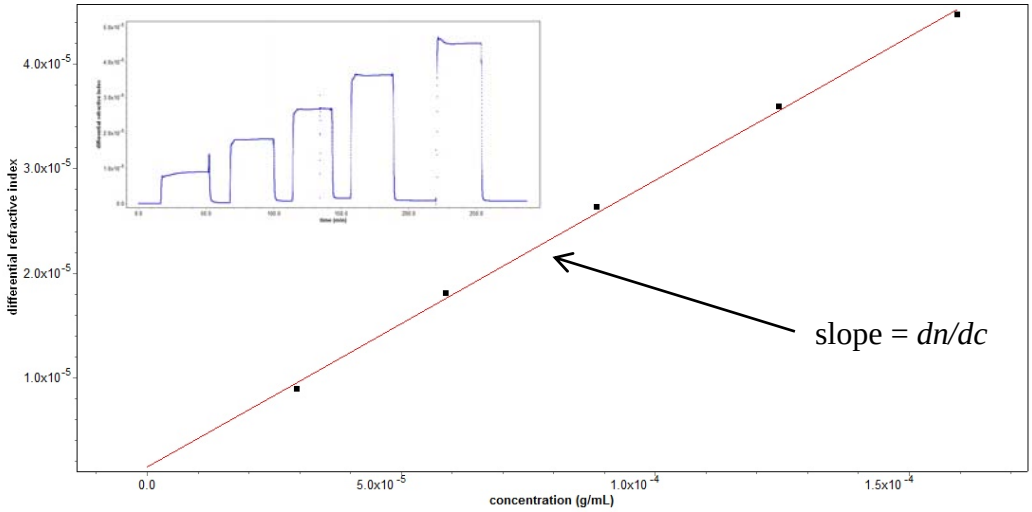

Figure 4.5 The slope of differential refractive index *vs* sample concentration equals *dn/dc*. Top left: optilab rEX data collection of differential refractive index changing gradually with time and stepwise with sample concentration.

In order to process the collected light scattering data manually, it has to be clarified how the DAWN HELEOS measures the excess Rayleigh ratio, R_θ (cm^{-1}) defined as:

$$R_\theta = \frac{(I_\theta - I_{\theta,solvent})r^2}{I_o V} \tag{4.4.3-1}$$

where I_θ is the scattered intensity; I_0 is the intensity of the incident beam; $I_{\theta,\,solvent}$ is the scattered intensity from the solvent; V is the volume of the scattering medium, and r is the distance between the scattering volume and detector.

In practice, the quantities measured by the light scattering photometer are detector voltages which are proportional to scattered light intensities (eq. 4.4.3-2).

$$R_\theta = N_\theta A_{CSCC} \left(\frac{V_\theta - V_{\theta,baseline}}{V_{laser} - V_{laser,dark}} \right) \tag{4.4.3-2}$$

where V_θ and $V_{\theta,baseline}$ are the θ angle detector signal voltage and baseline voltage respectively, and V_{laser} and $V_{laser,dark}$ are the laser monitor signal and dark offset respectively. The configuration specific calibration constant, A_{CSCC}, can be obtained from calibration with pure toluene. The normalization coefficient at θ angle, N_θ, is specific for a certain solvent system, and it can be determined by implementing normalization with an isotropic scatterer in the target solvent.

Before Debye plot fitting, the absorbance of scattered light by lignin macromolecules in the sample solution was compensated for by using a correction factor (Eq. 4.4.3-3) derived from the Beer-Lambert law, where F and F_0 are the forward laser monitor signal intensities with and without absorbance respectively; I_{true} is the intensity of

the laser at the center of the flow cell and I_0 is the intensity of the incident laser beam. Eq. 4.4.3-4 is derived from Eq. 4.4.3-2 and Eq. 4.4.3-3; therefore the corrected excess Rayleigh ratio at θ angle, $R_{\theta,corrected}$, can be obtained accordingly. Both the corrected M_w and R_g can be obtained through Debye fitting as described above.

$$\frac{I_{true}}{I_0} = \sqrt{\frac{F}{F_0}} \tag{4.4.3-3}$$

$$R_{\theta,corrected} = N_\theta A_{CSCC} \frac{[V_\theta/\sqrt{F/F_0} - V_{\theta,baseline}]}{(V_{laser} - V_{laser,dark})} \tag{4.4.3-4}$$

The experimental values of R_θ, V_θ, F and (V_θ-$V_{\theta,baseline}$) can be exported from ASTRA files in the following manner (ASTRA 5.3.2.15): go to menu Experiment → Graph → Add custom plot. Select the plots that are required for data processing from the "available" list in the menu window: (1) instrument data in physical units, despiked, baseline subtracted; (2) forward laser monitor (under "original data"); (3) raw data; (4) raw data, despiked, baseline subtracted. Plots (1) ~ (4) in ASTRA correspond to R_θ, F, V_θ and (V_θ-$V_{\theta,baseline}$) changing with time, respectively. $N_\theta A_{cscc}/(V_{laser}$-$V_{laser,\ dark})$, the ratio of R_θ to (V_θ-$V_{\theta,baseline}$), is constant for the corresponding detector.

Note that only detectors of odd number were employed in this study. Interference filters were installed on the odd-number detectors to avoid an overestimation of molecular weight of lignin due to fluorescence.

It is important to remember that the sample concentration involved in Debye fitting (Eq. 4.4.1-1~5) was the total concentration of salicylate hydroxylase and lignin substrate. The actual concentration of water-soluble lignin substrate was estimated on the basis of the

UV absorbance of the corresponding sample solution at 280 nm ($A_{280,sample}$). The average absorptivity of BML 10k fractions in pH 6.3 25 mM phosphate buffer at 280 nm ($a_{280,lignin}$) is 15.9 $g^{-1}Lcm^{-1}$. Salicylate hydroxylase, xylanase and NADH at the highest concentrations employed in this study contributed less than 3% to the absorbance of the sample solution at 280 nm, so that $A_{280,\ sample} \approx A_{280,\ lignin}$. The concentration of sample solution (c_{sample}) employed in the M_w and R_g determinations by Debye fitting can be estimated by using Eq. 4.4.3-5, where c_{lignin} and c_{SH} (g/L) are the concentrations of lignin substrate and salicylate hydroxylase in the original stock solution prior to dilution for each assay.

$$c_{sample} = A_{280,lignin} a_{280,lignin} \frac{c_{lignin} + c_{SH}}{c_{lignin}} \qquad (4.4.3\text{-}5)$$

Due to the poor stability of the Optilab rEX when low lignin substrate and enzyme concentrations were used, the dn/dc's obtained experimentally for the assay solution varied significantly from one another. However, accuracy of the DAWN HELEOS was not affected by low solute concentrations. Therefore, the dn/dc used in estimating M_w and R_g was the weight-average dn/dc (Eq. 4.4.3-6) of the proteins that contribute to scattering and the water-soluble lignin substrate. In Eq. 4.4.3-6, $(dn/dc)_{lignin}$ and $(dn/dc)_{protein}$ are the differential refractive index increments of water-soluble lignin and proteins, respectively, in the aqueous solutions.

$$dn/dc = \frac{c_{lignin}\,(dn/dc)_{lignin} + \sum c_{protein}(dn/dc)_{protein}}{c_{lignin} + \sum c_{protein}} \qquad (4.4.3\text{-}6)$$

4.5 Methylation of Ball-milled Lignin Preparations

20 g/L ball-milled lignin preparation was dissolved in 60% dioxane-aqueous 0.10 M NaOH solution followed by 2 mL/g lignin dimethyl sulfate (Aldrich) under N_2. During the reaction, the pH of the mixture tended to decrease; it was kept around 13.5 by adding 60% dioxane-aqueous 2.0 M NaOH. When the pH stopped decreasing, another 2mL/g lignin dimethyl sulfate was added. The preceding methylation procedure was repeated 4 times. At the end of the fifth dimethyl-sulfate methylation step, the reaction mixture was neutralized with 0.5 M H_2SO_4. The dioxane was removed exhaustively by means of rotary evaporation at 35ºC. The residue was washed with distilled water until the complete removal of SO_4^{2-} and then air-dried.

The partially methylated products were further methylated by diazomethane prepared by heating Diazald **(***N*-Methyl-*N*-nitroso-*p*-toluenesulfonamide, Aldrich) in a base-chloroform mixture. 30 mL chloroform was added to a cold bi-phasic mixture containing 30 mL aqueous 1 g/mL KOH and 30 mL 2-ethoxyethanol in a 250 mL clear-seal-joint distilling flask from the Diazald kit. The chloroform-aqueous KOH–2-ethoxyethanol mixture was magnetically stirred and heated in a water bath to 80ºC. When the first drop of chloroform appeared on the end of the condenser connected to the flask, 150 mL 0.1 g/mL Diazald in chloroform was slowly introduced into the mixture through a dropping funnel over a period of 15~20 min, and then an additional 75 mL volume of fresh chloroform was added to the boiling mixture. The diazomethane dissolved in chloroform was collected in a receiving flask immersed in an ice-water bath. The diazomethane–chloroform solution was mixed with 1 g of the lignin preparation that had

been pre-dissolved in 25 mL chloroform. After overnight incubation in the dark, the mixture was extracted with aqueous 0.5 M H_2SO_4 5 times to discharge the unreacted diazomethane, and then washed thoroughly with distilled water. After centrifugation at 3000 rpm, the clear chloroform layer after separation from the aqueous solution was dried with anhydrous Na_2SO_4 and then filtered through a 150 mL Büchner funnel (medium fritted disc). The chloroform was removed through rotary evaporation.

4.6 Preparation of Lignin-based Polymeric Materials by Solution Casting

0.6 g methylated lignin with or without other blend components was dissolved in 4.0 mL of dimethyl sulfoxide (DMSO) in a 10 x 20 mm teflon mold. The solution was thoroughly degased under reduced pressure in a vacuum oven at 50°C. The corresponding test piece was produced by solution casting at a suitable temperature. The resulting solid rectangular piece was filed into a dog-bone-shaped specimen, in which the typical distance between shoulders was ~8 mm and the width was ~5 mm.

When monomeric plasticizers (MP) were employed, their contents in the cast material can be estimated according to Eq. 4.6-1. 100% methylated lignin sample was prepared as the control for the blends containing MP produced under the same casting conditions.

$$MP\ \% = \frac{W_{L+MP} - W_L}{W_{L+MP}} \times 100\% \qquad (4.6\text{-}1)$$

W_{L+MP} and W_L are the weights of cast methylated lignin blends with and without MP, respectively. Such an approach has to be used because both low-molecular-weight lignin components and plasticizer(s) may be partially lost during casting

4.7 Tensile Tests

The tensile behavior of the methylated lignin-based blends (in the form of dog-bone-shaped test pieces) were characterized by means of stress-strain curves measured with an Instron model 5542 unit equipped with a 500 N static load cell. Serrated jaws were used to hold all test pieces in place. A crosshead speed of 0.05 mm/min was employed with specimen gauge lengths of ~8 mm. The tensile stress (σ_{max}) and elongation ($\Delta\varepsilon_b$) at fracture were calculated on the basis of initial sample dimensions.

4.8 Differential Scanning Calorimetry (DSC)

DSC measurements were carried out with a TA Q2000 differential scanning calorimeter (TA Instruments) equipped with Refrigerated Cooling System 90. About 8 mg of the sample to be tested was encapsulated in an aluminum Tzero pan and lid using the Tzero Press (TA Instruments) after flushing thoroughly with N_2 in a glove box overnight. The sample was pre-scanned from 40 to 200 °C at 10 °C min^{-1} to remove any trace of moisture and uniformize its thermal history. The second scan was performed from -90 to 200 °C with a cooling rate of 5 °C min^{-1} and a heating rate of 10 °C min^{-1}. The glass

transition temperature was taken to be the half-height point of the glass transition region in the DSC thermogram obtained.

Successive thermal cycles for uncast parent and high molecular weight methylated ball-milled lignins were scanned from 40 to 180 °C and from 40 to 200 °C, respectively. The heating rate was 10 °C min^{-1} and the samples were kept in an isothermal state for 5 min when the temperature reached the upper end.

4.9 X-ray Powder Diffraction

X-ray diffraction scans were obtained with a Bruker AXS D5005 diffractometer operating in a reflection mode using Cu Kα radiation (λ = 1.542 Å) and employing a diffracted beam monochromator. The powdered samples were compressed onto a zero background holder. When the sample rotates at a constant angular velocity, the detector (scintillation counter) rotates at double that angular velocity around the sample so that the diffraction angle is always equal to 2θ, where θ is the angle of the incident beam. The scans were taken within a range of 5° to 36.02° for 2θ with a step size of 0.06° and dwell time of 6 s.

The diffraction patterns from the amorphous MBML-based polymeric materials were fitted to the sums of two Lorentzian functions (Eq. 4.9-1) [Murthy and Minor, 1990]:

$$I(x) = I(0)/(1 + x^2/hwhm^2), \;\; x = 2\theta - 2\theta_k \tag{4.9-1}$$

where I(x) is the scattered intensity at angular distance x from the Bragg angle $2\theta_k$ at the centers of the reflection, 2θ is the scattering angle, and hwhm is the half-width at the half-maximum of the peak. The best fits of the two Lorenztian peaks were determined with respect to an algebraic baseline identified with SigmaPlot 10.0 to be below that for the experimental data; the contributions of the two peaks to the overall diffraction pattern were then taken to be proportional to the Lorenztian-peak areas relative to the experimental baseline.

Chapter 5

Enzymatic Lignin Degradation

5.1 Identification of Lignin-depolymerase Candidates

Mechanistically likely enzymes with true lignin-depolymerase activity were identified by careful comparisons of secretome models among three white-rot fungi, *Phanerochaete chrysosporium*, *Trametes cingulata* and *Heterobasidion annosum,* and one brown-rot fungus, *Postia placenta* (Yi-ru Chen, unpublished). White-rot fungi are capable of degrading a large proportion of lignin in plant cell walls completely and rapidly to carbon dioxide and water. Brown-rot fungi, on the other hand, were thought to be limited to removing aromatic methoxy groups in lignin macromolecules [Agosin *et al.*, 1989]. Recent 2D NMR studies reveal that about 55% of the alkyl aryl β-*O*-4 ether subunits have been cleaved after 16 weeks wood decay of aspen by brown-rot *P. placenta* [Yelle *et al.*, 2011], and the fungus genome encodes no lignin peroxidase, manganese peroxidase or versatile peroxidase [Martinez *et al.*, 2009]. Moreover, the recently sequenced genomes of white-rot *Botryobasidium botryosum* and *Jaapia argillacea* are found to lack high-oxidation potential ligninolytic peroxidases, yet they can degrade woody plant cell walls completely like *P. chrysosporium* does [Riley *et al*, 2014]

Unlike lignolytic peroxidases and laccases, which are poised between depolymerization and polymerization of the lignin substrates, certain flavin-dependent monooxygenases look as though they are mechanistically capable of being lignin-cleaving

enzymes without repolymerizing the degraded products. Flavin-dependent monooxygenases are not among the extracellular *P. chrysosporium* proteins identified in the ***absence*** of lignin substrates in carbon- and nitrogen-limited cultures [Vanden Wymelenberg *et al.*, 2006]. Yet, extracellular salicylate-hydroxylase-like flavin-dependent oxidoreductases are definitely expressed in *P. chrysosporium* cultures containing milled hybrid poplar wood. Indeed, a salicylate-hydroxylase-like enzyme and two other flavin-dependent monooxygenases were identified in extracellular solutions from cultures containing transgenic poplar with very high syringyl lignin contents [Gaskell *et al.*, 2014]. Transgenic poplar with 94% syringyl lignin content is more difficult to biodegrade than the parental poplar line [Skyba *et al.*, 2013]. As a result, two *P. chrysosporium* genes encoding salicylate-hydroxylase-like enzymes were upregulated, but the same effect was not observed for lignin peroxidase and manganese peroxidase genes [Gaskell *et al.*, 2014].

By analogy with the action of salicylate hydroxylase, in the proposed mechanism of Cα-arene cleavage catalyzed by a flavin-dependent monooxygenase (Fig. 5.1), the 4a-hydroperoxyflavin intermediate hydroxylates the C1 on the aromatic ring of an alkyl aryl β-*O*-4 ether subunit, and immediately thereafter a free phenolic component is released.

A commercially available flavin-dependent monooxygenase, salicylate hydroxylase (SH) from *Pseudomonas* sp., was chosen in this research to study its putative depolymerase activity toward water-soluble native polymeric ball-milled lignin fractions. This enzyme catalyzes the hydroxylation and simultaneous decarboxylation of salicylate to catechol with the stoichiometric consumption of NADH and O_2 [Katagiri, *et al.*, 1965]. It also exhibits broad substrate versatility in hydroxylating and cleaving the C–N and C–X

bonds of *ortho*-substituted phenols [Suzuki, *et al.*, 1991]. Pseudosubstrates such as benzoate, *o*-nitrobenzoate, *m*-hydroxybenzoate, *p*-hydroxybenzoate can bind to salicylate hydroxylase and facilitate FAD reduction without being hydroxylated, the consumed O_2 being reduced to H_2O_2 rather than becoming incorporated into the aromatic rings [White-Stevens and Kamin, 1972] [White-Stevens *et al.*, 1972].

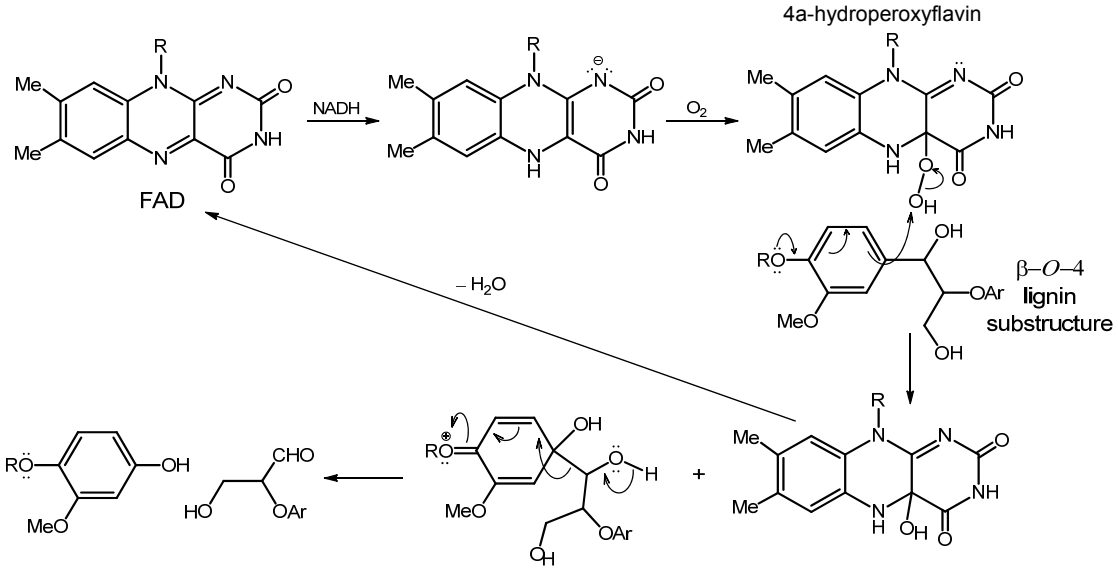

Figure 5.1 Flavin-dependent monooxygenase activity in the cleavage of lignin substructures.

5.2 Characterization of Water-soluble Native Lignin Substrate and Proteins by Rayleigh Light Scattering

Elsewhere during the past 25 years, the substrates most commonly employed in studies of lignin-modifying enzymes have been lignin model dimers (or even monomers) [Higuchi, 2004]. There is the distinct possibility that using such low molecular weight substrates, regardless of their convenience, could be akin to choosing cellobiose in a search

for cellulases. On the other hand, using solid native polymeric lignin preparations instead would invite complications arising from heterogeneous assay conditions. Consequently, soluble high-molecular weight ball-milled lignin preparations were developed for use as lignin depolymerase assay substrates.

5.2.1 Native polymeric lignin fractions

The underivatized paucidisperse ball-milled lignin (BML) fractions were generated by consecutive ultrafiltration of a parent milled-wood lignin preparation through 30,000, 10,000 and 5,000 nominal molecular weight cutoff membranes in aqueous 0.10 M NaOH, and these fractions were named according to the ultrafiltration membranes with which they were retained, e.g. BML 30k, BML 10k, BML 5k. In this part of the work, the freeze-dried fractions were re-dissolved in aqueous carbonate buffer at pH 10.0, and their weight-average molecular weights (M_w) and z-average radii of gyration (R_g) were determined by Rayleigh light scattering measurements. Six sample solutions, with increasing concentrations for each fraction, were weighed separately and then dissolved in 15 mL pH 10.0 aqueous carbonate buffer with concentrations ranging from 0.1 to 0.9 mg/mL.

Interestingly, the differential refractive index increments (dn/dc) are independent of the molecular weight of these BML fractions; actually their values remain approximately the same at 0.2 mL/g in pH 10.0 aqueous carbonate buffer. The measured molecular weights of the same BML fractions vary considerably depending on the pore size of the membrane (0.45 μm and 1.0 μm) through which they are filtered prior to the light scattering measurements (Fig 5.2).

It is obvious that the M_w's and R_g's obtained by means of Rayleigh light scattering at pH 10.0 are attributable to supramacromolecular complexes composed of many individual molecular lignin components. The relationship between R_g and M_w of these complexes can be summarized by means of an empirical polynomial curve fit (Fig. 5.2).

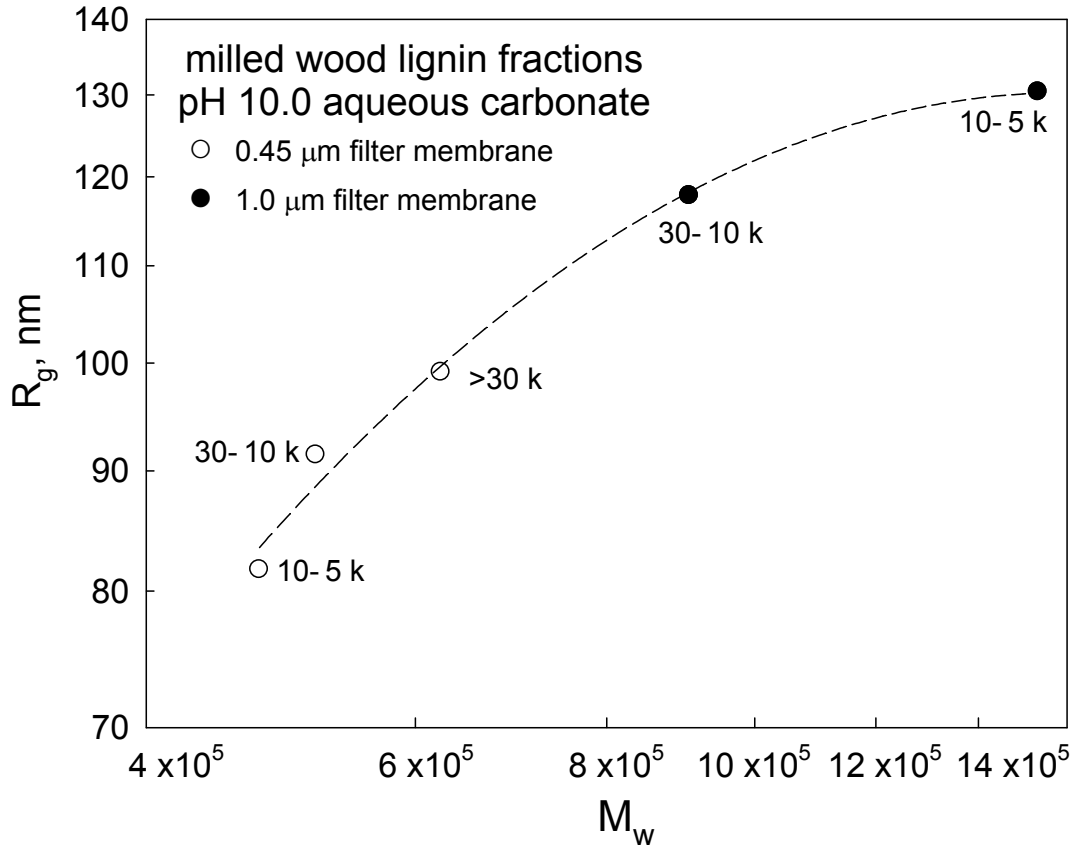

Figure 5.2 Relationship between radius of gyration and weight-average molecular weight for a series of paucidisperse native lignin fractions that have been filtered through membranes with two different pore sizes. Dashed curve represents empirical correlation between the two parameters.

5.2.2 Weight-average molecular weights and radii of gyration of water-soluble lignin substrates and proteins in aqueous solutions

A 10 k ball-milled lignin fraction (BML 10 k) has been employed as the substrate for detecting lignin-depolymerase activity in this research. It remains soluble in aqueous solution at pHs as low as 6.0, and therefore it is preferable as a substrate to any corresponding insoluble native lignin preparation that would call for heterogeneous assay conditions. Four batches of BML 10 k fractions including BML #7 (2.6 g/L), BML #8 (3.4 g/L), BML #9 (5.6 g/L) and BML #10 (3.7g/L), were produced (according to the procedures described in section 4.2) as native polymeric lignin substrates during the period between 2010 and 2012. They were kept in triply-distilled water under N_2, and hence the configurations of the complexes formed under these conditions may well be different from the freeze-dried fractions mentioned in section 5.2. The values of the refractive index increment (dn/dc), M_w and R_g for these BML 10 k fractions, determined through Rayleigh light scattering in different aqueous conditions, are listed in Tables 5.1 and 5.2.

The proteins employed in the following sections, including salicylate hydroxylase from *Pseudomonas* sp. (mw 52 kDa, 47% pure, Sigma-Aldrich), alcohol dehydrogenase from baker's yeast (mw 141-152 kDa, 90% pure, Sigma-Aldrich), xylanase from *Trichoderma viride* (mw 22 kDa, 50% pure, Sigma-Aldrich) and bovine serum albumin (mw 66 kDa, 98% pure, Sigma-Aldrich), were used as received. Their dn/dc's (Table 5.1) were estimated on the basis of the weight concentrations for the crude proteins. However, the molar concentrations presented in the following figures represent ones for the pure proteins (based upon the purities provided by the vendor). The weight-average molecular

weights and radii of gyration of the proteins in different aqueous solutions have been determined by Rayleigh light scattering (Table 5.3). Attempts to determine M_w and R_g of SH alone at pH 6.3 failed due to severe protein aggregation. Such behavior was signified by a rapid continuous increase in the scattered-light intensities with time when a sample solution was passed through the flow cell of the DAWN HELEOS, although the corresponding determination for dn/dc was not affected.

Assuming that they are not affected significantly by pH, the dn/dc values for individual proteins obtained at pH 6.3 (Table 5.1) were adopted in the estimation of weight average dn/dc's of the assay components in ethanol-free aqueous solutions at different pHs. Similarly, for the assay solutions containing 5 mM ethanol, their dn/dc's included the weight average values of those for proteins measured at pH 8.0. Note that NADH (mw 663.34 g/mol) was excluded from the estimation of weight average dn/dc because of its negligible contribution to scattered-light intensities during light scattering measurements.

The sources of the discrepancies between the molecular weights of the enzymes reported by the vendor and those determined by our light scattering measurements (Table 5.3) are not known, but it is clear that substantial association between the protein molecules takes place under the experimental conditions employed in our work. The majority of the dn/dc values estimated for the proteins (Table 5.1) are below the values (0.18 – 0.20 mL/g [Zhao, 2011]) calculated from the amino acid sequences, but here the discrepancies arise from the purities of the proteins reported by the vendor (with the sole exception of ADH).

Table 5.1 Refractive index increments (dn/dc) of 10k water-soluble ball-milled lignin (BML) fractions and salicylate hydroxylase (SH), xylanase (XYL), alcohol dehydrogenase (ADH), bovine serum albumin (BSA) and NADH in aqueous solutions at different pHs with or without 5 mM ethanol.

aqueous solution[a]	Refractive Index Increment, dn/dc (mL/g)							
	BML #7[b]	BML #8	BML #9	BML #10	SH	XYL	ADH	BSA
pH 6.3		0.2264	0.2167	0.1983	0.1497	0.1682		
pH 6.3 with 5 mM EtOH		0.2213						
pH 6.6		0.2201	0.2213					
pH 6.6 with 5 mM EtOH		0.2208						
pH 7.1	0.2154	0.2198	0.2037					
pH 7.1 with 5 mM EtOH	0.2234	0.2241	0.1934		0.1510			
pH 8.0		0.2178						
pH 8.0 with 5 mM EtOH		0.2209			0.1509		0.1556	0.1829
pH 8.6		0.2290						
pH 8.6 with 5 mM EtOH		0.2306						

a. pH 6.3~8.6 aqueous buffers

25 mM phosphate	KH_2PO_4, g/L	$Na_2HPO_4 \cdot H_2O$, g/L
pH 6.3	2.7973	1.1917
pH 6.6	2.3420	2.0880
pH 7.1	1.4386	3.8678
pH 8.0	0.2321	6.2438
Tris sulfate	Tris base, g/L	0.05 M H_2SO_4, mL
pH 8.6	3.6430	82.8500

b. batch number of the corresponding BML 10 k fraction.

The light scattering measurements were carried out as soon as possible after mixing the two solutions containing the enzymes and lignin substrate, respectively. Each data point in the plots of M_w *vs* time and R_g *vs* time (for example, Figs. 5.3 and 5.4) represents one measurement involving 5 sample solutions containing 0.01 ~ 0.06 g/L lignin substrate. Usually, it took 1 h for measuring one concentration, hence ~5 h to acquire the data for each experimental point. The results of the first set of measurements for each series of experimental assays were assigned to 2 h on the overall time scale.

Table 5.2 Weight-average molecular weights and radii of gyration of the 10k water-soluble ball milled lignin (BML) fractions in aqueous solutions at different pHs with and without 5 mM ethanol.

aqueous solution	BML #7		BML #8		BML #9		BML #10	
	M_w g/mol	R_g nm	M_w g/mol	R_g nm	M_w g/mol	R_g nm	M_w g/mol	R_g nm
pH 6.3			781×10^3	97	502×10^3	112	905×10^3	107
pH 6.3 with 5 mM EtOH			888×10^3	100				
pH 6.6			652×10^3	113	331×10^3	94		
pH 6.6 with 5 mM EtOH			655×10^3	102				
pH 7.1	589×10^3	125	592×10^3	115	423×10^3	108		
pH 7.1 with 5 mM EtOH			546×10^3	106	441×10^3	106		
pH 8.0			635×10^3	102				
pH 8.0 with 5 mM EtOH			628×10^3	102				
pH 8.6			504×10^3	112				
pH 8.6 with 5 mM EtOH			409×10^3	107				

Table 5.3 Weight-average molecular weights and radii of gyration of salicylate hydroxylase (SH) and alcohol dehydrogenase (ADH) in aqueous solutions at different pHs with ethanol.

aqueous solution	SH		ADH	
	M_w g/mol	R_g nm	M_w g/mol	R_g nm
pH 8.0 with 5 mM ethanol	228 x 10^3	58	526 x 10^3	60
pH 7.1 with 10 mM ethanol	222 x 10^3	55		

5.3 Early Exploration for Putative Lignin-depolymerase Activities with Alcohol Dehydrogenase as an Auxiliary Enzyme

A system involving two enzymes, salicylate hydroxylase (the putative lignin depolymerase, LD) and alcohol dehydrogenase (ADH) as an auxiliary enzyme interacting through a cofactor, NADH, was devised to look for putative lignin depolymerase activity towards the soluble native polymeric lignin substrate. In this system, ADH was expected to facilitate NADH regeneration from NAD^+ by catalyzing the oxidation of ethanol to acetaldehyde.

In aqueous solution at pH 7.1 containing 5 mM ethanol, M_w increased by 25~50% after ~28 h incubation with 4 μM LD in the presence or absence of ADH and NADH, while in contrast R_g decreased by ~10% (Figs. 5.3 and 5.4). Modulation of other factors failed to reveal conditions where a reduction of M_w takes place. On the other hand, when the concentration of ADH was doubled (from 0.2 to 0.4 μM), the increase in M_w within 28 h was accelerated ~1.5 fold. Actually, ADH itself may interact strongly with lignin

components so as to bring about further association beyond that characteristic of the polymeric substrate under the initial solution conditions: without LD, the M_w increased slowly by 28% over a 52 h incubation period of the lignin substrate with 0.2 μM ADH and 10 μM NADH, while R_g remained stable around 120 nm (Figs. 5.3 and 5.4).

At pH 8.0 with 5 mM ethanol, M_w increased rapidly by ~50% over the first 30 h exposure of the lignin substrate to 4 μM LD in the presence of 0.2 μM ADH and 10 μM NADH, but under these conditions R_g tended not to increase with time (Figs. 5.5 and 5.6). In the absence of LD, M_w for the assay composed of 0.67 g/L substrate (BML #8) and 2 μM ADH increased by ~45% after 28 h with or without NADH. Beyond 28 h, however, the assay solutions containing 2 μM ADH became visibly milky, and the corresponding results for the resulting heterogeneous systems are not included in Figs 5.5 and 5.6.

When 3 μM BSA alone was mixed with the soluble native lignin fraction at pH 8.0 under the same conditions, M_w remained stable around 400,000 g/mol (Fig. 5.7). Actually, such an experimental value of M_w is quite close to the one calculated on the basis of the weight concentrations and the molecular weights of BSA (mw 66 kDa) and lignin substrate (Tables 5.2) assuming that no association occurs between BSA and lignin components. Hereby, the two distinct patterns of M_w varying with time (Figs. 5.5 and 5.7) can be correlated with the magnitude of the interactions between the proteins and lignin macromolecules. Under non-lignolytic conditions, for example, the assay solution composed of 0.67 g/L lignin substrate and 2 μM ADH, the increase in M_w (Fig. 5.5) with time can be viewed as an outcome of further association of the lignin components when they interact strongly with the protein molecules in the system. Meanwhile, R_g (Fig. 5.6)

hardly changes or increases slightly depending on the configurations of participating complexes and the degree of association.

The addition of 3 μM BSA into the assay solution containing 4 μM LD, 0.2 μM ADH and 10 μM NADH seems to reduce the rate at which M_w increases (Fig. 5.7), and more markedly, as shown in Fig. 5.8, it caused an instantaneous 10% reduction in R_g to a value of 92 nm for the z-average radius of gyration (Eq.5.2.2.1, where c_i, M_i and $R_{g,i}$ are the weight concentration, molecular weight and radius of gyration of the individual components, respectively) of all the assay components excluding BSA. This unexpected result suggests that the presence of the BSA may interfere with the interactions of the other two proteins with the lignin components.

$$\left\langle R_g^2 \right\rangle_z = \frac{\sum c_i M_i R_{g,i}^2}{\sum c_i M_i} \qquad (5.2.2.1)$$

5.4 pH-Dependence of Lignin-depolymerase Activity

The pH-dependence of the enzyme exhibiting lignin-depolymerase activity toward the native polymeric lignin fractions has revealed some important aspects about the nature of the transformations observed. The manner in which M_w and R_g of the lignin substrates vary with time in the presence of 0.2 μM ADH and 10 mM NADH over the pH range 6.6~8.6 is particularly instructive (Figs. 5.9 and 5.10). Precipitation occurred after 8 h incubation at pH 6.6, as a result of which the subsequent data points were removed from Figs. 5.9 and 5.10; at pH 7.0, the corresponding phenomenon was observed after 28 h.

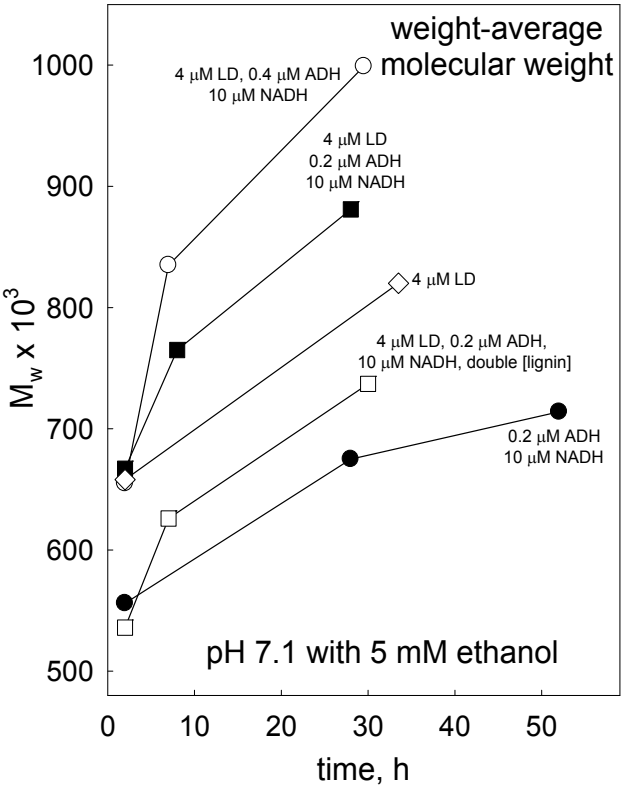

Figure 5.3 Effects of salicylate hydroxylase, the putative lignin depolymerase (LD), on the weight-average molecular weight of the native lignin substrate (0.65 g/L BML #7) with alcohol dehydrogenase (ADH) and NADH in homogeneous aqueous solution at pH 7.1 (25 mM phosphate) containing 5 mM ethanol.

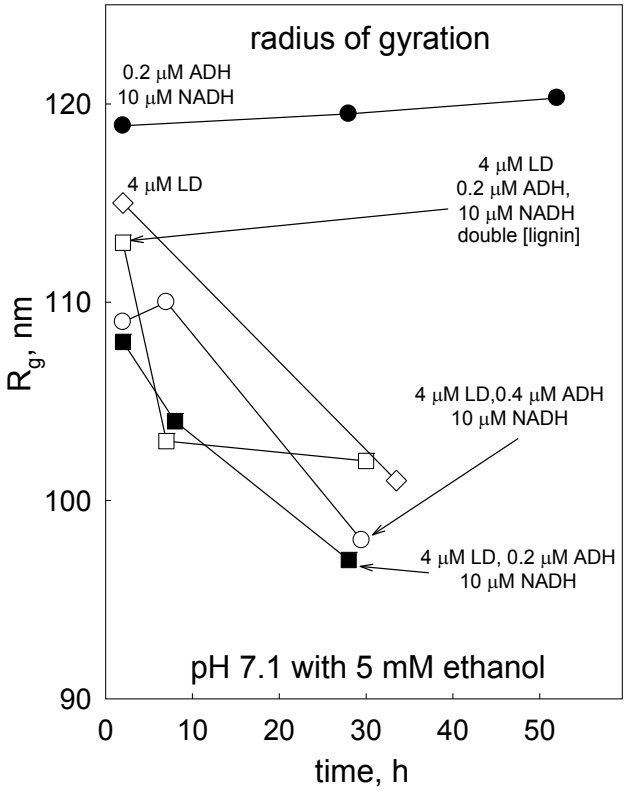

Figure 5.4 Effects of LD on the radius of gyration of native lignin substrate (0.65 g/L BML #7) with ADH and NADH in homogeneous aqueous solution at pH 7.1 (25 mM phosphate) containing 5 mM ethanol.

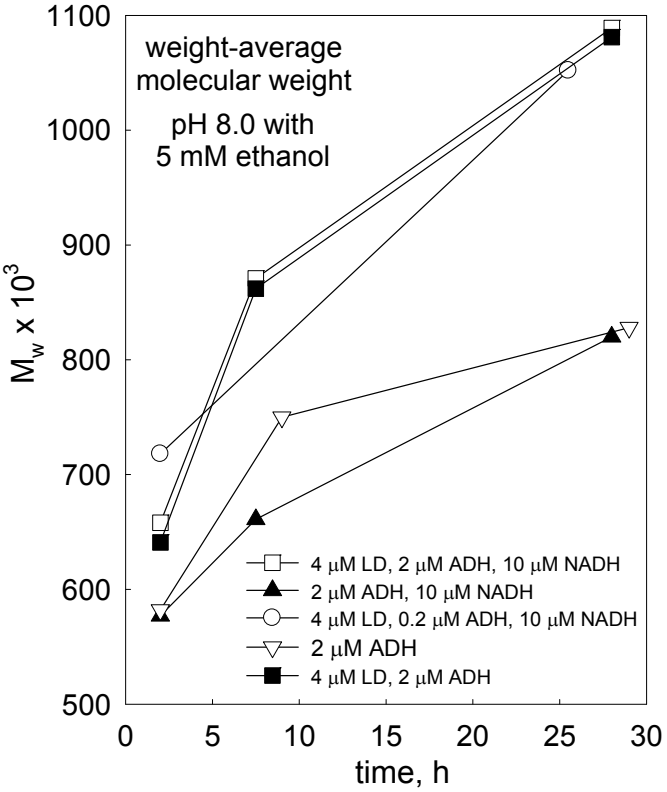

Figure 5.5 Effects of LD and ADH on weight-average molecular weight of the native polymeric lignin substrate (0.67 g/L BML #8) in homogeneous aqueous solution at pH 8.0 (25 mM phosphate) containing 5 mM ethanol.

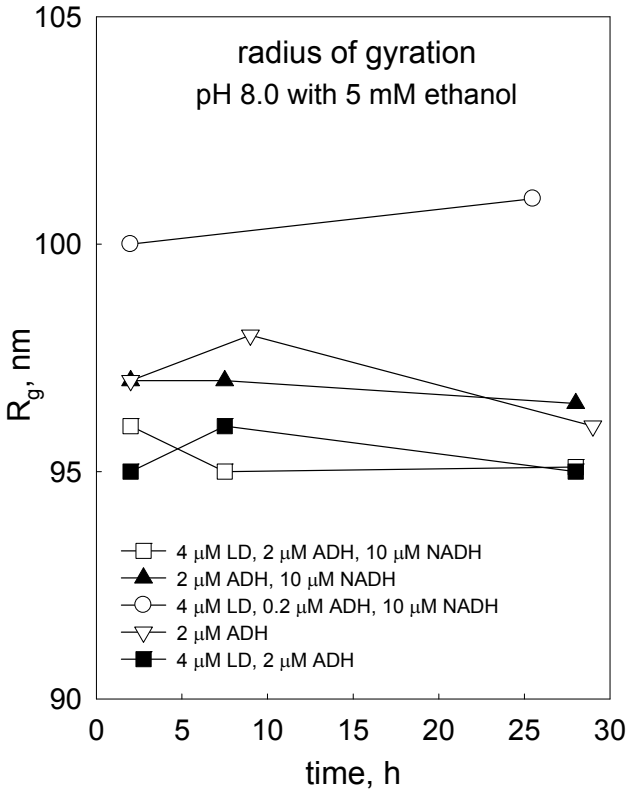

Figure 5.6 Effects of LD and ADH on the radius of gyration of the native polymeric lignin substrate (0.67 g/L BML #8) in homogeneous aqueous solution at pH 8.0 (25 mM phosphate) containing 5 mM ethanol.

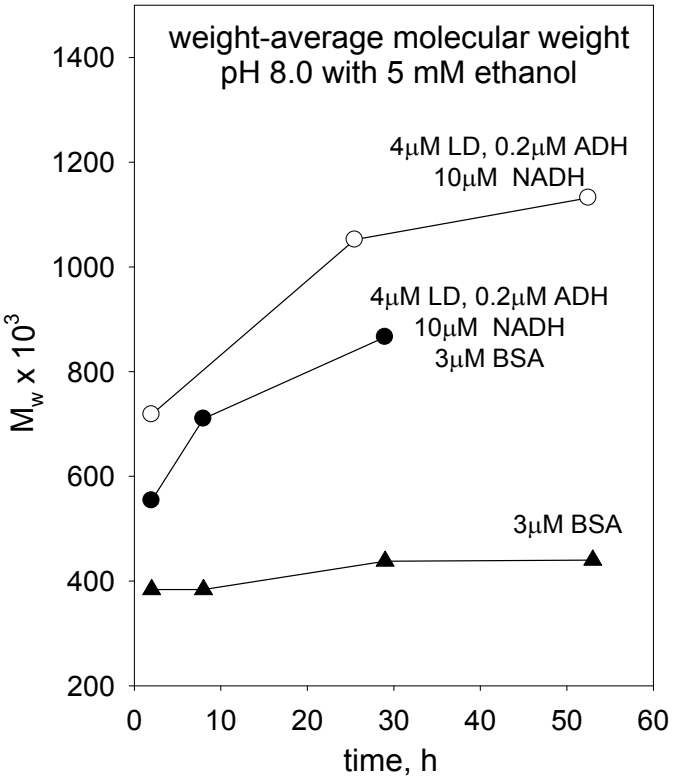

Figure 5.7 Effect of 4 μM LD, 0.2 μM ADH and 10 μM NADH on molecular weight of native polymeric lignin substrate (0.67 g/L BML #8) in presence and absence of 3 μM BSA at pH 8.0.

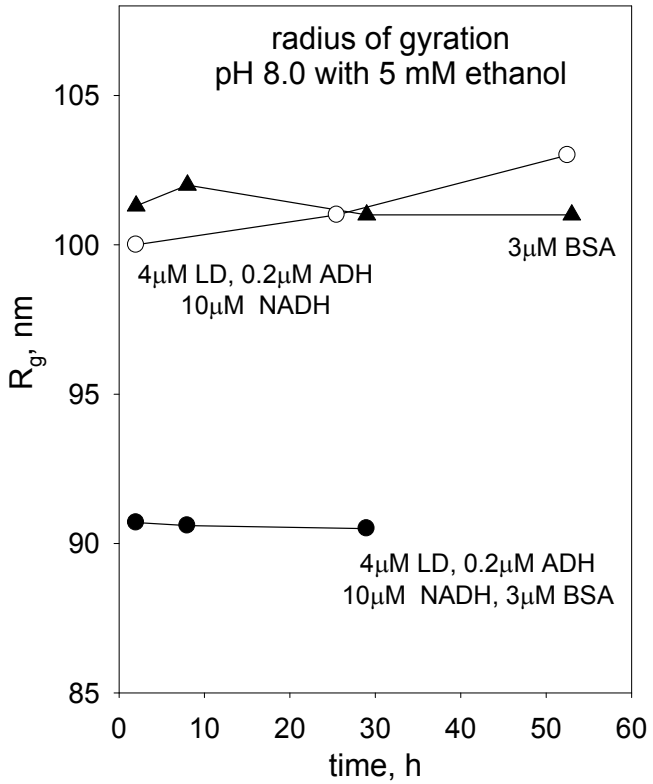

Figure 5.8 Effect of 4 μM LD, 0.2 μM ADH and 10 μM NADH on radius of gyration of native polymeric lignin substrate (0.67 g/L BML #8) in presence and absence of 3 μM BSA at pH 8.0.

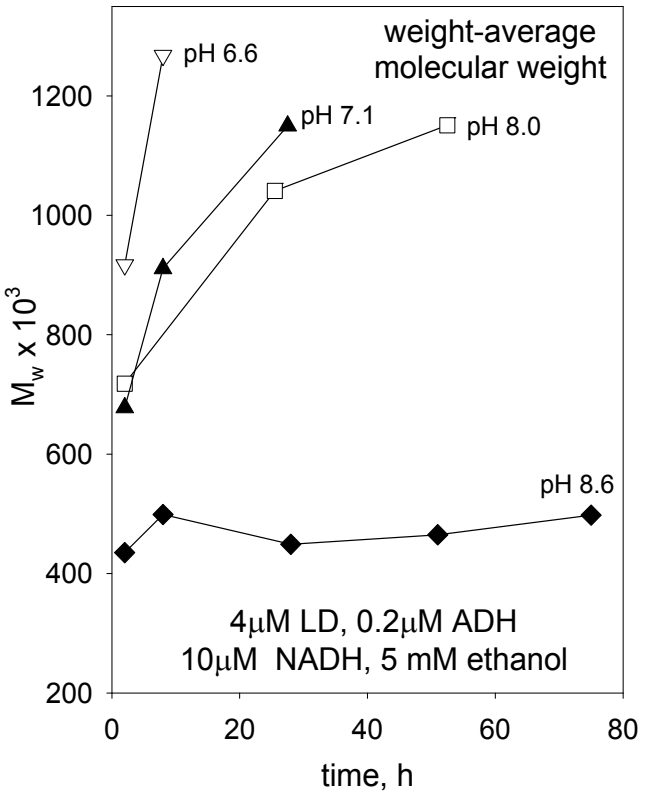

Figure 5.9 Enzyme-catalyzed changes in weight-average molecular weight of native lignin substrate (0.67 g/L BML #8) with 4 μM LD, 0.2 μM ADH and 10 mM NADH in aqueous solutions containing 5 mM ethanol at pHs 6.6 ~ 8.6.

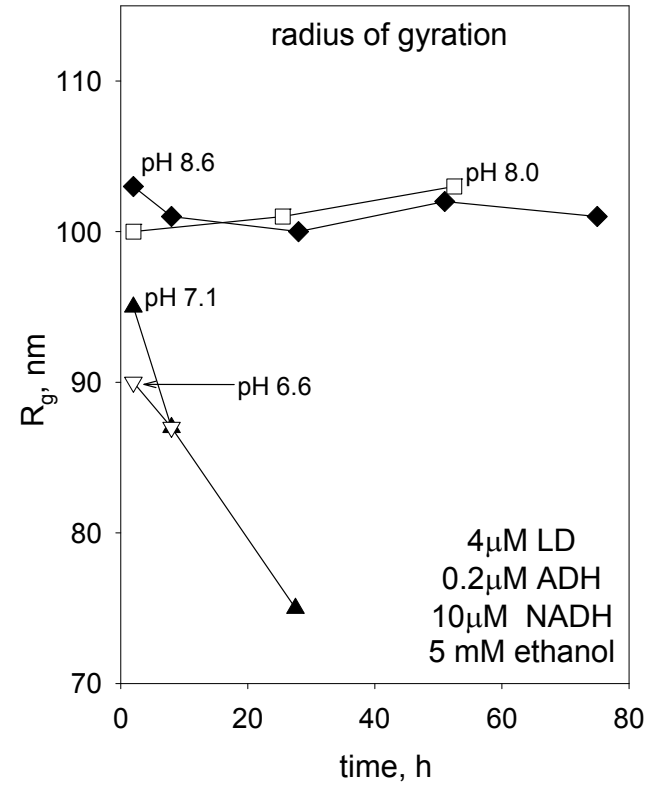

Figure 5.10 Enzyme-catalyzed changes in radius of gyration of native lignin substrate (0.67 g/L BML #8) with 4 μM LD, 0.2 μM ADH and 10 mM NADH in aqueous solutions containing 5 mM ethanol at pHs 6.6 ~ 8.6.

A similar but clearer pattern of the variation in M_w and R_g that occurs as a result of lignin-depolymerase activity towards the lignin substrate has been observed even when ADH is not included in the assay solutions. As shown in Figs. 5.11 and 5.12, the increase in M_w becomes more rapid as the pH of the aqueous solution falls, but on the other hand, a more dramatic rate of reduction in R_g was observed at pH 6.3. In contrast, catalytic lignin cleavage may not be possible after the LD protein molecules bind to the native lignin substrate in aqueous solution at pH 8.6 where neither M_w nor R_g vary appreciably with time.

In principle, the lignin depolymerase has the catalytic capability of covalently modifying a significant proportion of aromatic rings in the lignin components, causing the lignin substrate to undergo cleavage. Careful consideration has been given to the sequence of events necessary for native lignin macromolecules to be degraded by LD around or slightly below neutral pH. Enzyme-catalyzed cleavage may not automatically facilitate extensive release of degraded native lignin components because the latter remain assembled into supramacromolecular complexes containing numerous individual molecules held together through strong noncovalent forces. Therefore, one reasonable working hypothesis is that the decrease in R_g arises from lignin depolymerase-catalyzed cleavage of the lignin macromolecules, while the concomitant increase in M_w is caused by protein-mediated association of the cleaved components into complexes with more compact configurations.

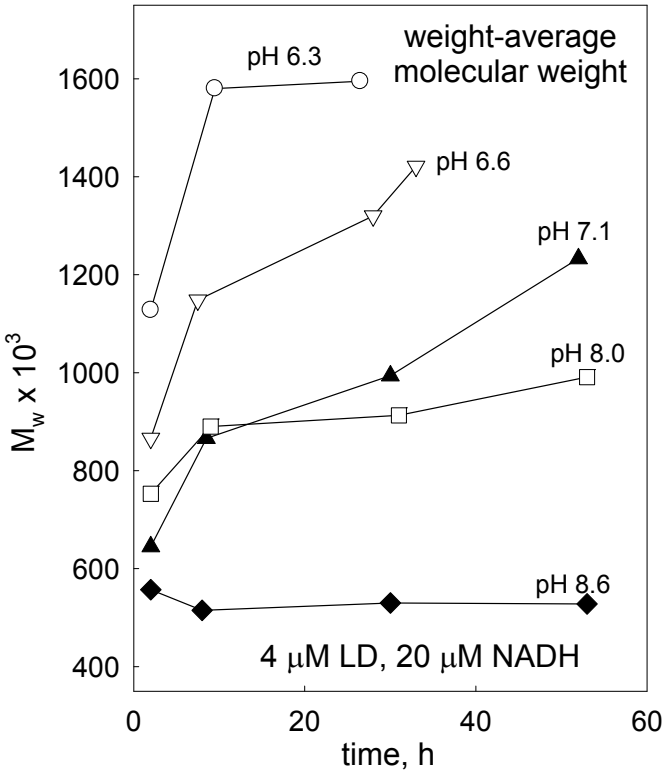

Figure 5.11 4 μM lignin depolymerase (LD) – catalyzed changes in weight-average molecular weight of native polymeric lignin substrate (0.67 g/L BML #8) with 20 μM NADH in aqueous solutions at pHs 6.3 ~ 8.6.

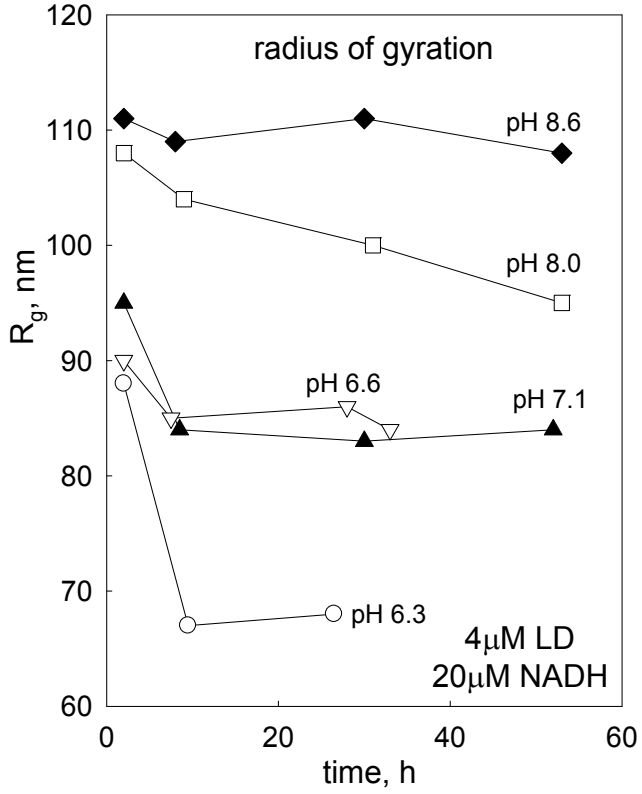

Figure 5.12 4 μM lignin depolymerase (LD) – catalyzed changes in radius of gyration of native polymeric lignin substrate (0.67 g/L BML #8) with 20 μM NADH in aqueous solutions at pHs 6.3 ~ 8.6.

5.5 NADH Requirement for Lignin-depolymerase Activity of Salicylate Hydroxylase

5.5.1 Changes in M_w and R_g of native lignin substrate catalyzed by lignin depolymerase with and without NADH

The results disclosed in sections 5.3 and 5.4 revealed a complication associated with the manner in which the enzyme, salicylate hydroxylase, acts as a lignin depolymerase toward soluble native polymeric lignin substrates. Originally, lignin-depolymerase activity had been investigated in the presence of the reputedly obligatory cofactor NADH that can be turned over by alcohol dehydrogenase, ADH. The effects of NADH on M_w are somewhat complicated at pHs 6.6 and 7.1 in the absence of ADH (Fig. 5.13). However, it has been clearly demonstrated that 20 μM NADH under these conditions does not necessarily accelerate the rate at which the R_g of the lignin substrate is reduced by the action of LD at pHs 6.6 and 7.1 (Fig. 5.14), and a similar effect (Figs. 5.15 and 5.16) was fully confirmed at pH 6.3 where the initial rate of reduction in R_g of the same substrate is 5 times faster than at pH 6.6 (Fig. 5.16). The question naturally arose as to whether, in this context, the polymeric lignin substrate can replace the cofactor NADH in its reductive effect on LD (Fig. 5.1).

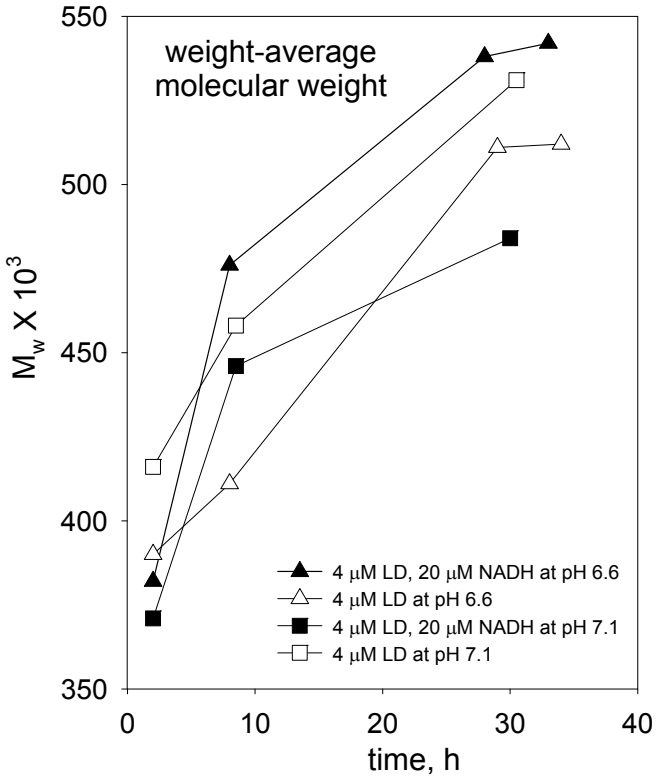

Figure 5.13 Effect of 4 μM LD on weight-average molecular weight of native polymeric lignin substrate (0.93 g/L BML #9) in presence and absence of 20 μM NADH at pHs 6.6 and 7.1 (25 mM phosphate).

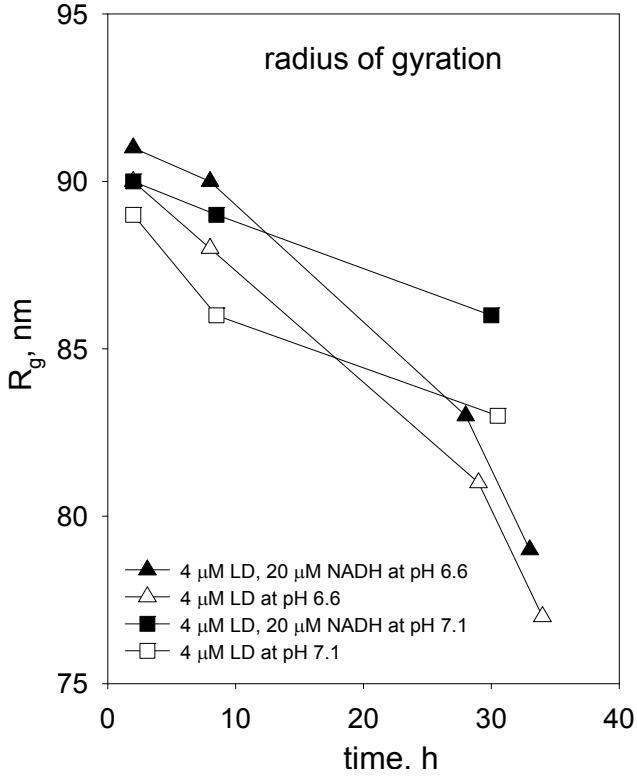

Figure 5.14 Effect of 4 μM LD on radius of gyration of native polymeric lignin substrate (0.93 g/L BML #9) in presence and absence of 20 μM NADH at pHs 6.6 and 7.1 (25 mM phosphate).

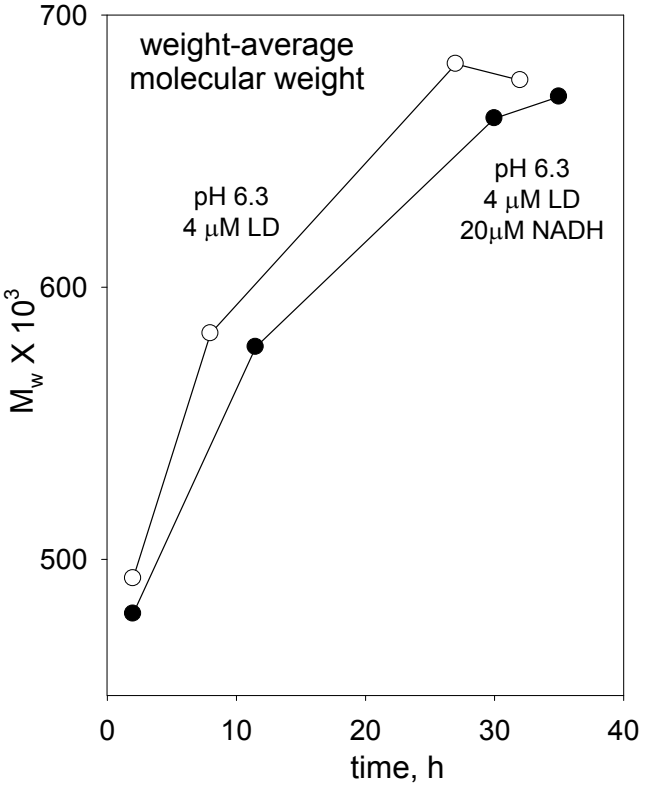

Figure 5.15 Effect of 4 μM LD on weight-average molecular weight of native polymeric lignin substrate (0.93 g/L BML #9) in presence and absence of 20 μM NADH at pH 6.3 (25 mM phosphate).

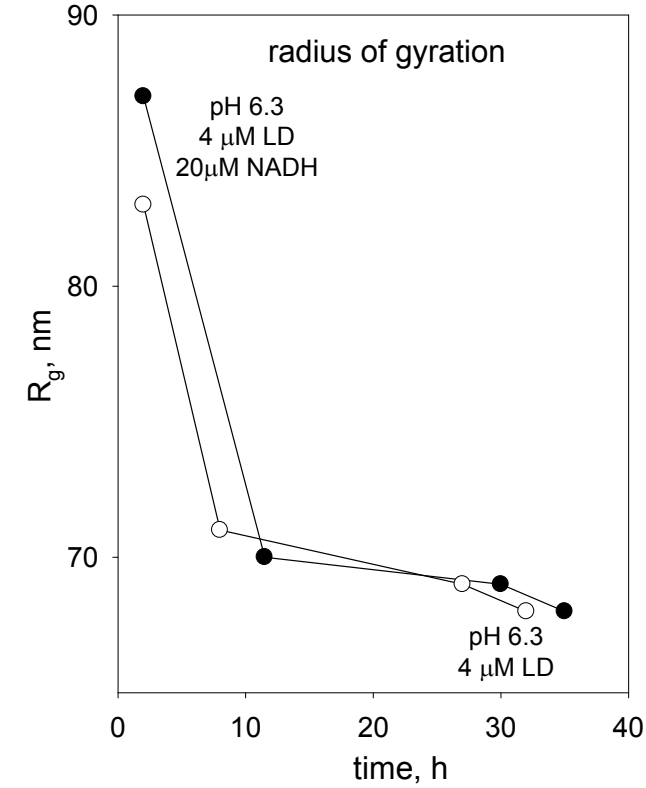

Figure 5.16 Effect of 4 μM LD on radius of gyration of native polymeric lignin substrate (0.93 g/L BML #9) in presence and absence of 20 μM NADH at pH 6.3 (25 mM phosphate).

5.5.2 Reductive capacity of native lignin substrate in the salicylate hydroxylase-catalyzed decarboxylation of salicylate

It must be borne in mind that the flavin-dependent monooxygenase employed here as a lignin depolymerase exhibits pronounced salicylate hydroxylase activity in decarboxylating salicylate. Actually, the reductive capability of 0.14 g/L lignin is sufficient to confer salicylate hydroxylase activity on the lignin depolymerase with respect to the monomeric substrate, salicylate, at pH 8.0. As shown in Fig. 5.17, the evolving differences between the UV-visible spectra of the lignin-containing solutions, as the monomeric substrate is being transformed by the enzyme, are identical to the UV-visible spectrum of salicylate in terms of the peak maximum and peak width. Indeed, the overall change in the difference spectrum of Fig. 5.17 is equivalent to the transformation of 98% of the monomeric substrate; no spectral change was observed in the absence of the lignin before pre-emptive precipitation began to appear around 240 h after initiating the reference assay.

The salicylate hydroxylase-catalyzed decarboxylation kinetics of salicylate in the presence of native polymeric lignin are illustrated at pH 8.0 in Fig. 5.18. The rate of 86 μM salicylate depletion deviates only to a small extent from zero-order kinetics, and sharply changes to zero when substrate transformation reaches completion. The aromatic salicylate-hydroxylase catalyzed reaction product, catechol, can undergo further changes alone in solution (Fig. 5.19) through a process that is approximated reasonably well by first-order kinetics (Fig. 5.20), and these transformation rates are affected only to very small extents by salicylate hydroxylase and lignin. The consequences of any further

reaction(s) have not been detected in the UV-spectral changes that characterize the salicylate-hydroxylase catalyzed transformation of salicylate in the first place.

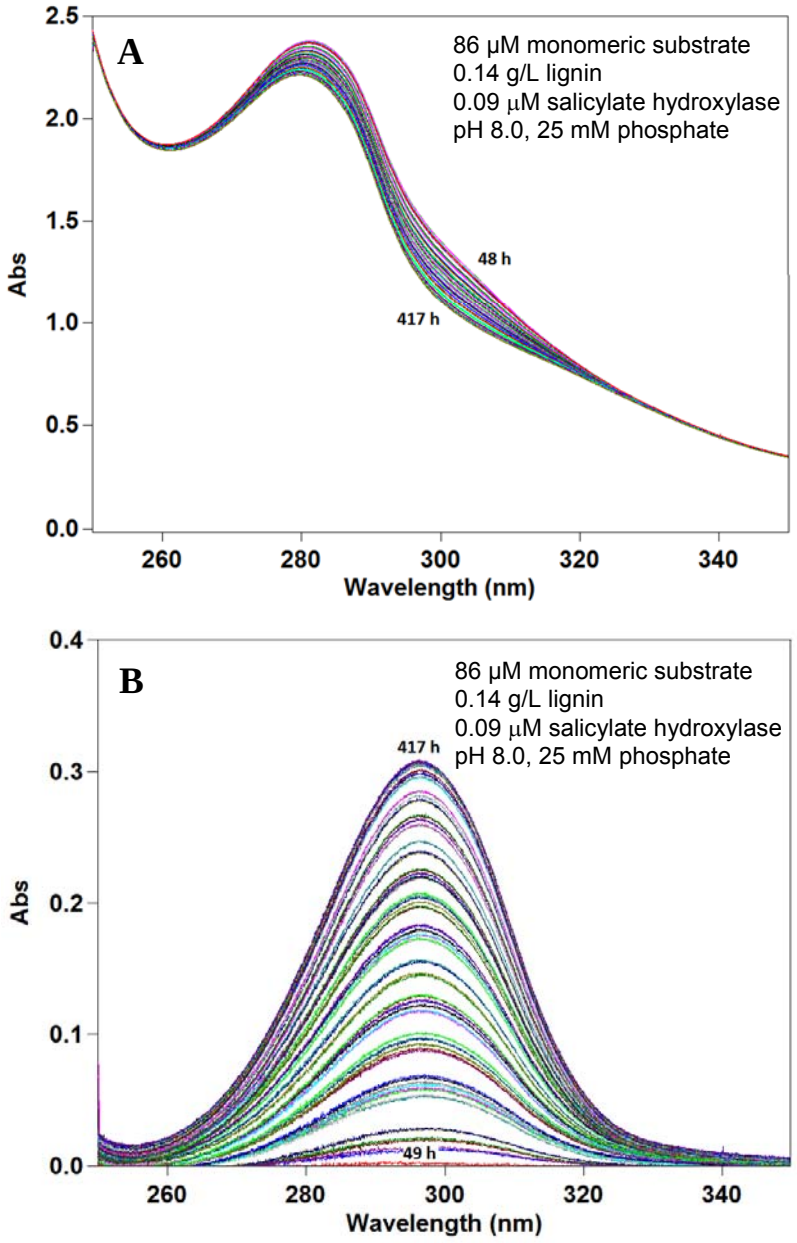

Figure 5.17 UV-visible spectral changes (**A**) and difference spectra (**B**) resulting from salicylate hydroxylase–catalyzed transformation of natural monomeric substrate (salicylate) without NADH in the presence of native polymeric lignin (BML #9) at pH 8.0.

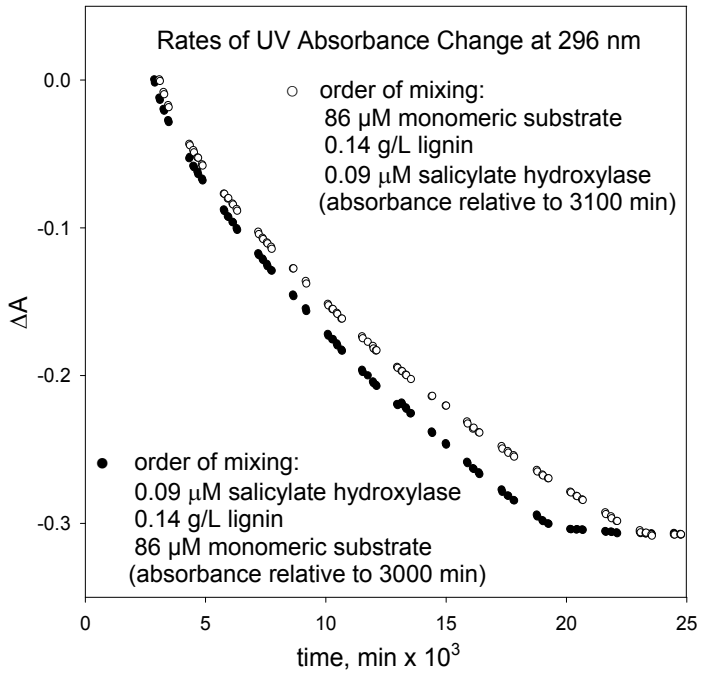

Figure 5.18 Kinetics of salicylate hydroxylase–catalyzed transformation of salicylate (the natural monomeric substrate) in the presence of native polymeric lignin (BML #9) at pH 8.0 (25 mM phosphate).

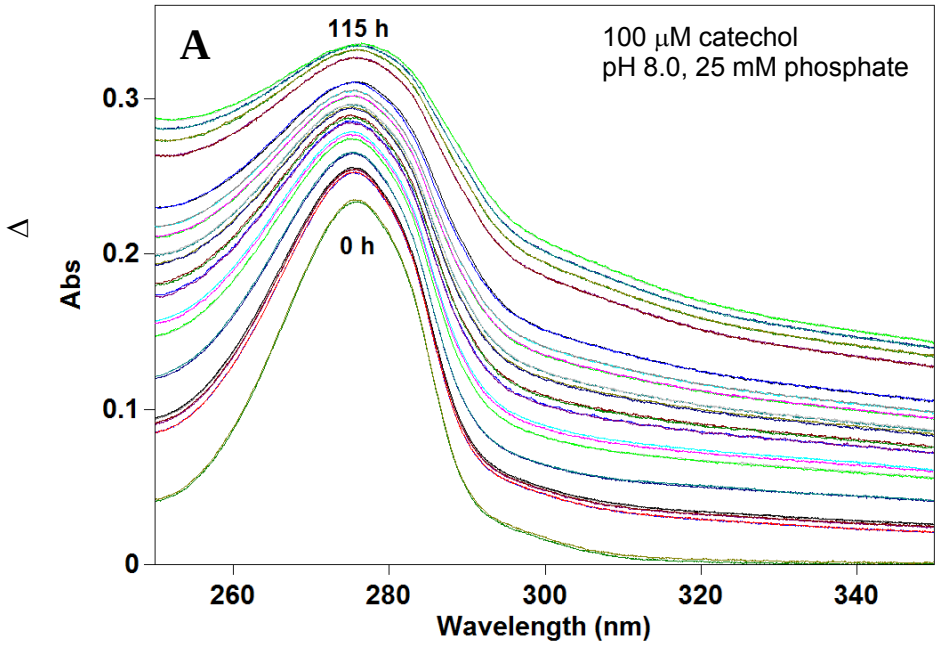

Figure 5.19 (**A**) UV-visible changes of catechol alone in aqueous pH 8.0 (25 mM phosphate).

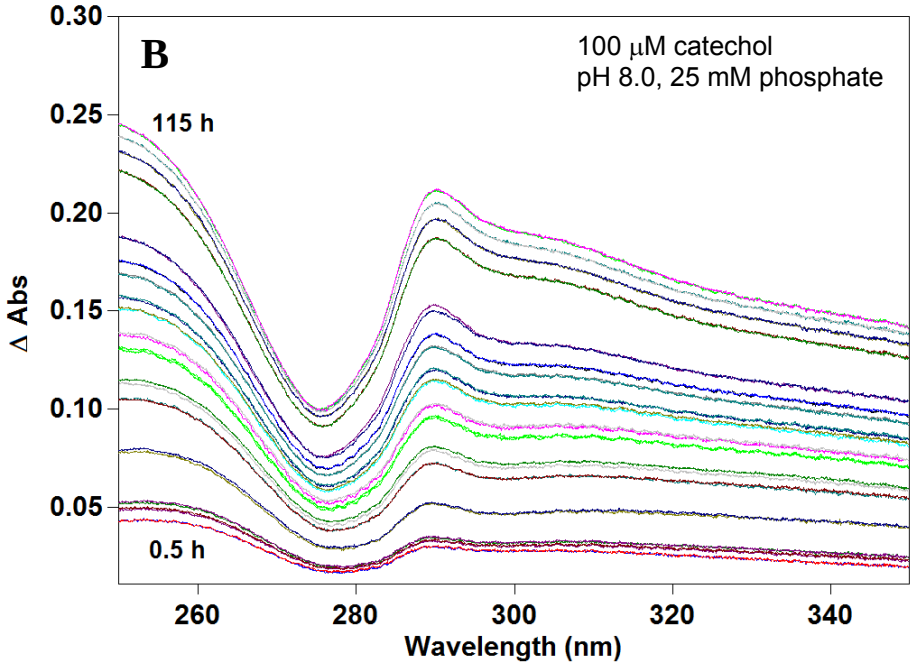

Figure 5.19 (**B**) UV-visible difference spectra of catechol alone in aqueous pH 8.0 (25 mM phosphate).

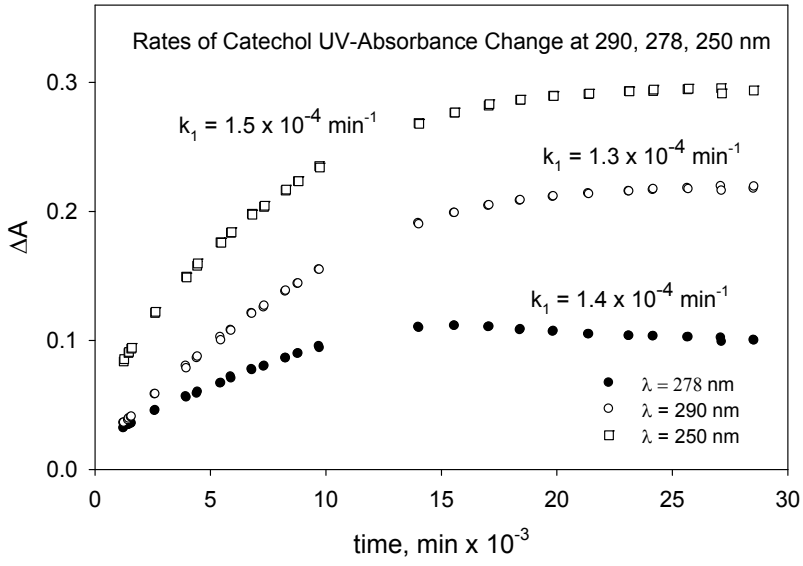

Figure 5.20 The transformation kinetics of 110 μM catechol in the presence of 0.09 μM salicylate hydroxylase at pH 8.0 (25 mM phosphate) monitored at three different wavelengths (λ).

5.6 Lignin–lignin and Lignin–protein Interactions during Lignin Depolymerization

As described previously, the impact of lignin-depolymerase activity on the soluble macromolecular native lignin substrate adopted as a standard in these studies is two-fold: a decrease in R_g is routinely accompanied by an increase in M_w. The effect is enhanced as the pH is reduced from 8.6 to 6.3.

Macromolecular lignin complexes tend to undergo dissociation in aqueous alkaline solutions. Hence, such conditions may be expected to provide better estimates of the molecular weight distributions for the enzymatically cleaved lignin samples. In preparation for studies along these lines, incubation of the polymeric native lignin fractions was carried out in aqueous 0.10 M NaOH in the presence and absence of the ADH employed in earlier studies to bring about turnover of NAD^+ if and when necessary (Fig. 5.21). Before incubation in 0.1 M NaOH, the polymeric native lignin fractions were pre-incubated with and without ADH in pH 8.0 (25 mM phosphate) aqueous solution for 48 h. The changes in the molecular weight distributions were significant during a 288 h incubation period in 0.10 M NaOH solution. The monotonic depletion of highest molecular weight species is consistent with the observations in section 5.3 that ADH promotes further association among lignin components (Fig. 5.21a) although the overall changes in the molecular weight distribution arise from a combination of effects. Comparison of the outcomes from corresponding aqueous alkaline solutions containing the substrate and protein separately (Figs. 5.21b and 5.22) reveal that changes in both the protein and the lignin contribute to the variations observed in the overall molecular weight distributions.

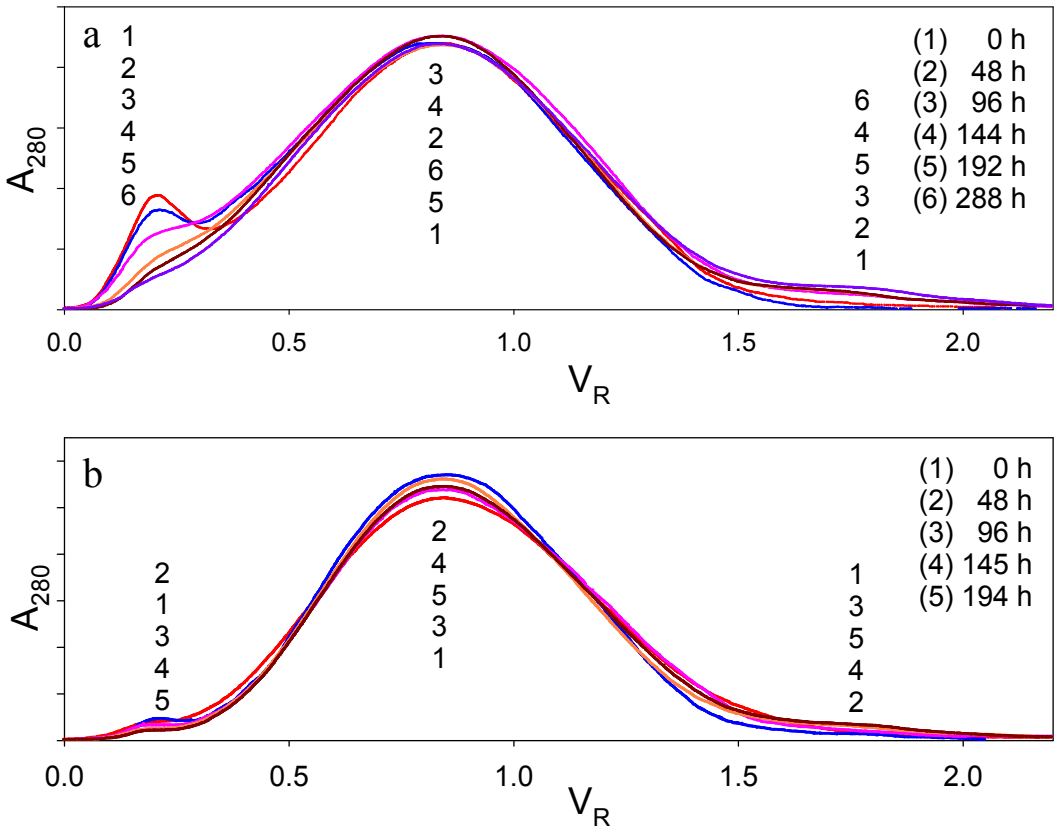

Figure 5.21 Incubation of polymeric native lignin fraction (BML #9) at 0.37 g/L in aqueous 0.10 M NaOH in the (a) presence and (b) absence of 0.8 μM ADH. The substrate was pre-incubated at 0.93 g/L in the presence and absence, respectively, of 2.0 μM ADH in 25 mM phosphate at pH 8.0 for 48 h. (Sephadex G100/aqueous 0.10M NaOH elution profiles.)

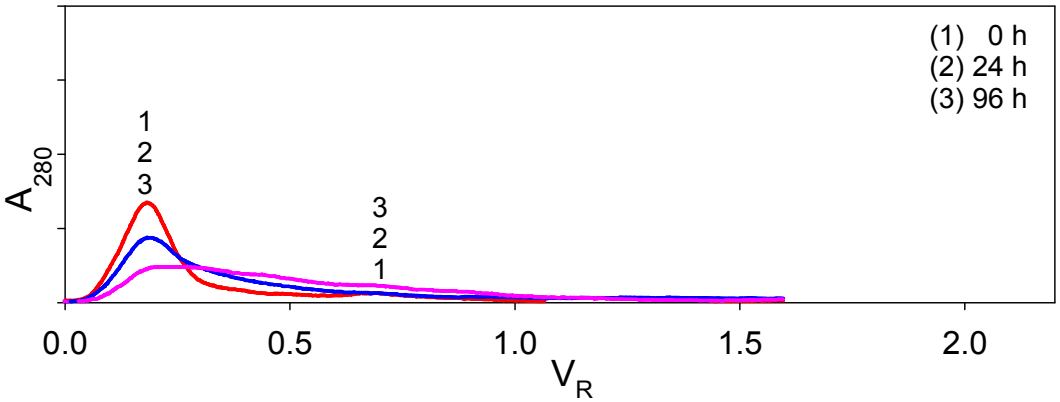

Figure 5.22 Incubation of 1.8 μM ADH alone in aqueous 0.10 M NaOH in absence of lignin substrate. (Sephadex G100/aqueous 0.10M NaOH elution profiles.)

In exploiting the propensity of macromolecular lignin complexes to dissociate in aqueous alkaline solution, the native polymeric substrate was pre-incubated for 40 h at pH 6.3 in the presence of the salicylate hydroxylase (SH) with lignin depolymerase activity. The changes in the molecular weight distribution of the resulting product mixture during subsequent incubation in aqueous 0.10 M NaOH are shown in Fig. 5.23a. At the very beginning, there were considerably more of the highest molecular weight species evident in the Sephadex G100/aqueous 0.10 M NaOH elution profile than when SH was entirely absent (Fig. 5.23b). This presumably arises from quite strong interactions on the part of lignin components with the protein. Indeed, a marked increase in the proportion of high molecular weight species initially occurred within the first 26 h incubation in 0.1 M NaOH as a result of interactions between (partially cleaved) lignin components that, under alkaline conditions, adopt more extended conformations which exhibit greater compatibility with association. Thereafter, the high molecular weight entities were systematically depleted owing to resolute dissociation on the part of the macromolecular lignin complexes. The rate of the latter process is thought to be controlled by conformational changes in the individual components that preclude their (re)association [Li and Sarkanen, 1999].

It is the consecutive increase and decrease in the proportions of high molecular weight species under aqueous alkaline conditions that is prototypical of the overall impact of lignin depolymerase activity on the native lignin substrate. Without exposure to lignin depolymerase activity, the corresponding change in the molecular weight distribution of the polymeric substrate was very small (Fig. 5.23b). Moreover, during incubation in

aqueous 0.10 M NaOH without the native lignin substrate, there was very little change in the molecular weight distribution of the salicylate hydroxylase preparation (Fig. 5.24).

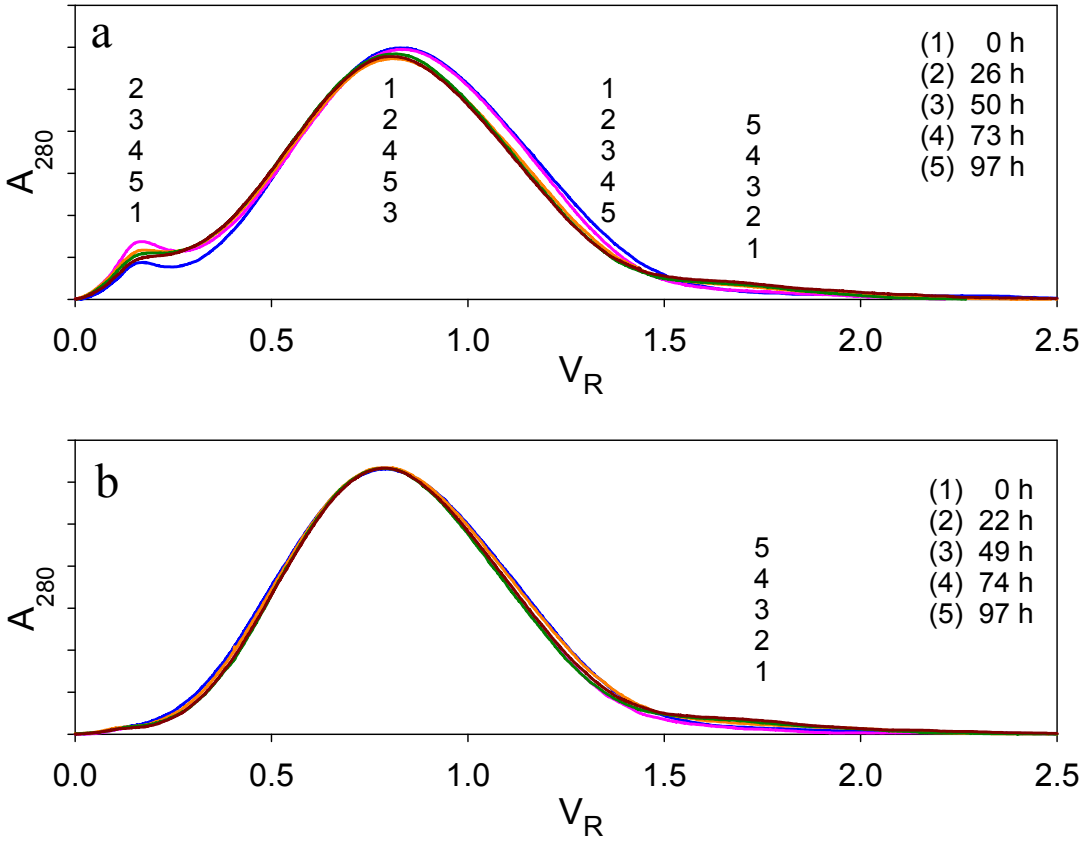

Figure 5.23 Incubation of polymeric native lignin fraction (BML #9) in aqueous 0.10 M NaOH in the (a) presence and (b) absence of the salicylate hydroxylase with lignin depolymerase activity. Substrate has been pre-incubated for 40 h at 0.93 g/L in presence and absence of 4 μM protein in 25 mM phosphate at pH 6.3. (Sephadex G100/aqueous 0.10M NaOH elution profiles.)

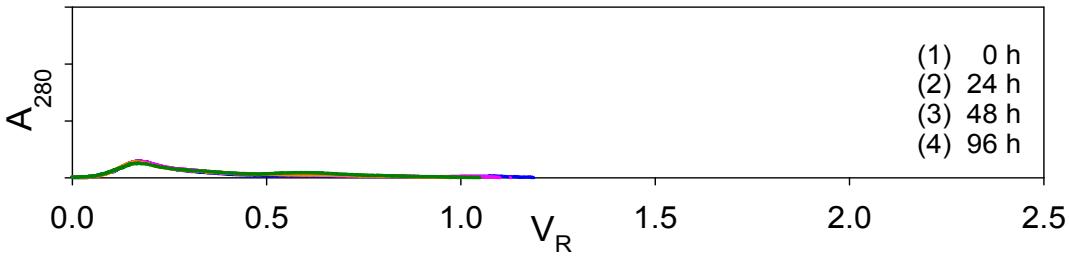

Figure 5.24 Incubation of enzyme with lignin depolymerase activity in aqueous 0.10 M NaOH under same conditions as in Fig. 5.23 (a) but without preincubation and without lignin substrate. (Sephadex G100/aqueous 0.10M NaOH elution profiles.)

Two requirements must be met for the enzyme-catalyzed depolymerization of macromolecular lignin substrates to be successful. Covalent bonds linking successive monomer residues within the polymer chains must be cleaved, and the powerful noncovalent forces between the aromatic rings in interacting lignin macromolecules must be overcome. It might be anticipated that incubation of enzymatically depolymerized macromolecular lignin preparations in aqueous alkaline solution would lead to rapid dissociation of the degraded components from the polymer chains with which they continue to interact. This possibility was investigated during the incubation of ball-milled lignin fractions at pHs 6.3 and 6.6 in the presence of salicylate hydroxylase that exhibits lignin-depolymerase activity under both solution conditions, and in both cases the assay solutions were subjected to SEC examination without any further incubation in 0.10 M NaOH (Fig. 5.25 and 5.26, respectively). The unexpected substantial increase in the proportions of the highest molecular weight species at pHs 6.3 and 6.6 suggested that an entirely different approach had to be developed to overcome the noncovalent interactions between the lignin components and enzyme that acts as lignin depolymerase.

In summary, the enzyme-catalyzed degradation of lignin macromolecules requires two steps to reach fulfillment. Macromolecular lignin chains are first cleaved by a lignin depolymerase so that R_g of the polymeric substrate falls rapidly. However, the individual lignin components (whether degraded or not) cannot automatically dissociate from one another in solution because of the strong intermolecular interactions between them, which may be mediated by the lignin depolymerase. Actually, further association between the cleaved lower-molecular-weight components leads to a possible increase in M_w of the

substrate (Fig. 5.27 profiles a1 and a2). Such effects can be annulled by a suitable protein like xylanase acting in an auxiliary capacity (Fig. 5.27 profiles d1, d2 and d3) that competes with the interactions of the lignin depolymerase with the degraded lignin components.

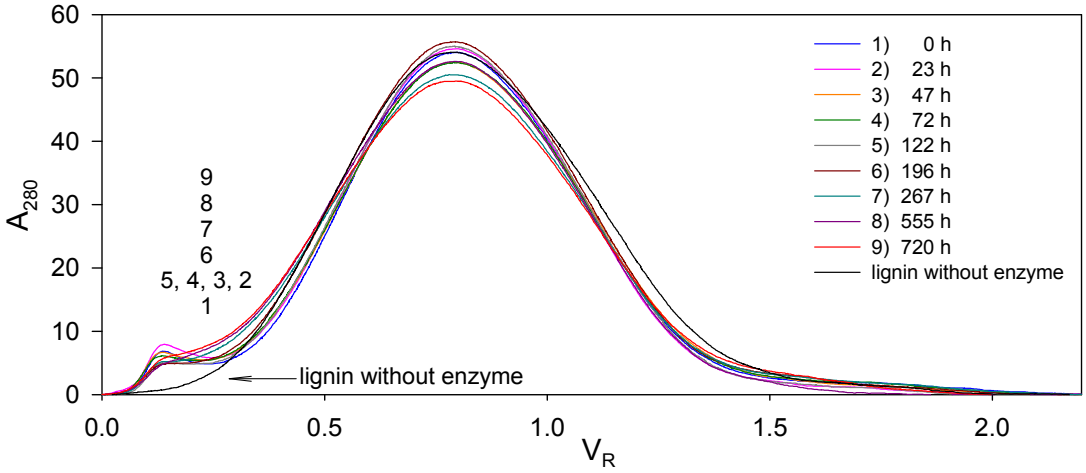

Figure 5.25 Incubation of 0.93 g/L native polymeric lignin fraction (BML #9) in 25 mM phosphate at pH 6.3 in the presence of 4 µM salicylate hydroxylase with lignin depolymerase activity. Sephadex G100/aqueous 0.10M NaOH elution profiles for components present in solution after times indicated.

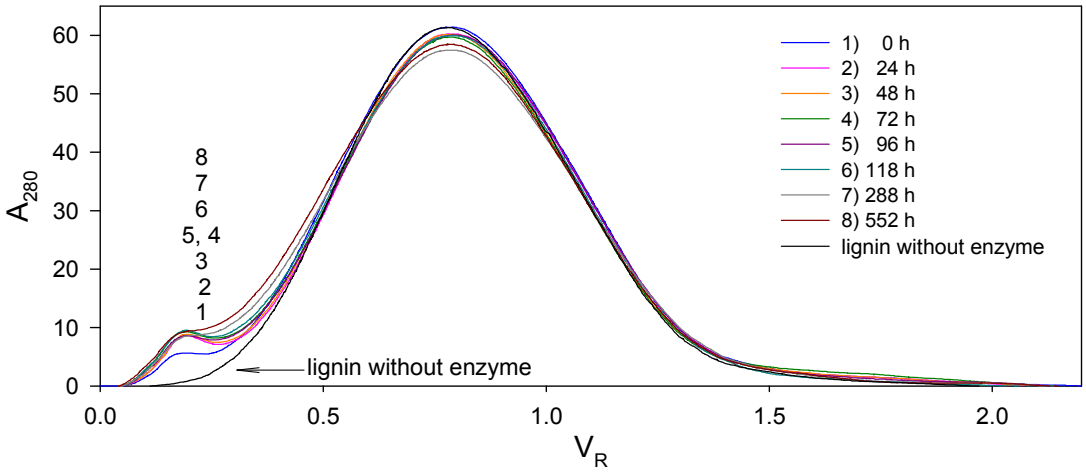

Figure 5.26 Incubation of 0.93 g/L native polymeric lignin fraction (BML #9) in 25 mM phosphate at pH 6.6 in the presence of 4 µM salicylate hydroxylase with lignin depolymerase activity. Sephadex G100/aqueous 0.10M NaOH elution profiles for components present in solution after times indicated.

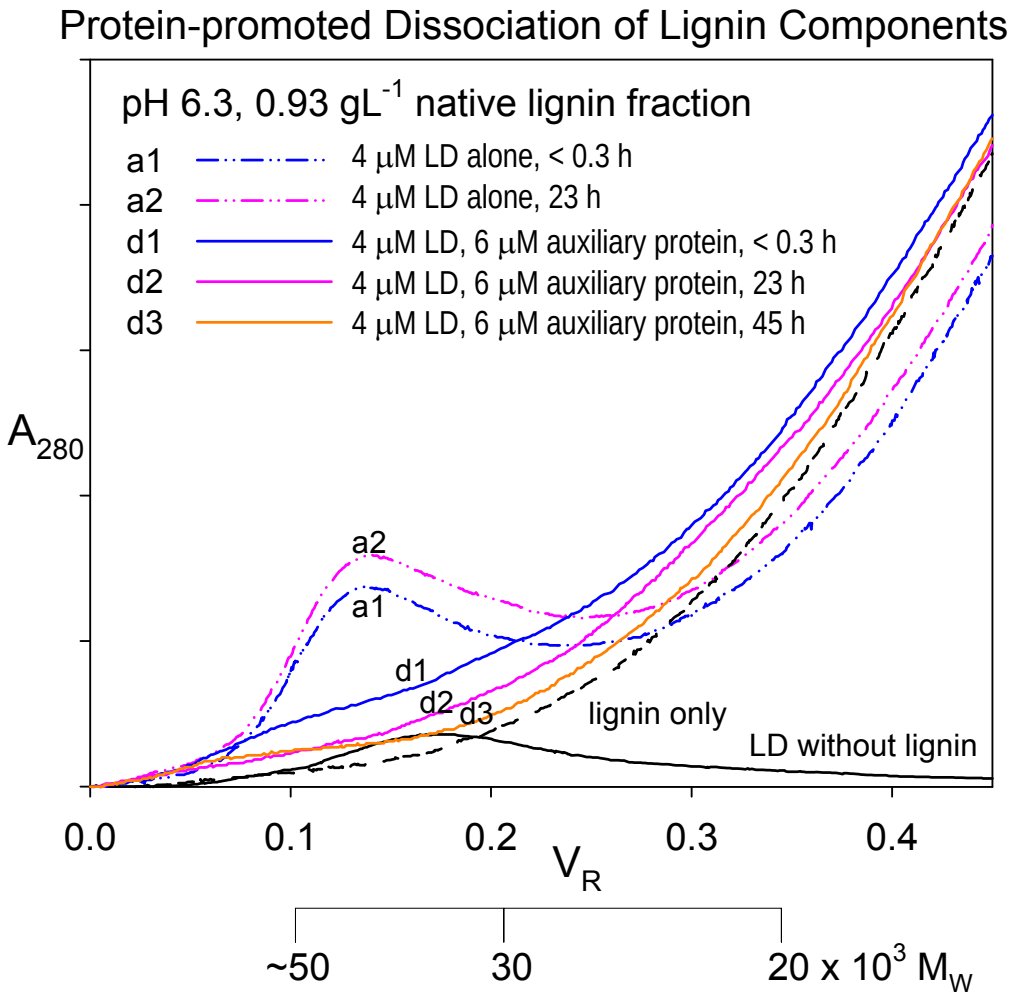

Figure 5.27 Interactions of native polymeric lignin fraction (BML #9) with LD (salicylate hydroxylase) in absence and presence of xylanase acting in an auxiliary capacity at pH 6.3 in 25 mM phosphate. (0.0–0.45 V_R segments of Sephadex G100/aqueous 0.10 M NaOH profiles after incubation times indicated.)

5.7 Lignin–depolymerase Activity with Xylanase as an Auxiliary Protein

The manner in which an auxiliary protein like xylanase can overcome the effects of LD–lignin noncovalent interactions has been clearly demonstrated in Fig. 5.27 by comparing the relevant molecular weight distributions under aqueous alkaline conditions.

More insights about the changes in M_w and R_g of the partially degraded or intact substrates in the presence of xylanase have been revealed through systematic Rayleigh light scattering studies.

The contribution of 6 μM xylanase to the scattered light intensities from the assay solutions is less than 1% of the total; therefore M_w of the lignin substrate in the assay solution containing 6 μM xylanase (Fig. 5.28) can be estimated using dn/dc of lignin alone (BML #9, Table 5.1) in aqueous 25 mM phosphate at pH 6.3.

It is important to remember that xylanase alone has no discernible effect on M_w and R_g of the native lignin substrate at pH 6.3 (Fig. 5.28 and 5.29). Indeed, this lignin substrate contains no detectable monosaccharide residues as a result of the fractionation procedure used in its preparation. Thus xylanase acts in an auxiliary capacity by competing with the interactions of the partially degraded lignin components toward LD (salicylate hydroxylase).

When the native lignin substrate was treated with 4 μM LD in the presence of 6 μM xylanase at pH 6.3, M_w increased to a small extent in the presence of 20 μM NADH, but a rather slow decrease of M_w with time was observed when NADH was absent (Fig. 5.30); on the other hand, R_g fell by ~15 % within 35 h whether or not NADH was present (Fig. 5.31). The impact of xylanase is revealed in terms of its marked inhibitory effect on the increase in M_w and decrease in R_g of the lignin substrate that normally accompanies the action of SH in its capacity as LD (Figs. 5.30 and 5.31).

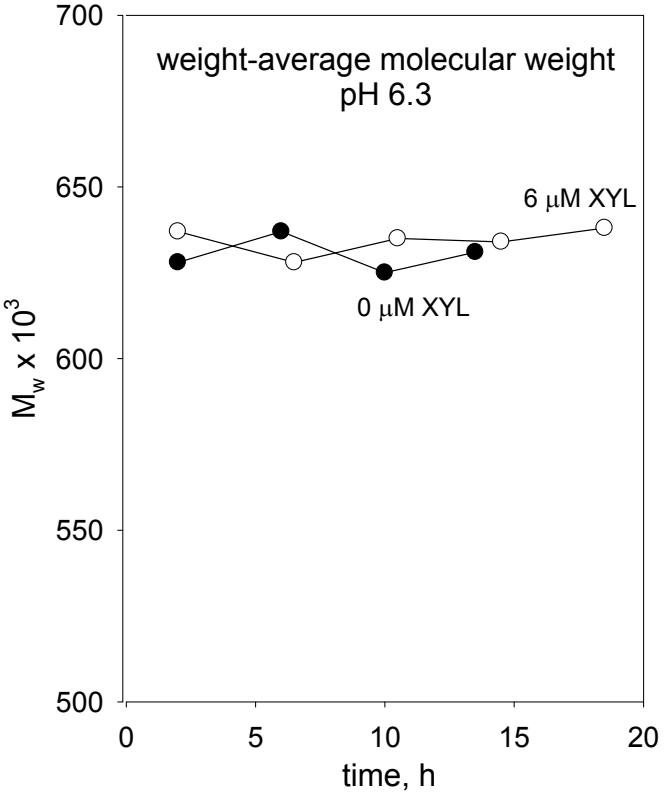

Figure 5.28 Effect of xylanase (XYL) alone on weight-average molecular weight of soluble native polymeric lignin preparation (BML #9, 0.93 g/L) at pH 6.3 (25 mM phosphate).

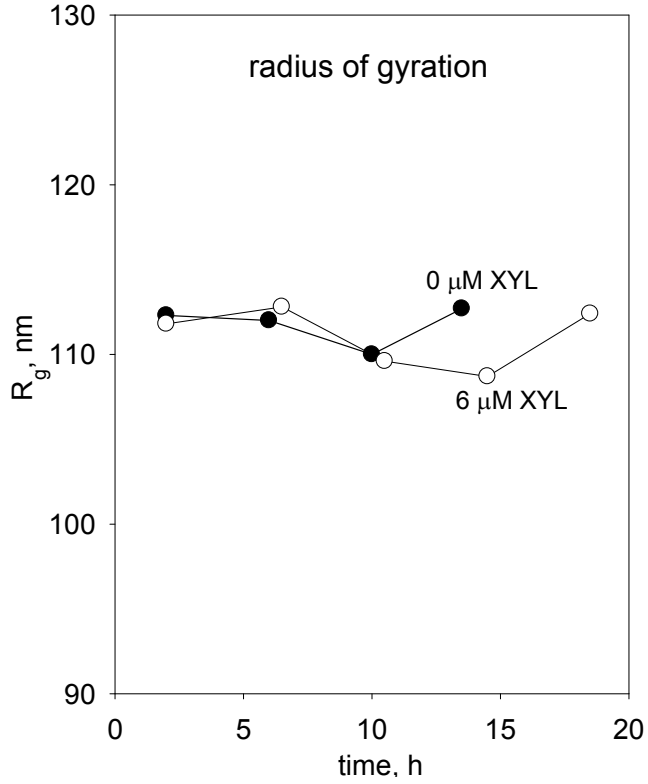

Figure 5.29 Effect of xylanase (XYL) alone on radius of gyration of soluble native polymeric lignin preparation (BML #9, 0.93 g/L) at pH 6.3 (25 mM phosphate).

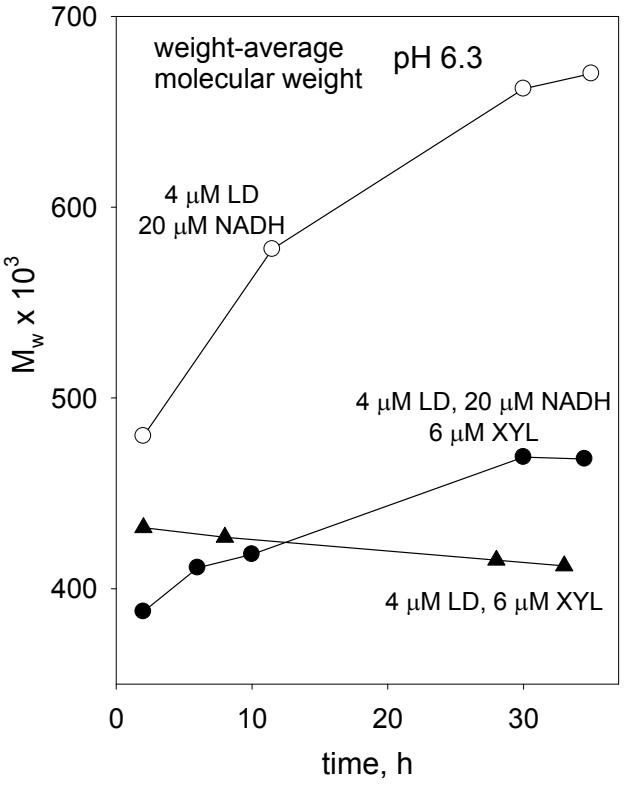

Figure 5.30 Change in weight-average molecular weight of soluble native polymeric lignin fraction (0.93 g/L BML #9) in aqueous 25 mM phosphate containing 4 μM LD in the presence and absence of 6 μM xylanase (XYL) and 20 μM NADH at pH 6.3.

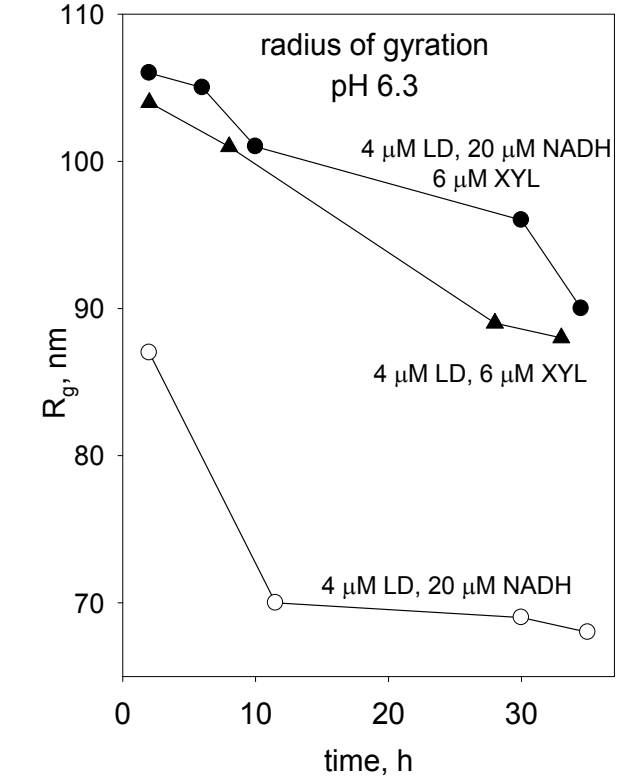

Figure 5.31 Change in radius of gyration of soluble native polymeric lignin fraction (0.93 g/L BML #9) in aqueous 25 mM phosphate containing 4 μM LD in the presence and absence of 6 μM xylanase (XYL) and 20 μM NADH at pH 6.3.

Without xylanase (XYL), the salicylate hydroxylase that exhibits depolymerase activity toward the polymeric native lignin preparation has a two-fold effect on the M_w and R_g of the substrate in solution at pH 6.3 containing 30 μM NADH (Fig. 5.32 and 5.33). The characteristic rise in M_w is enhanced by increasing enzyme concentration, but the corresponding impact on the reduction in R_g is smaller.

In Figs. 5.34–5.37, the native lignin substrates were initially treated under the same conditions as shown in Figs. 5.32 and 5.33, but the incubations were disrupted at a time point around 13 h by the introduction of aqueous xylanase (XYL) solutions at pH 6.3 (25 mM phosphate) to the repective assay solutions, as a result of which the pre-existing solute components were diluted 1.5 fold. In this connection, the M_w's presented in Fig. 5.34 and 5.37 are the weight-average molecular weights of the macromolecular assay components except for the xylanase (XYL).

Both 6 μM and 10 μM XYL are able to engender rapid dissociation of the lignin–LD complexes that are spontaneously assembled in the presence of 6 μM lignin depolymerase at pH 6.3 (Fig. 5.34). M_w falls to almost the same value whether 6 μM or 10 μM XYL is added to the assay solution. On the other hand, R_g attains an appreciably higher value with 10 μM rather than 6 μM XYL in solutions containing 4 μM LD (Fig. 5.35). Remarkably, R_g of the partially cleaved lignin substrate tends to approach its original value (before exposure to lignin depolymerase) after introducing progressively more XYL into the assay solution, especially when the LD concentration is low (Fig. 5.36). Such an observation suggests that a memory of the original macromolecular configuration

(embodied in the associated complexes of the substrate) can survive LD-catalyzed cleavage of the native lignin components under these conditions.

At first sight, however, the findings above could prompt an entirely different kind of interpretation where the consecutive physicochemical effects of the putative LD and the xylanase acting as an auxiliary protein arise from conformational changes in the substrate components. Thus, the rapid initial reduction in R_g could be viewed as an outcome of noncovalent interactions with the LD resulting in more compact and rigid conformations of the individual lignin components that lead to enhancement in the degree of association between them. In this context, the latter would be the facilitator of the dramatic increase in M_w that occurs in the presence of higher LD concentrations (Fig. 5.37). The rapid decrease in M_w upon the introduction of xylanase would then arise from competition on the part of the glycoside hydrolase (acting simply as an auxiliary protein) in disrupting the prevailing noncovalent interactions between the lignin components and LD or other lignin components.

Be that as it may, such an alternative working hypothesis is not consistent with the finding that the introduction of xylanase brings about appreciable increases in M_w at higher XYL:LD molar ratios (6:1 and 6:2) (Fig. 5.37). Moreover, when LD concentrations are high (4 μM and 3 μM) in the assay solutions containing 6 μM XYL, the resulting M_w of the substrate is significantly lower than in the former two cases as a result of greater lignin-depolymerase activity. Therefore simple reversible physicochemical processes cannot account for the observations. The final R_g of the partially cleaved lignin substrate in the

presence of LD and XYL is determined by several of interconnected equilibria between the species in solution.

It is important to remember that some proteins acting non-catalytically in solution can bring about a marked increase in M_w of the native polymeric lignin substrate without affecting R_g. Such effects (prominent ones at that) have been encountered with alcohol dehydrogenase in the absence and presence of NADH (Figs. 5.7 and 5.8). Thus, the principal criterion for LD-catalyzed cleavage of the lignin substrate should be a reduction in R_g regardless of whether M_w rises or falls. It would be surprising if conformational changes alone could be responsible for a significant decrease in R_g since the substrate consists of associated complexes composed of 50 or more individual components held in relatively rigid structures.

5.8 Lignin–depolymerase Activity under Limiting Conditions

The variations in R_g and M_w of the native lignin substrate incorporate complicated relationships with respect to each other that are governed by intermolecular interactions with one another, the LD and auxiliary protein (if present) under a range of conditions. A strategy that may engender a degree of clarification recognizes the fact that the flavin-dependent monooxygenase needs to be reduced (commonly by NADH) to exhibit activity toward its natural substrate. Nevertheless, it has been demonstrated that the native lignin can furnish the necessary reductive capacity when the natural cofactor is absent (Fig. 5.17). Under such conditions, the relative rates of the steps in the catalytic cycle of the enzyme will be altered, but any impact on the overall process of enzymatic catalysis will depend

on what is rate-limiting. Certainly, it would be worthwhile examining the effects of lignin-depolymerase activity conferred by low concentrations of enzyme in the absence of NADH on the native lignin substrate.

The results obtained in solutions containing 0.25 μM LD without NADH at pH 6.3 have revealed a distinctive relationship between the R_g and M_w of the native lignin preparation (Fig. 5.38 and 5.39) as the two parameters vary with time. R_g fell markedly (Fig. 5.38), although more slowly than in the presence of NADH (Fig. 5.33). Concomitantly, M_w of the substrate now underwent an initial reduction before beginning to rise as a result of intermolecular association between the degraded lignin components and the enzyme (Fig. 5.39). Hereby, important insights about the consequences of lignin-depolymerase activity have been confirmed under limiting conditions with respect to the concentrations of enzyme and substrate in the absence of NADH. Under these circumstances, the slower reduction of the flavin-dependent monooxygenase (by the macromolecular lignin substrate) impedes the rate of formation of the complexes between the lignin-product and enzyme; hence, LD-mediated association of the cleaved lignin components is delayed.

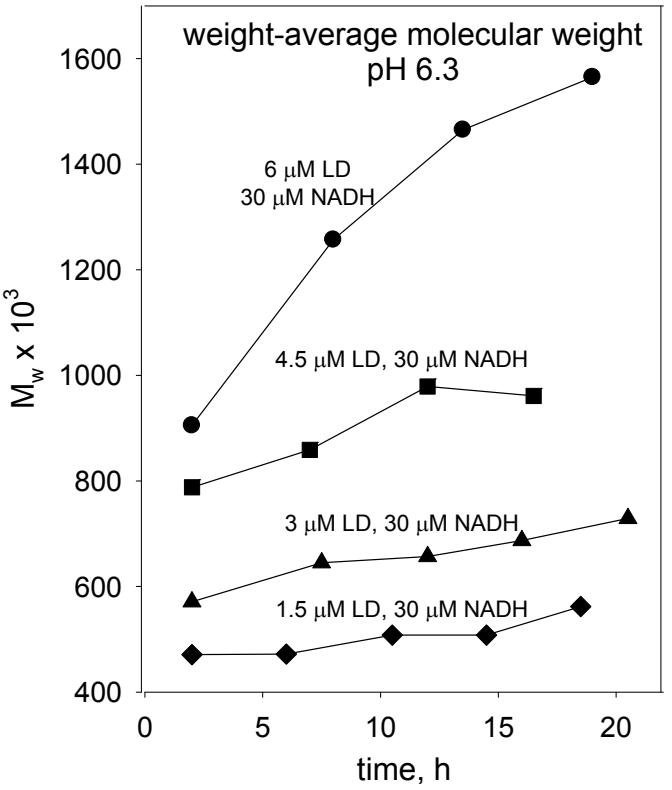

Figure 5.32 Changes in weight-average molecular weight of soluble native polymeric lignin preparation (1.40 g/L BML #9) caused by LD at pH 6.3 in 25 mM phosphate containing 30 μM NADH.

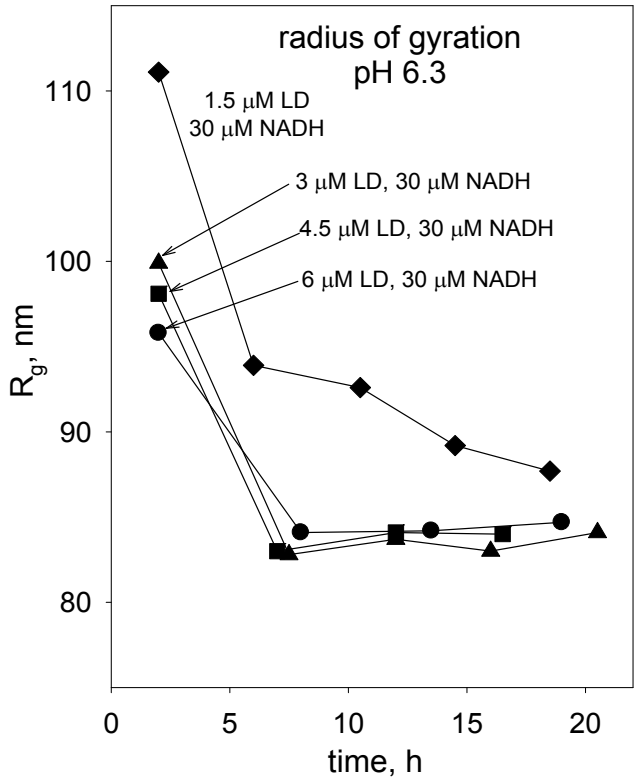

Figure 5.33 Changes in radius of gyration of soluble native polymeric lignin preparation (1.40 g/L BML #9) caused by LD at pH 6.3 in 25 mM phosphate containing 30 μM NADH.

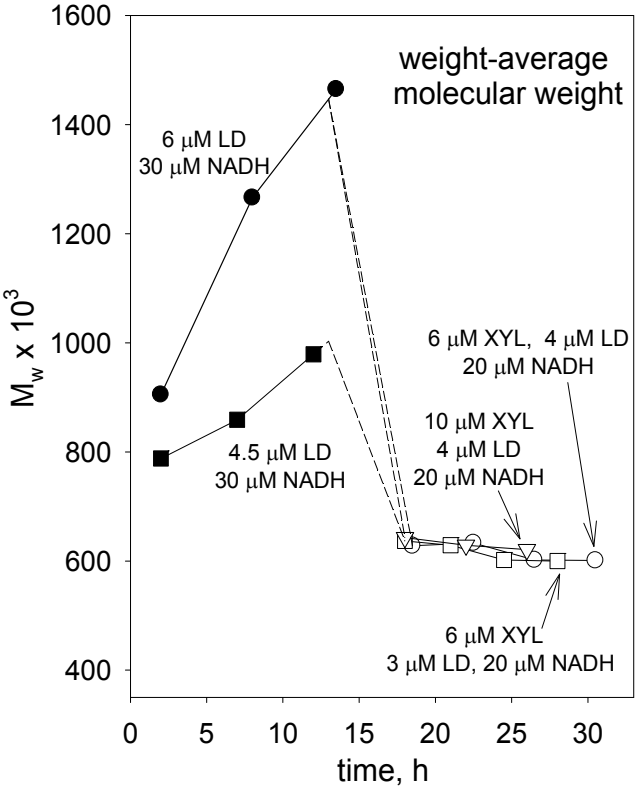

Figure 5.34 Xylanase-generated changes in weight-average molecular weight of soluble native polymeric lignin preparation (open symbols, 0.93 g/L BML #9) after 13 h incubation in presence of LD (closed symbols, 1.40 g/L BML #9) at pH 6.3 (25 mM phosphate).

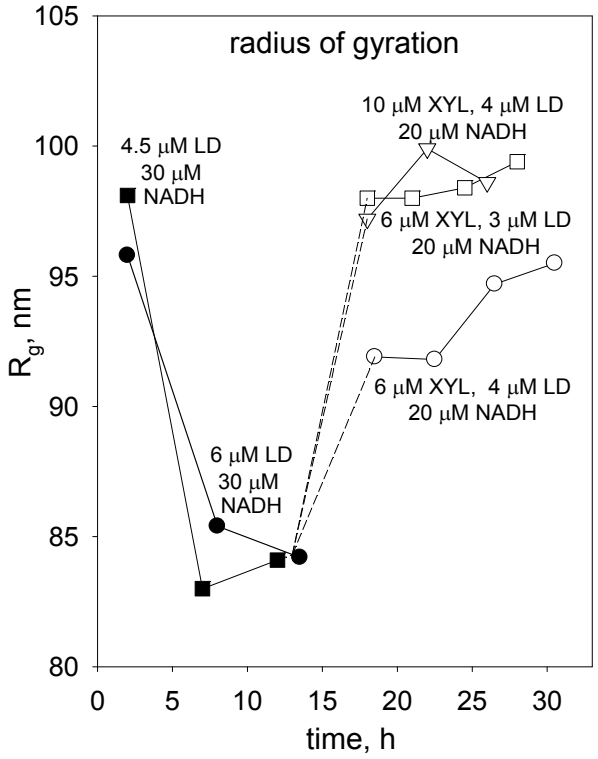

Figure 5.35 Xylanase-generated changes in radius of gyration of soluble native polymeric lignin preparation (open symbols, 0.93 g/L BML #9) after 13 h incubation in presence of LD (closed symbols, 1.40 g/L BML #9) at pH 6.3 (25 mM phosphate).

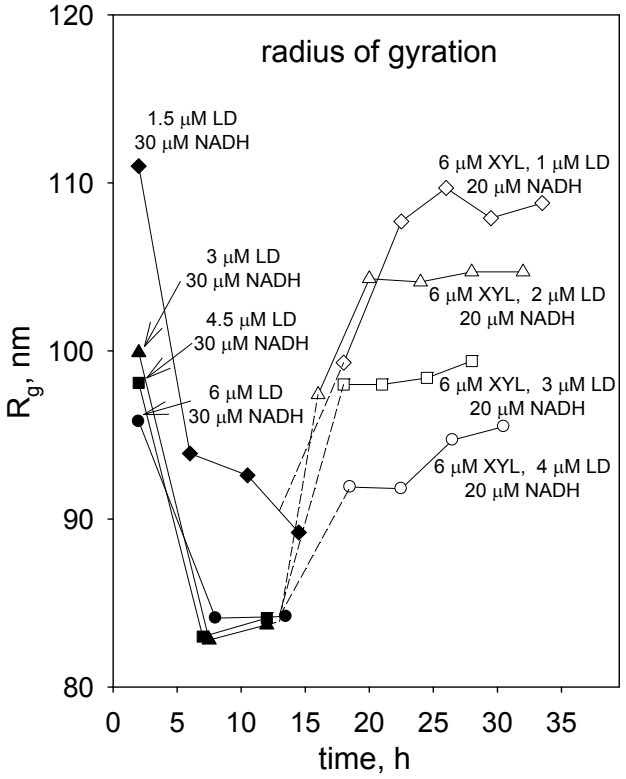

Figure 5.36 Xylanase-generated changes in radius of gyration of soluble native polymeric lignin preparation (open symbols, 0.93 g/L BML #9) after 13 h incubation in presence of LD (closed symbols, 1.40 g/L BML #9) at pH 6.3 (25 mM phosphate).

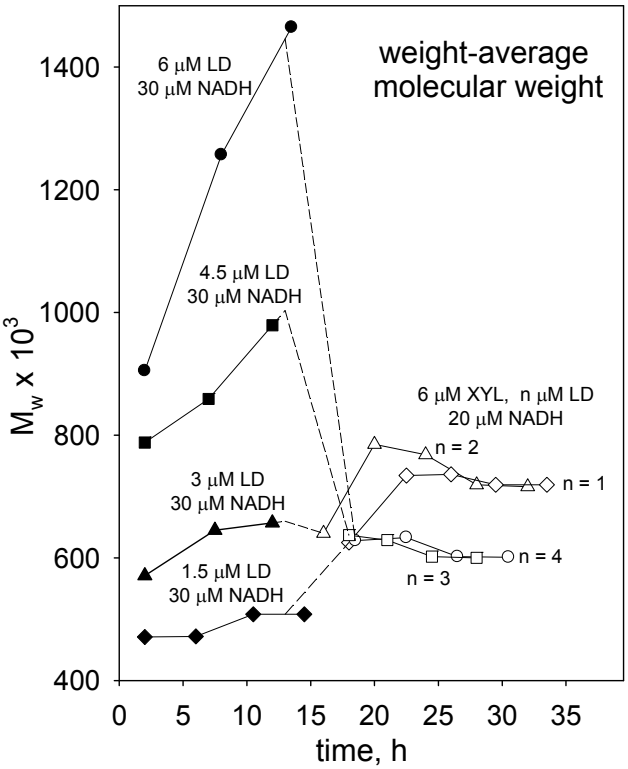

Figure 5.37 Xylanase-generated changes in weight-average molecular weight of soluble native polymeric lignin preparation (open symbols, 0.93 g/L BML #9) after 13 h incubation in presence of LD (closed symbols, 1.40 g/L BML #9) at pH 6.3 (25 mM phosphate).

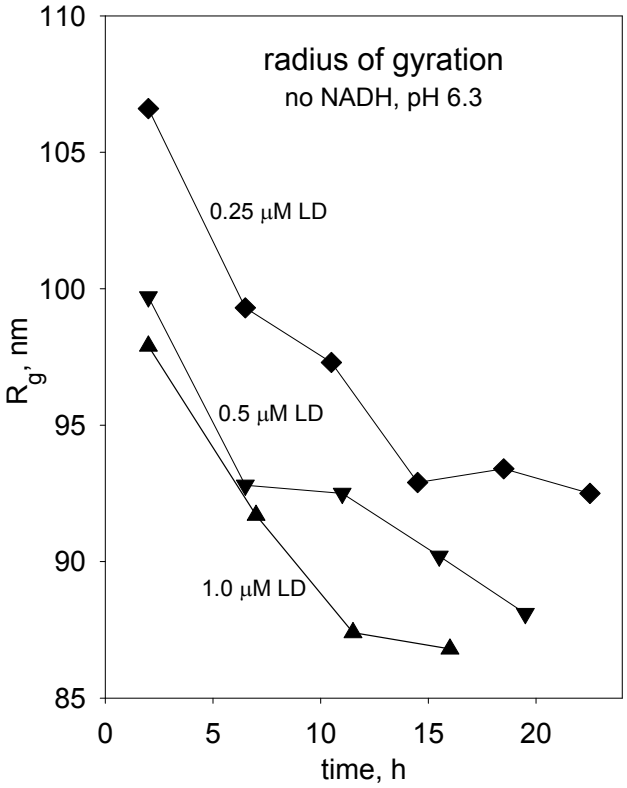

Figure 5.38 Changes in radius of gyration of soluble native polymeric lignin preparation (1.42 g/L BML #10) caused by low concentrations of LD without NADH at pH 6.3 in 25 mM phosphate.

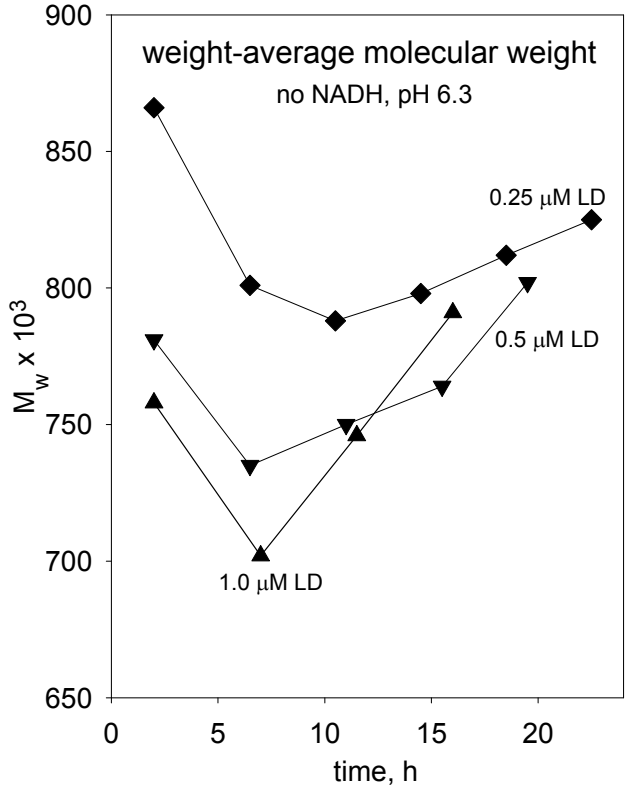

Figure 5.39 Changes in weight-average molecular weight of soluble native polymeric lignin preparation (1.42 g/L BML #10) caused by low concentrations of LD without NADH at pH 6.3 in 25 mM phosphate.

5.9 Conclusions

The soluble native polymeric lignin substrates have been treated with the putative lignin-depolymerase, salicylate hydroxylase, under a carefully chosen range of conditions. Rayleigh light scattering studies have revealed that this enzyme exhibits a two-fold effect on native polymeric lignin substrates. In general, M_w rises to an extent determined by the enzyme concentration, while R_g falls much more rapidly to approximately constant values that have a weaker dependence on the lignin-depolymerase activity. On other hand, the alcohol dehydrogenase that was originally employed for NADH turnover is able to associate with lignin components even when LD is absent from the assay solution; as a result, the M_w of the substrate increases as R_g remains approximately constant when no ligninolysis occurs.

The cleaved lignin fragments cannot automatically be released into open solution at a pH below neutrality; further association occurs between them and the partially degraded complexes to form noncovalently assembled macromolecular species with smaller R_g. Therefore, a reduction of R_g with time can be viewed as convincing evidence for functional lignin-depolymerase activity. Yet, for such a complicated biopolymer that exhibits associative behavior, it is essential to select meaningful conditions under which lignins are exposed to enzymes expressing lignin-depolymerase activity *in vitro* [Gilardi and Cass, 1993]. In this regard, it has been demonstrated that xylanase is capable of promoting dissociation of the associated lignin complexes formed as a result of (non-productive) interactions between the lignin components and enzyme.

The native lignin substrate is capable of furnishing the necessary capacity for reducing the LD (a flavin-dependent monooxygenase) when the natural cofactor, NADH, is absent. Under limiting conditions, i.e. with no NADH and at low LD concentrations, the rate-limiting step in the catalytic cycle of LD has been altered, and consequently the initial reduction in M_w that must accompany the decrease in R_g (resulting from covalent lignin-component cleavage) has be discerned for the first time. LD does indeed degrade the individual lignin components before they participate in enzyme-mediated association to form higher molecular weight complexes.

Chapter 6

Methylated Ball-milled Softwood Lignin-based Thermoplastics

6.1 Methylated Ball-milled Softwood Lignin in Blends with Low-T_g Polyesters

In order to explore the feasibility of converting biorefinery co-product lignins into value-added plastics, the systematic approach to formulations [Li and Sarkanen, 2002; 2005] that led to promising kraft lignin-based polymeric material blends have been adapted to produce a new generation of lignin-based plastics. The co-product lignins may differ dramatically from one another depending on the pretreatment process employed prior to enzymatic saccharification of lignocellulose; therefore native softwood lignin (ball-milled lignin) was employed in this research to develop initial guidance for subsequently formulating thermoplastics from technical lignins. Ball-milled softwood lignin (BML) has been considered to be more representative of the total lignin in woody plant cell walls, because less degradation of *β–O–*4 inter-unit linkages occurs for softwood than for hardwood lignins during ball milling [Hu *et al.*, 2006].

Formulations containing >70% methylated ball-milled softwood lignin (MBML) with low T_g polyesters represent the beginning of a new generation of lignin-based polymeric materials. The blends initially discussed in this section were prepared through solution casting from DMSO at 150 °C for 20 h, and then 180 °C under vacuum for 3 h to remove the last trace of DMSO.

At first glance, methylated kraft lignins [Li and Sarkanen, 2005] tend to form more ductile materials than MBML when both are blended with polyesters such as poly(butylene adipate) (PBA, M_w ~ 12,000, Aldrich) at 25~30% incorporation levels. Yielding has not been observed during uniaxial extension of MBML-PBA blends when the content of MBML was reduced to 70% (Fig. 6.1). Other MBML-based materials containing poly(trimethylene succinate) (PTMS, M_w ~ 9,500, Scientific Polymer Products, Inc., Ontario, NY) or poly(ethylene succinate) (PES, M_w ~ 10,000, Scientific Polymer Products, Inc., Ontario, NY) are also quite disappointing: none of them possesses a tensile strength approaching 40 MPa (Fig. 6.1) except the one containing 15% poly(trimethylene glutarate) (PTMG, M_w ~ 4,000, Scientific Polymer Products, Inc., Ontario, NY).

By contrast, multiphase blends of MBML and poly(ε-caprolactone) (PCL, Polymer Source, Inc, Dorval, QC, Canada) embody a substantial improvement in tensile properties that have been achieved by polymeric materials containing even more than 80% lignin. For example, blends containing 15% PCL can easily attain a tensile strength (σ) above 50 MPa with ~7% elongation at break ($\Delta\varepsilon$) (Fig. 6.1), even though homogeneity of the materials was limited by the experimental conditions employed.

6.2 Methylated Ball-milled Lignin in Blends with Block Copolymers

With the incorporation of 15~20% poly(ethylene oxide-*b*-1,2-butadiene-*b*-ethylene oxide) (EBE, M_n 4300-800-4300, Polymer Source, Inc, Dorval, QC, Canada), MBML-based polymer materials start to demonstrate their potential as excellent candidates for sustainable engineering plastics with tensile strengths well above 60 MPa (Fig. 6.2). On

the other hand, their tensile properties are surprisingly sensitive to the EBE content when the latter is increased beyond 20%.

A methylated higher molecular-weight ball-milled lignin fraction (10k MBML, ~67% of the total parent BML preparation) was progressively plasticized by EBE in the same manner as the parent MBML preparation. The lower molecular weight lignin components had been removed during exhaustive ultrafiltration in 0.1 M NaOH through a 10,000 nominal molecular weight cutoff membrane (~19% of the total parent BML preparation was then retained during subsequent ultrafiltration through a 1,000 nominal molecular weight cutoff membrane). Hereby, it was found that the plasticization efficacy of 15~20 % levels of EBE toward 10k MBML are weakened substantially so that neither the tensile strength nor elongation at break is comparable to those of the corresponding parent MBML-based blends (Fig. 6.2). As the EBE content increases to 25~30%, the 10 k MBML-based blends become more ductile than the corresponding parent MBML ones, but no obvious improvement in their tensile strength can be observed. Those missing lower molecular-weight lignin components may be responsible for the occurrence of chain re-arrangements within the macromolecular complexes during solution casting, without which the mechanical properties of the materials tend to be compromised when the plasticizer content is low.

The diblock co-polymer poly(ethylene oxide-*b*-1,2-butadiene) (EB, M_n 4000-1800, Polymer Source, Inc, Dorval, QC, Canada) has been blended with MBML with the expectation that the longer polybutadiene chain could enhance the mechanical properties of the lignin-based materials. However, EB is not as miscible as EBE with MBML, and the

corresponding MBML-based materials are more fragile (Fig. 6.3). In fact, polybutadiene alone is not miscible with MBML, and thus it acts as a toughening component in the blends only when it is covalently bound to the miscible PEG fragments at both ends.

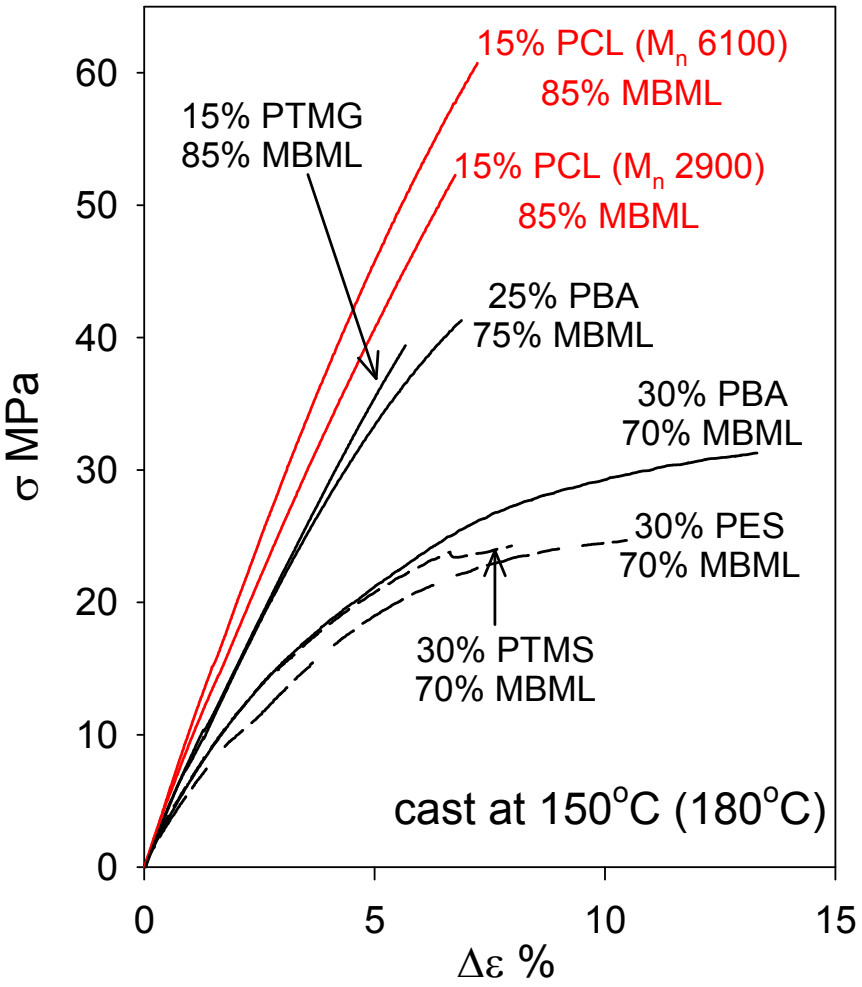

Figure 6.1 Tensile behavior of parent methylated ball-milled lignin (MBML) in blends with poly(butylene adipate) (PBA), poly(trimethylene succinate) (PTMS), poly(ethylene succinate) (PES), poly(trimethylene glutarate) (PTMG) and poly(ε-caprolactone) (PCL).

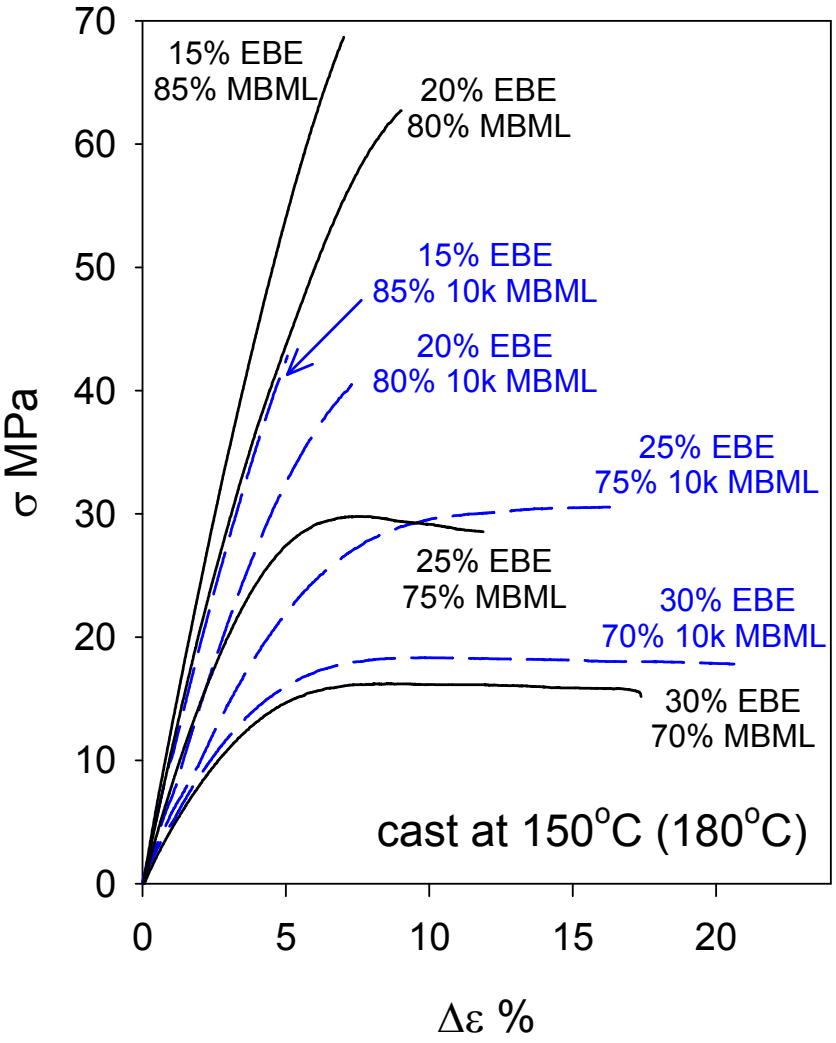

Figure 6.2 Progressive plasticization of methylated ball-milled lignin (MBML) based blends by poly(ethylene oxide-*b*-1,2-butadiene-*b*-ethylene oxide) (EBE): effect of lower molecular weight lignin components on plastic deformation. The 10k MBML was prepared by exhaustive ultrafiltration of the unmethylated parent ball-milled lignin through a 10,000 nominal molecular weight cutoff membrane (Amicon YM10, Millipore) in aqueous 0.1 M NaOH.

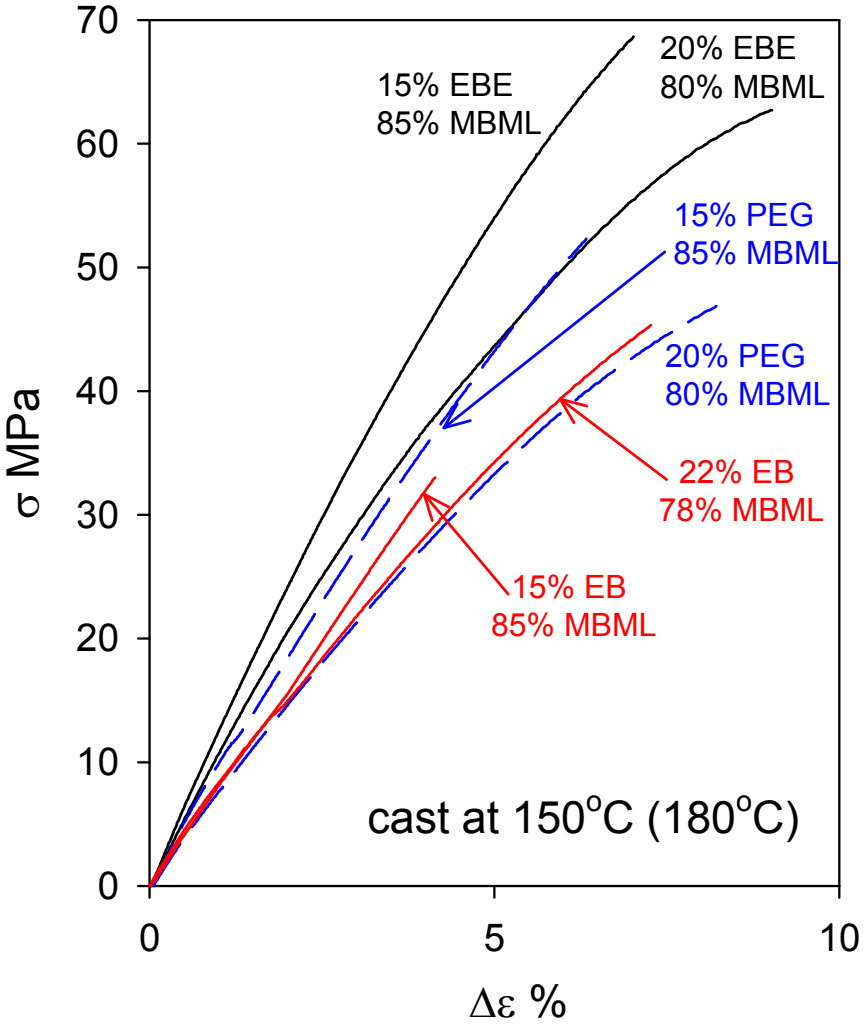

Figure 6.3 Tensile behavior of parent methylated ball-milled lignin (MBML) in blends with EBE, poly(ethylene oxide-b-1,2-butadiene) (EB) and poly(ethylene glycol) (PEG): introduction of potentially toughening polybutadiene segments.

6.3 Methylated Ball-milled Lignin in Blends with Monomeric Plasticizers

6.3.1 MBML-based blends containing diesters

Tertiary MBML-based material blends containing 13% poly(ethylene glycol) (PEG, M_n = 10,000, Aldrich) and 2% diesters were found to be more ductile than the corresponding binary blends with PEG when solution cast at 150 °C (Fig. 6.4). Among the three diesters employed in these tertiary blends, diethyl glutarate (DEG, Aldrich) was the most effective monomeric plasticizer in terms of enhancing the tensile strength of the binary-blend material (Fig. 6.4).

When the casting temperature was lowered from 150 to 140 °C, the polymeric materials composed of 100% MBML attained a tensile strength of ~50 MPa with ~8% elongation at break. Although the tensile properties of the materials were sensitive to the loss of volatile low molecular weight lignin components during the casting process (Fig. 6.5), this represents the first demonstration that polymeric materials made only of a simple lignin derivative can exhibit tensile properties comparable to those of common engineering plastics such as the examples listed in Table 6.1.

Alkylated kraft lignins can form miscible blends with aliphatic polyesters characterized by methylene/carboxylate group ratios (CH_2/COO) of 2.0~4.0; on the basis of the concavity of the T_g–composition curve, the interactions between the two blend components were found to be the most favorable when the CH_2/COO of the polyester lay between 2.5 and 3.0 [Li and Sarkanen, 2002]. The diesters selected in this work represent the repeating units of those polyesters with alkyl end groups that preclude hydrogen bond formation with lignin components. Most of the diesters evaporated at elevated temperature

during solution casting at 140 °C despite the fact that their boiling points are far above 200 °C. The lignin losses indicated in Figs. 6.6 and 6.7 were the mass losses from the control preparations composed of 100% MBML after casting under the same conditions as the binary blends containing the various diesters. The diester contents estimated in Figs. 6.6 and 6.7 are the amounts after solution casting (Eq. 4.4-1). 20~30% diethyl adipate (DEA, Aldrich), 30~45% DEG and 30% diethyl succinate (DES, Aldrich) were employed as initial diester contents in these blends (w/w).

Table 6.1 Room-temperature tensile properties of selected engineering plastics [Davis, 2004].

Thermoplastic	**Tensile strength**	**Elongation at break**	**Tensile modulus**
	MPa	**%**	**KPa**
Styrene	46	2.2	320
Styrene-acrylonitrile (SAN)	72	3	390
Acrylonitrile-butadiene-styrene (ABS)	48	8	210
Flame-retardant ABS	40	5.1	240
Polypropylene (PP)	32	15	130
Polyethylene (PE)	30	9	100

ASTM D 638 test method

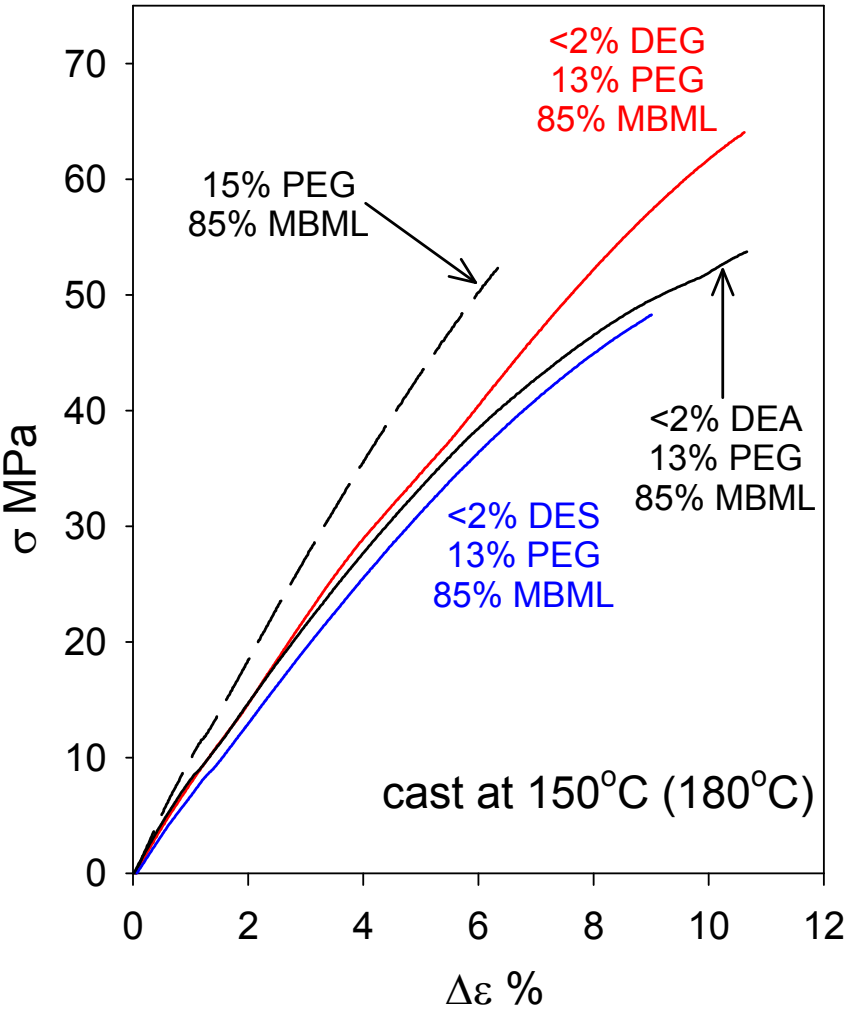

Figure 6.4 Tensile behavior of parent methylated ball-milled lignin (MBML) in blends with PEG initially containing 2% w/w quantities of diethyl glutarate (DEG), diethyl adipate (DEA) and diethyl succinate (DES) respectively.

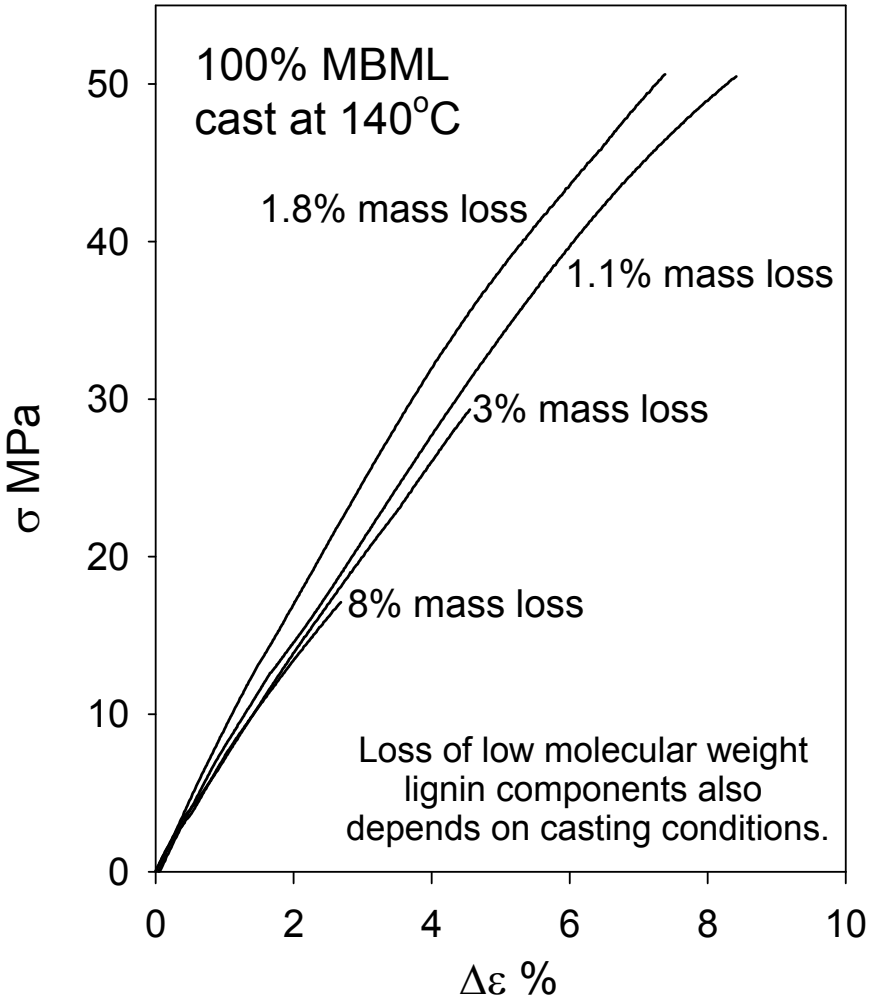

Figure 6.5 Tensile behavior of methylated ball-milled lignin (MBML)-based polymeric materials formed by casting for differing periods of time at 140 °C.

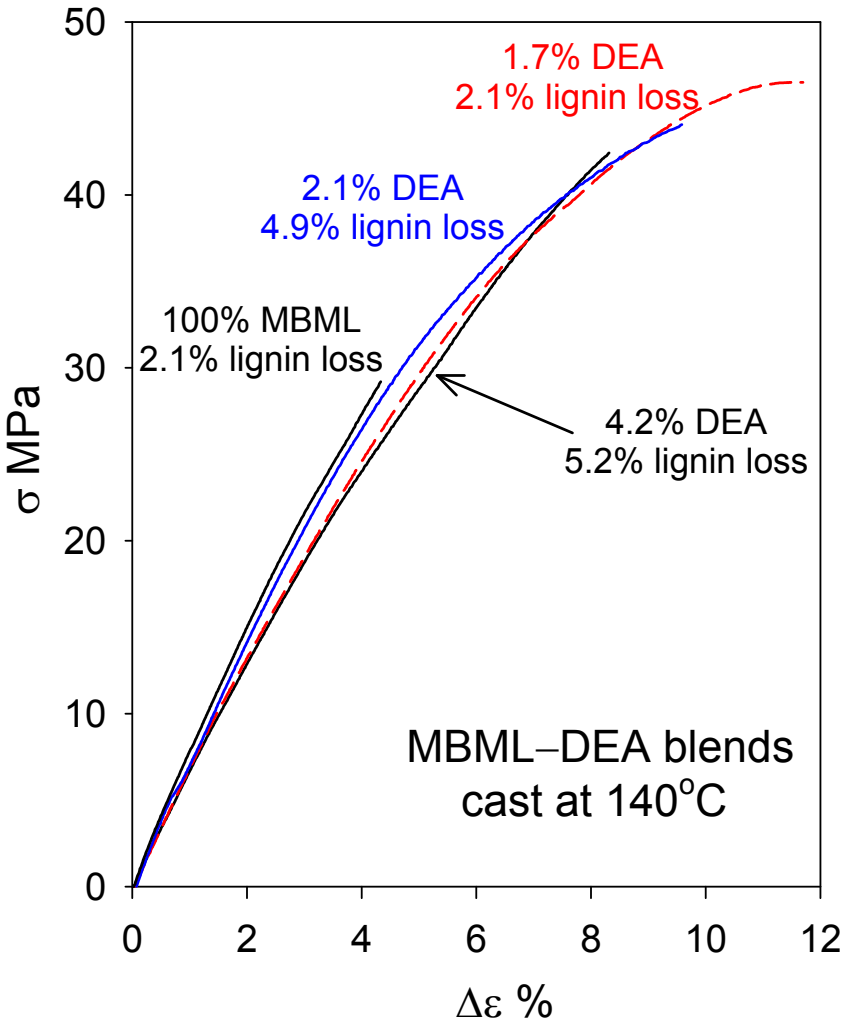

Figure 6.6 Tensile behavior of methylated ball-milled lignin (MBML)-based polymeric materials in blends with differing small quantities of diethyl adipate (DEA).

As shown in Fig. 6.6, the impact of the lost volatile low molecular weight lignin components can be compensated for by the monomeric plasticizer, DEA. For example, the ductility of 100% MBML with a 2.1% lignin loss during casting is improved 3-fold in the presence of 1.7% DEA, and its tensile strength is enhanced by 50% (Fig. 6.6). Although the contents of DEA remaining in the blends cannot be determined accurately in this study, it is obvious that its presence facilitates particular conformational changes in the

components making up the macromolecular lignin complexes and hereby reduces the brittleness of these lignin-based materials (Figs. 6.4 and 6.6). The intermolecular interactions between DEG and lignin components are so weak that the inherent cohesion of the material is compromised by the presence of this diester, and as a result the strength of the material falls rapidly when more DEG molecules are preserved in the blends cast at 140 °C (Fig. 6.7). The effect of DES does not appear to be any better than that of DEG (Fig. 6.7)

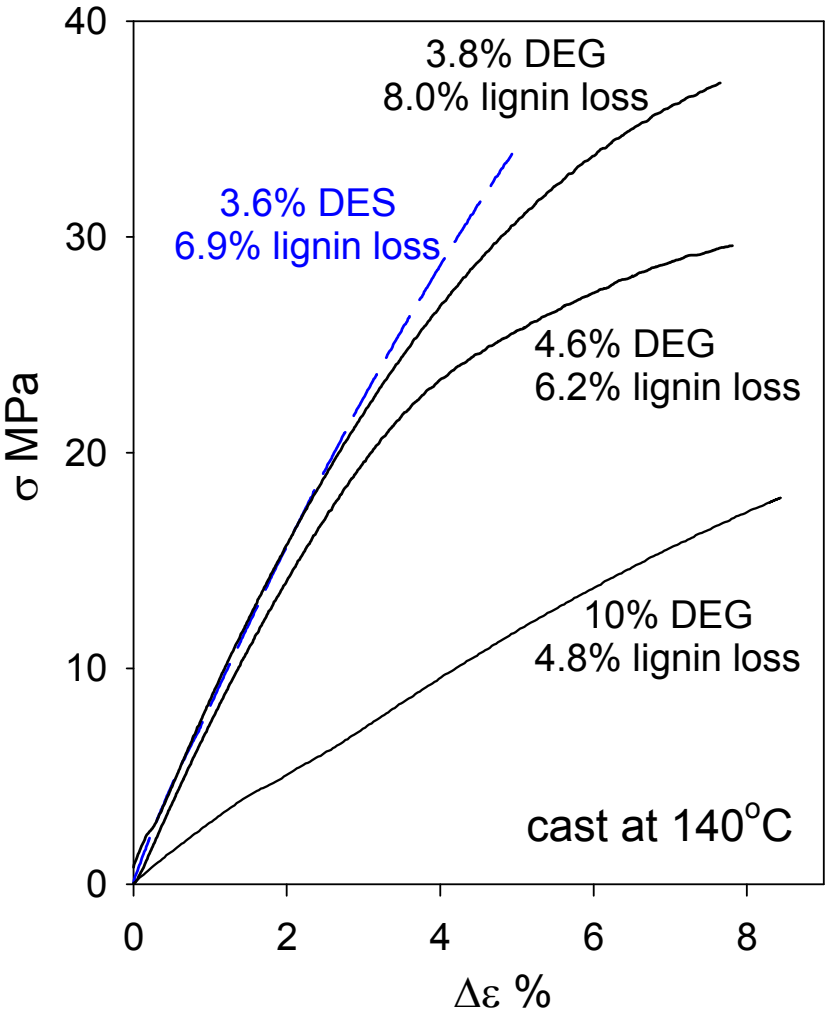

Figure 6.7 Tensile behavior of methylated ball-milled lignin (MBML)-based polymeric materials in blends with differing small quantities of diethyl succinate (DES) and diethyl glutarate (DEG).

6.3.2 MBML-based material blends with brominated aromatic compounds

Binary blends of MBML and aromatic compounds with bulky electron withdrawing substituents (Fig. 6.8) have suggested new avenues for formulating lignin-based polymeric materials.

3,3',5,5'-Tetrabromobisphenol A (TBBP-A) is widely used as a reactive flame retardant in epoxy and polycarbonate resins [Ortuño, *et al.*, 2014]; it also works as an additive flame retardant in acrylonitrile-butadiene-styrene (ABS), high impact polystyrene (HIPS) and phenolic resins [BSEF, 2013]. In the blends with MBML, TBBP-A (Aldrich) may act not only as a flame retardant, but also, more interestingly, as a plasticizer. When TBBP-A was cast alone in DMSO for 23 h, it decomposed to dark brown globular material at 150 °C with significant mass loss, but it formed a light grey globular material at 140 °C as a result of less degradation. However, its decomposition at elevated temperatures seems to be inhibited by the presence of MBML. The MBML-based materials containing 10% TBBP-A, whether solution cast at 140 or 150 °C, do not differ significantly from one another in terms of their tensile behavior; they were capable of attaining tensile strengths above 60 MPa with elongations at break of 8~9% regardless of their casting temperatures (Fig. 6.9). By comparison, 4,4'-dibromobenzophenone (DBBP), which possesses a lower frequency of electron-withdrawing groups on the aromatic rings, plasticized MBML-based materials less effectively as revealed by the fact that the material containing only MBML exhibited a similar tensile strength of ~40 MPa.

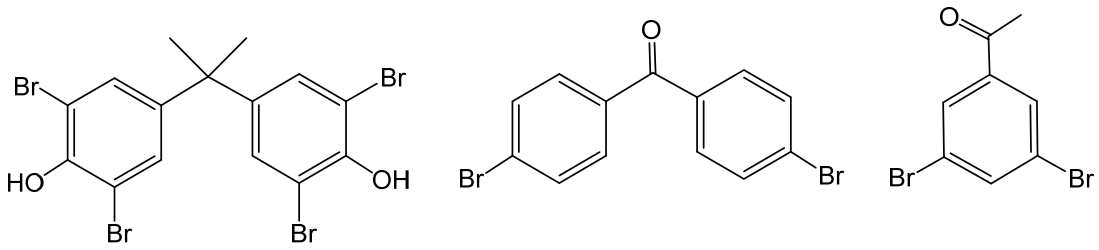

A B C

Figure 6.8 (**A**) 3,3',5,5'-tetrabromobisphenol A (TBBP-A); (**B**) 4,4'-dibromobenzophenone (DBBP); (**C**) 3',5'-dibromoacetophenone (DBAP).

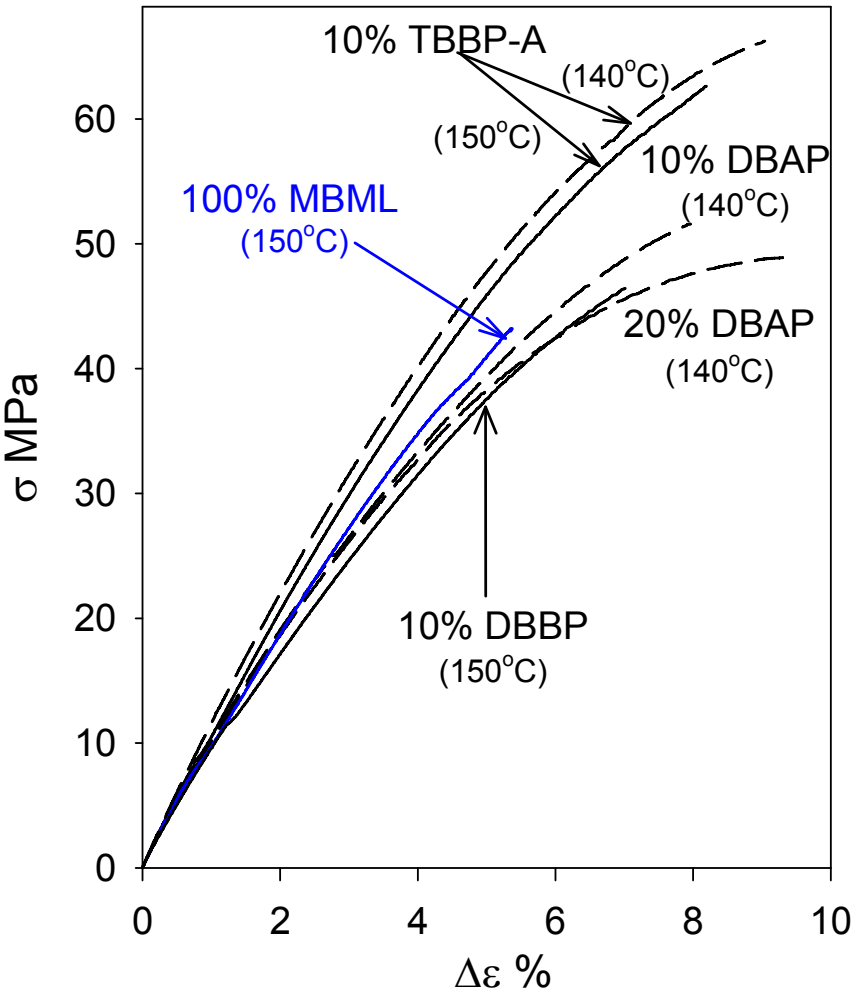

Figure 6.9 Tensile behavior of methylated ball-milled lignin (MBML)-based polymeric materials in blends with 3,3',5,5'-tetrabromobisphenol A (TBBP-A), 3',5'-dibromoacetophenone (DBAP) and 4,4'-dibromobenzophenone (DBBP).

The plasticizer contents indicated in Fig 6.9 represent the blend compositions for each test piece prior to casting. The contents of 3',5'-dibromoacetophenone (DBAP, American Custom Chemicals Corporation, San Diego, CA) in the cast material are lower than the initial values for the same reason as found with the diesters. The remaining contents of the initial 10% and 20% levels of DBAP in the blends are ~1.5% and 11% respectively, and yet the poor efficiency of plasticization by DBAP evident in Fig. 6.9 implies that the intermolecular interactions between DBAP and the peripheral components in the lignin complexes do not enhance blend deformability.

6.4 Methylated Ball-milled Lignin in Blends with Poly(ethylene glycol)

The efficiency of plasticizers for alkylated kraft lignin depends on two opposing tendencies: on one hand, the intermolecular attraction between plasticizer and individual lignin components has to be strong enough so that the plasticizer molecules can be incorporated into the peripheral regions of the associated lignin complexes; on the other hand, it would be counterproductive if such attraction becomes so powerful that the macromolecular complexes undergo dissociation [Li and Sarkanen, 2005].

In the case of derivatized milled wood lignin (Fig. 6.10), PEGs act as efficient plasticizers: in general, they are able to improve the ductility of the MBML polymeric material by 2~3 fold with increasing PEG levels up to 15%; concomitantly, the tensile strength of the material decreases significantly from 65 to 40 MPa as more PEG is added to the blend. It is remarkable that the MBML-based blend containing 15% poly(ethylene glycol) methyl ether (PEGM, M_n 5000) is more brittle than the corresponding blend with

PEG (M_n 4600) (Fig. 6.10). It suggests that PEG molecules interact with lignin components partially through hydrogen bonding between the hydroxyl end groups of PEG chains.

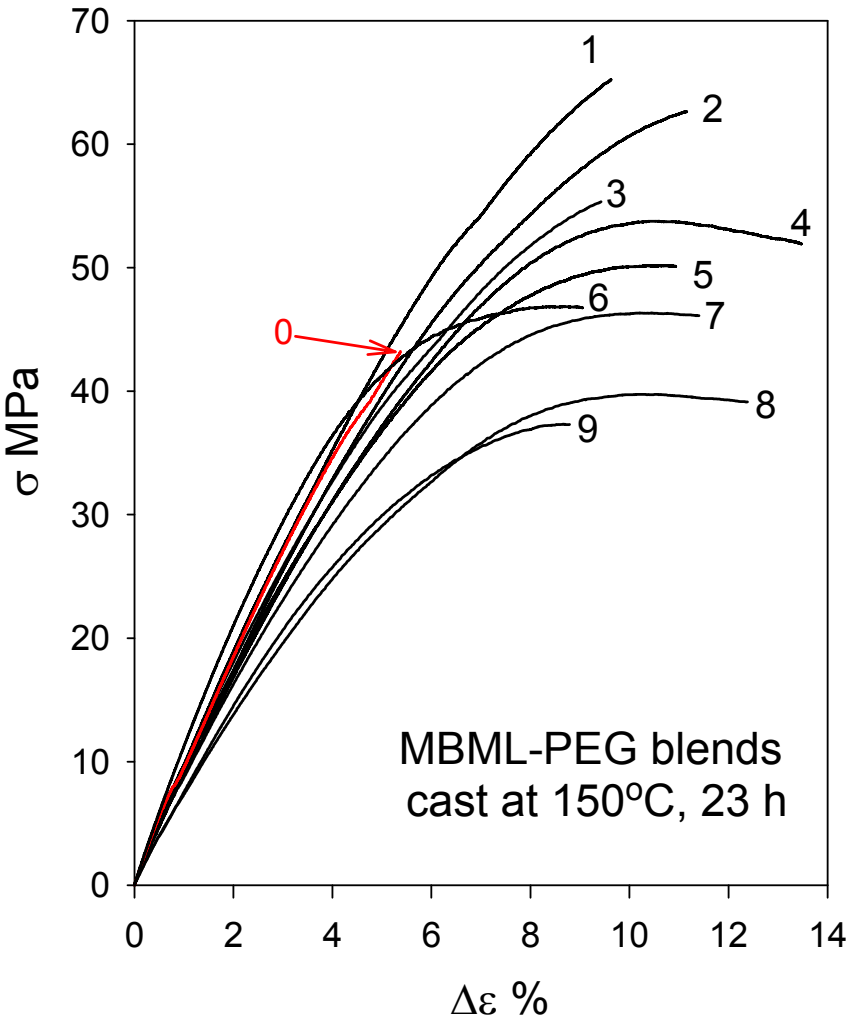

Figure 6.10 Tensile behavior of parent methylated ball-milled lignin (MBML) in blends involving homopolymer fractions, poly(ethylene glycol) (PEG), with different molecular weight distributions. [0] 100% MBML; [1] 5% PEG (M_n 400); [2] 5% PEG (M_n 400), 5% PEG (M_n 10,000); [3] 15% PEG (M_n 4600); [4] 5% PEG (M_n 400), 5% PEG (M_n 4600); [5] 10% PEG (M_n 400); [6] 5% PEG (M_n 1000); [7] 15% PEG (M_n 2000); [8] 15% PEG (M_n 10,000); [9] 15% poly(ethylene glycol) methyl ether (PEGM) (M_n 5000).

The PEGs selected in this work possess number-average molecular weights (M_n) ranging from 400 to 10,000, and their physical states vary from liquid to waxy solid materials depending on the molecular weight. Interestingly, the mechanical properties of the MBML-PEG blends seem to be sensitive to the molecular weight distribution of plasticizer: MBML-based blends plasticized by low molecular weight PEG tend to attain better tensile strengths. It is very likely that the incorporation of shorter-chain PEGs into the peripheral regions of the associated lignin complexes are more favored due to the higher concentration of hydroxyl end groups per unit volume of PEG, which contributes to increasing the stabilization energy when shorter chains interact with lignin components.

6.5 X-ray Powder Power Diffraction

6.5.1 Introduction

X-ray scattering is primarily induced by the interactions between x-ray photons and electrons in atoms, and therefore the pattern of x-ray diffraction reflects the overall electron distribution in the material. The intensities of the x-ray scattering are related to the frequencies of the corresponding interatomic distances, in other words, an intensity maximum represents a preferred interatomic packing arrangement in the material. If the atoms are arranged in a periodic pattern as they are in crystals, a sharp diffraction peak will be observed and the inter-planar distance, d, can be estimated by means of the Bragg equation $\lambda = 2d\sin\theta$. In noncrystalline polymeric materials, there is no three-dimensional long-range order, yet the short-range order of amorphous macromolecular chain segments is anisotropic because dense packing of those segments has to follow a certain correlation

between their relative position and orientation [Ruland, 1969]. The intramolecular distance and packing in an amorphous polymer can be specified by means of a radial distribution function (RDF) which can provide significant details about interatomic packing in a range below 5~6 Å [Klug and Alexander, 1954], but little information about intermolecular distances [Miller and Boyer, 1984]. The frequently occurring interatomic distances can be approximately estimated by the equivalent Bragg spacing, d, which is obtained by applying the Bragg equation at the maximum of an amorphous peak [Miller and Boyer, 1984]. For a more accurate value of interatomic distance, $R \approx 1.22d$, where R is the magnitude of some related frequently occurring interatomic vector.

The X-ray diffraction patterns for amorphous polymers usually contain one or more peaks that are related to the intramolecular or intermolecular packing of carbon atoms. For example, two prominent amorphous peaks centered at 10^{o} and 19^{o}, corresponding to Brag spacings of 8.84 Å and 4.67 Å respectively, have been observed in the x-ray diffraction pattern of unoriented polystyrene at room temperature. The former peak has been interpreted as arising from intermolecular effects because it is absent in the x-ray scattering diagram of monomeric styrene [Katz, 1936], and its intensity increases monotonically with temperature in the x-ray diffraction pattern of amorphous polystyrene.

Amorphous scattering patterns from x-ray diffraction scans of semicrytalline polymers have been correlated with the corresponding crystalline peaks and depicted by Lorentzian functions as reference templates to follow the changes in the amorphous regions [Murthy and Minor, 1990]. The intensity below the experimental baseline can be attributed to the unoriented, isotropic, amorphous components, and the intensity above the

experimental baseline can be attributed to the oriented, anisotropic, amorphous components [Murthy *et al.*, 1993]. Lignins are known to be noncrytalline polymers, and amorphous methylated kraft lignin fractions exhibit two prominent Lorentzian component peaks centered at $2\theta = 16.9^{o}$, d = 5.25 Å and $2\theta = 22.1 \pm 0.6^{o}$, d = 4.0 ± 0.1 Å [Li and Sarkanen, 2005] in their x-ray diffraction patterns.

6.5.2 X-ray diffraction patterns of MBML-based materials

The x-ray diffraction diagram of uncast 100% MBML shows a distinct bimodal distribution that can be decomposed into two Lorentzian peaks centered at $2\theta = 14.4^{o}$, d = 6.1 Å and $2\theta = 21.7^{o}$, d = 4.1 Å, respectively (Fig. 6.11 A); d or the d-spacing is the equivalent Bragg spacing at the maximum of the Lorentizan peak. These two predominant peaks have been found to be typical in the x-ray diffraction patterns of lignins and their simple derivatives [Rials and Glasser, 1989; Hatakeyama and Hatakeyama, 1982; Li and Sarkanen, 2005], and their origins can be correlated with two different configurations of interacting aromatic rings in neighboring lignin macromolecules. It was previously recounted in the x-ray diffraction study of methylated kraft lignin-based plastics [Li and Sarkanen, 2005] that the d-spacing of 4.0 Å (4.1 Å for MBML in this study) represents the average value of the intermolecular separations (3.4 ~ 4.6 Å) between co-facial aromatic rings in the crystal structures of lignin model compounds [Morokuma, 1977; Lundquist and Stomberg, 1988; Roblin *et al.*, 2000; Stomberg and Lundquist, 1987]. On the other hand, the Lorentzian component characterized through an equivalent Bragg spacing of 6.1 Å, which shifts to ~5.5 Å upon casting (Fig. 6.11 B), can be reasonably assigned to the

intermolecular separation between edge-on aromatic rings, which is 5.3 Å in the crystalline (nonphenolic) β-*O*-4' linked dilignol [Stomberg and Lundquist, 1986].

Upon casting, the peak maximum of the higher–θ Lorentzian component peak remains approximately in the same location; in fact the most frequent separation between co-facial aromatic rings in neighboring lignin macromolecules hardly changes regardless of the casting conditions or the blend composition (Fig. 6.11). Concurrently, the equivalent Bragg spacing of the lower–θ Lorentzian component peak maximum decreases by 0.5 Å and the relative proportions of edge-on configurations for interacting aromatic rings increases by a factor of 1.2 as a result of casting at 140 or 150 °C (Fig. 6.11 A~C).

The systematic changes in the separations and relative proportions of the two configurations for interacting aromatic rings suggest that individual lignin components, instead of existing as freely diffusing polymeric chains in the casting solvent, may well be incorporated in well-defined macromolecular complexes that are preserved during the casting process at temperatures around T_g. At a molecular level, a co-facial complex between two veratryl alcohol molecules is calculated to be more stable than the corresponding edge-on structure on the basis of an appropriate level of density functional theoretical computations in the gas phase [Chen and Sarkanen, 2010, and unpublished results]. Therefore, it is reasonable to assume that in these complexes, the predominant configurations of interacting aromatic rings in the interior regions are co-facial; on the other hand, interacting pairs of aromatic rings in the lignin chains in the peripheral regions presumably exhibit a higher proportion of edge-on configurations. In other words, the Lorenztian component peak centered at ~4.1 Å arises from the intermolecular separations

between the interior cofacial aromatic rings, while the Lorentzian component peak centered between 5.5 and 6.3 Å reflects the peripheral edge-on configurations for interacting aromatic rings.

During the solvent casting process, the macromolecular lignin complexes coalesce with one another to form continuous domains through their peripheral regions, and consequently among the individual complexes there is a 1.2-fold increase in interacting pairs of aromatic rings that embody edge-on configurations (Fig. 6.11 A~C). However, in the absence of lower-molecular weight lignin components (removed by ultrafiltration through a 10,000 nominal molecular weight cutoff membrane), hardly any inter-conversion between the cofacial and edge-on configurations takes place despite the fact that the d-spacing for the lower-θ Lorentzian component peak decreases by 0.5 Å (Fig. 6.12 A, B).

The ratios of cofacial and edge-on configurations for pairs of interacting aromatic rings in the cast and uncast high molecular weight MBML fractions are surprisingly close to that in the cast parent MBML preparation (Fig 6.13). Such a coincidence suggests that the ~8% loss in the cofacial configurations for pairs of interacting aromatic rings in the cast parent MBML preparation can arise from conformational changes in the shorter macromolecular lignin chains that are present in the peripheral domains of the complexes.

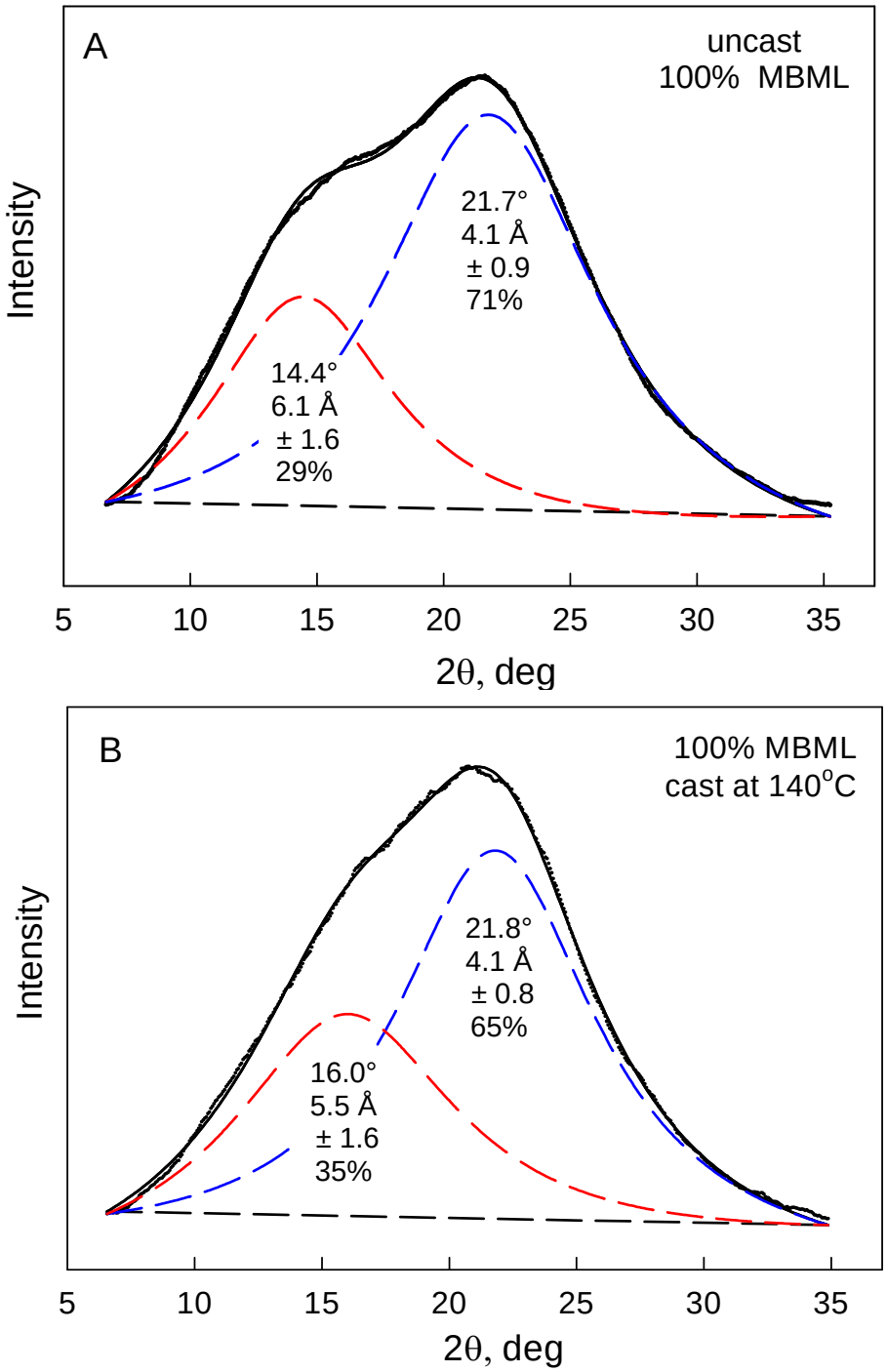

Figure 6.11 A & B Analysis of x-ray powder diffraction patterns of methylated ball-milled lignin (MBML)-based materials using two Lorentzian functions $I(x) = I(0)/(1 + x^2/\text{hwhm}^2)$, $x = 2\theta - 2\theta_k$, where $I(x)$ is the scattered intensity at x from the Bragg angle $2\theta_k$ for the peak, 2θ is the scattering angle, and hwhm is the half-width at the half-maximum of the peak.

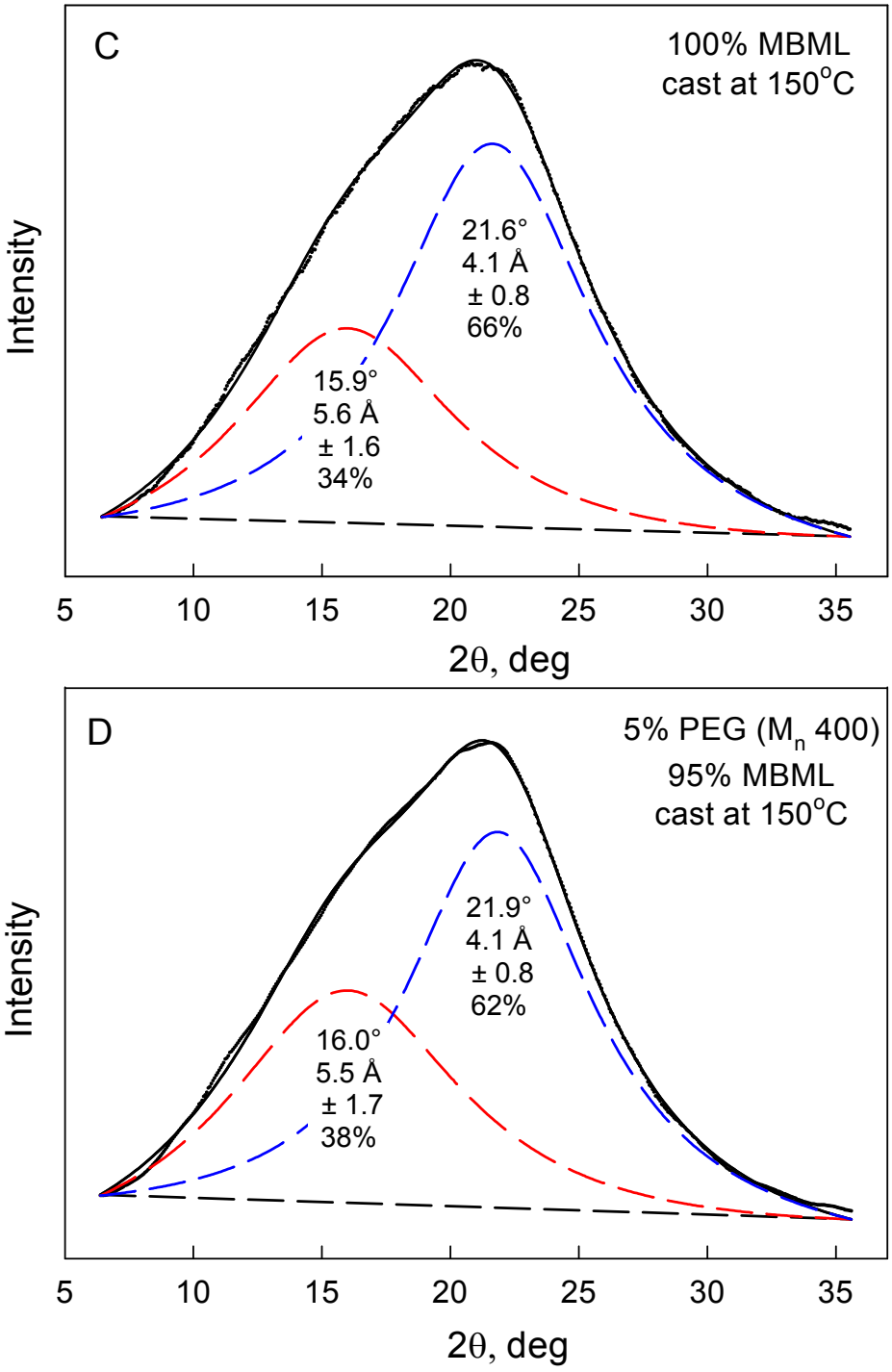

Figure 6.11 C & D Analysis of x-ray powder diffraction patterns of methylated ball-milled lignin (MBML)-based materials using two Lorentzian functions $I(x) = I(0)/(1 + x^2/\text{hwhm}^2)$, $x = 2\theta - 2\theta_k$, where $I(x)$ is the scattered intensity at x from the Bragg angle $2\theta_k$ for the peak, 2θ is the scattering angle, and hwhm is the half-width at the half-maximum of the peak.

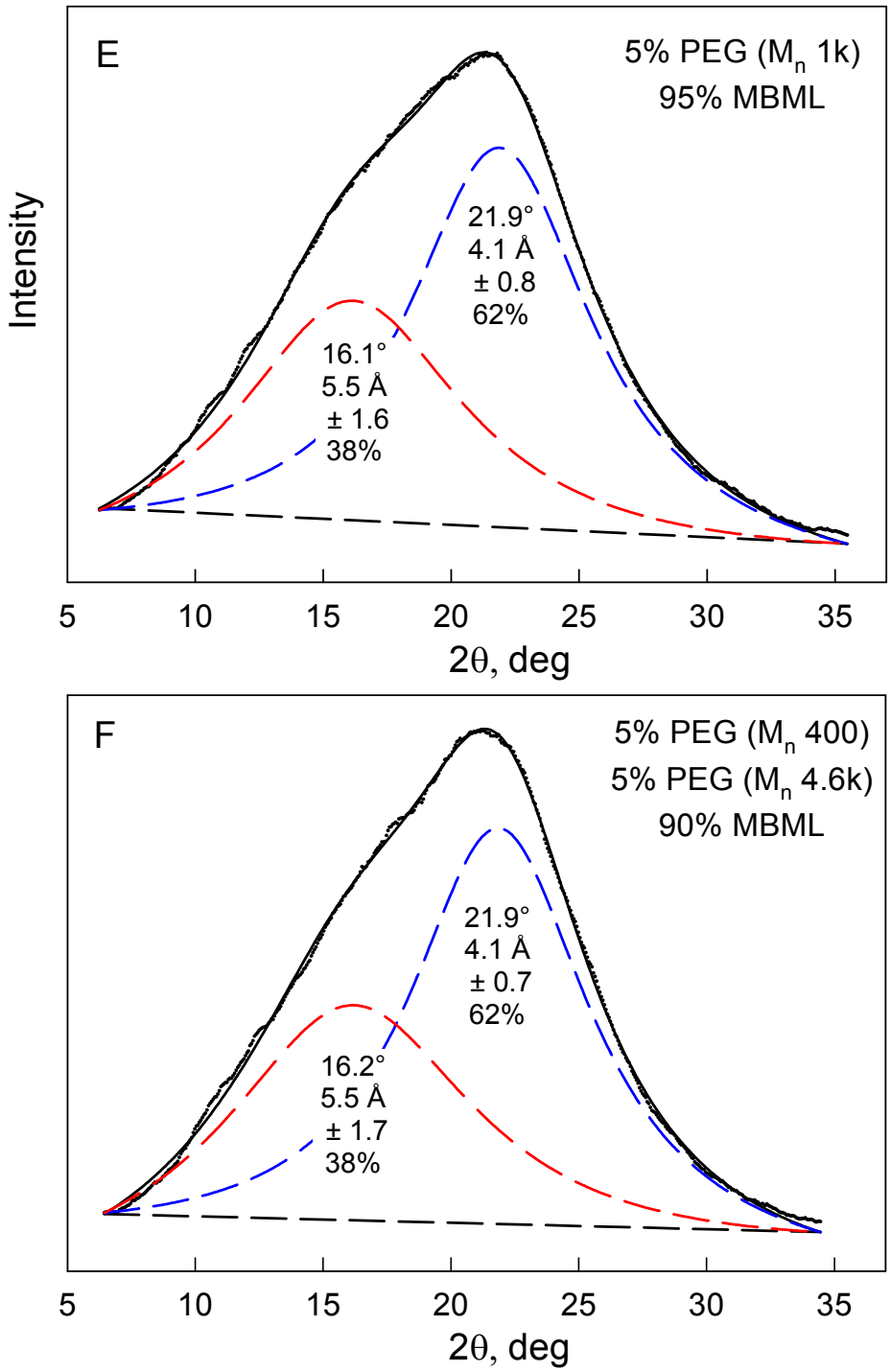

Figure 6.11 E & F Analysis of x-ray powder diffraction patterns of methylated ball-milled lignin (MBML)-based materials using two Lorentzian functions $I(x) = I(0)/(1 + x^2/\text{hwhm}^2)$, $x = 2\theta - 2\theta_k$, where $I(x)$ is the scattered intensity at x from the Bragg angle $2\theta_k$ for the peak, 2θ is the scattering angle, and hwhm is the half-width at the half-maximum of the peak.

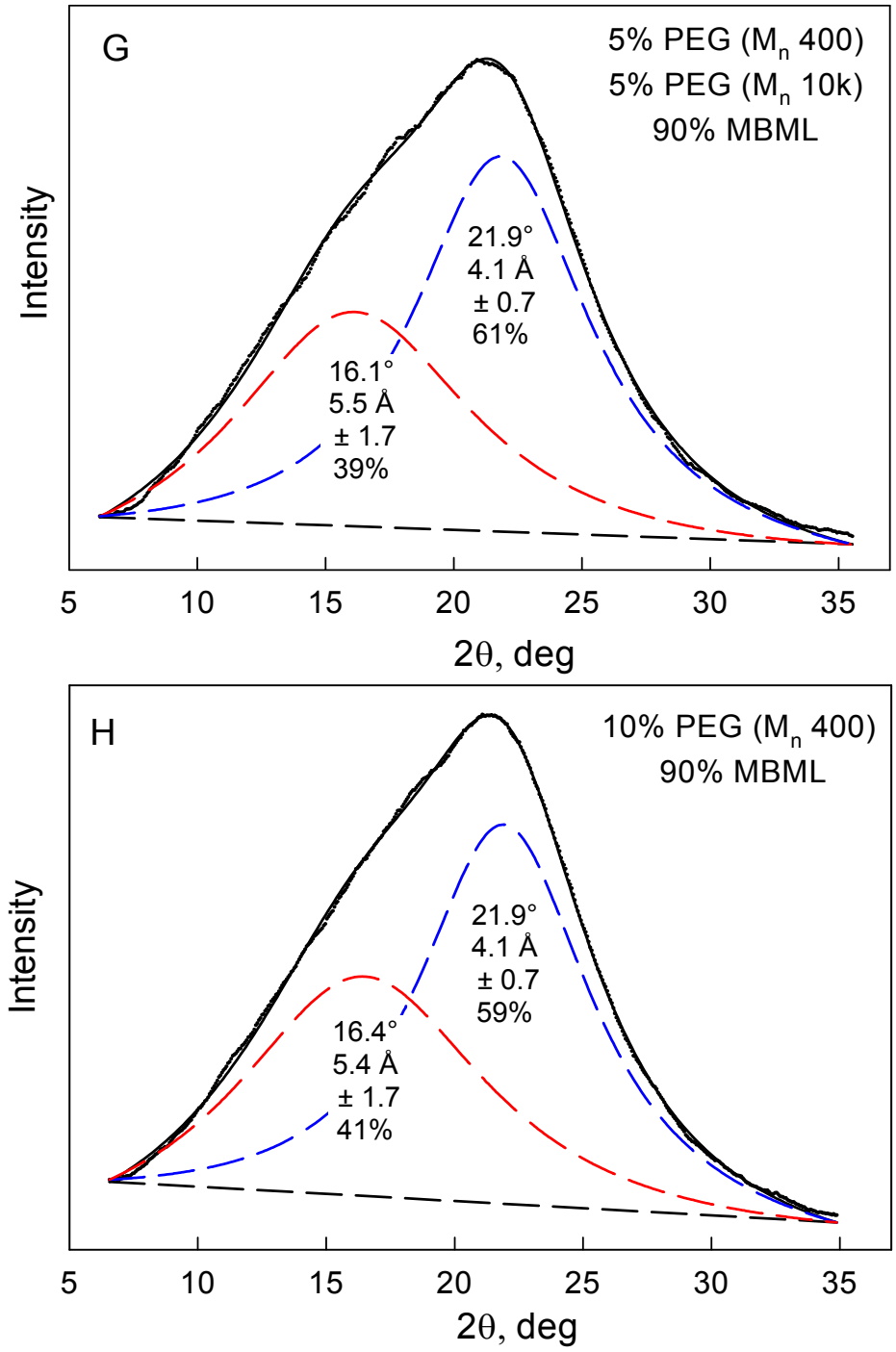

Figure 6.11 G & H Analysis of x-ray powder diffraction patterns of methylated ball-milled lignin (MBML)-based materials using two Lorentzian functions $I(x) = I(0)/(1 + x^2/\text{hwhm}^2)$, $x = 2\theta - 2\theta_k$, where $I(x)$ is the scattered intensity at x from the Bragg angle $2\theta_k$ for the peak, 2θ is the scattering angle, and hwhm is the half-width at the half-maximum of the peak.

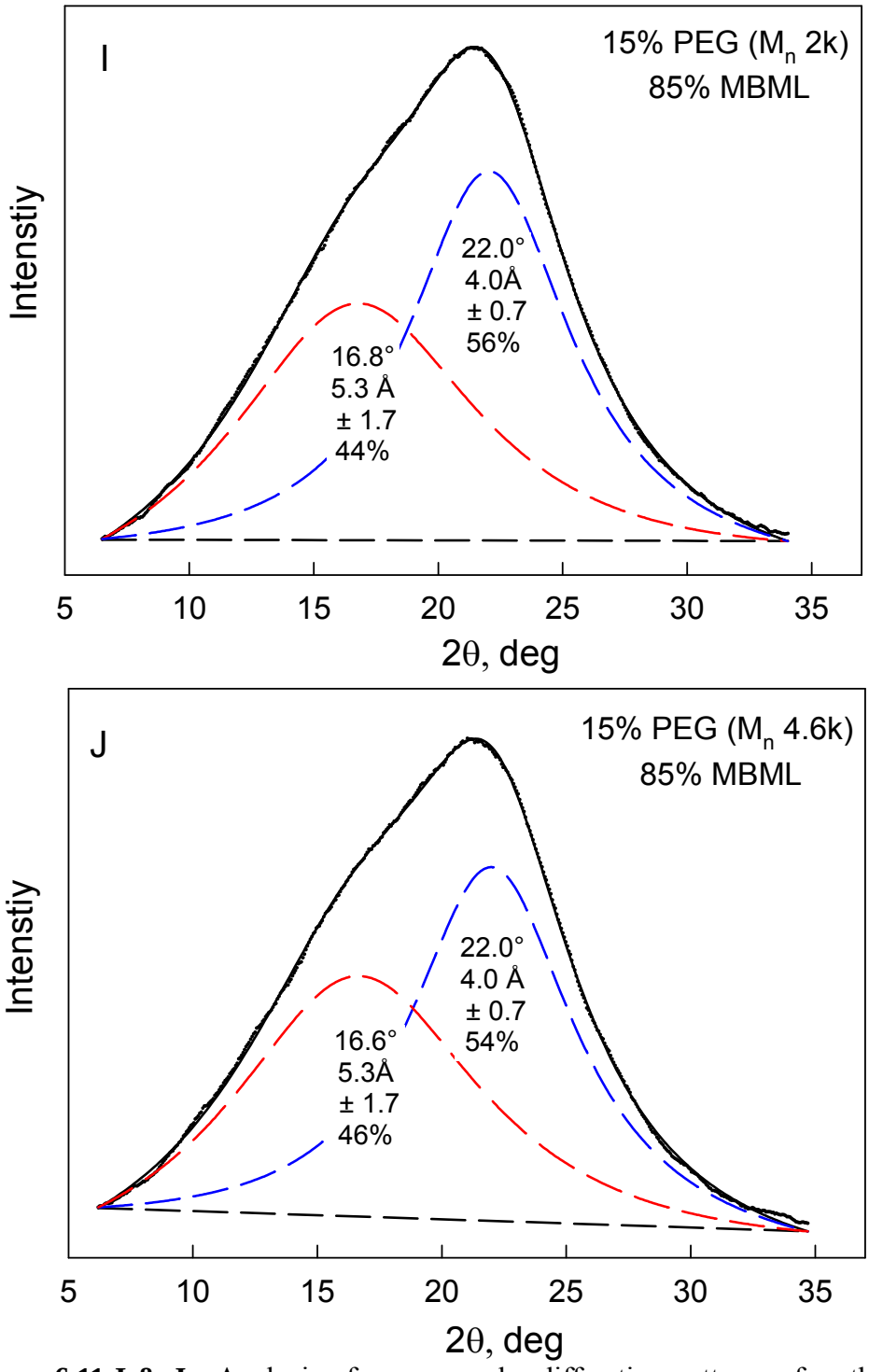

Figure 6.11 I & J Analysis of x-ray powder diffraction patterns of methylated ball-milled lignin (MBML)-based materials using two Lorentzian functions $I(x) = I(0)/(1 + x^2/\text{hwhm}^2)$, $x = 2\theta - 2\theta_k$, where $I(x)$ is the scattered intensity at x from the Bragg angle $2\theta_k$ for the peak, 2θ is the scattering angle, and hwhm is the half-width at the half-maximum of the peak.

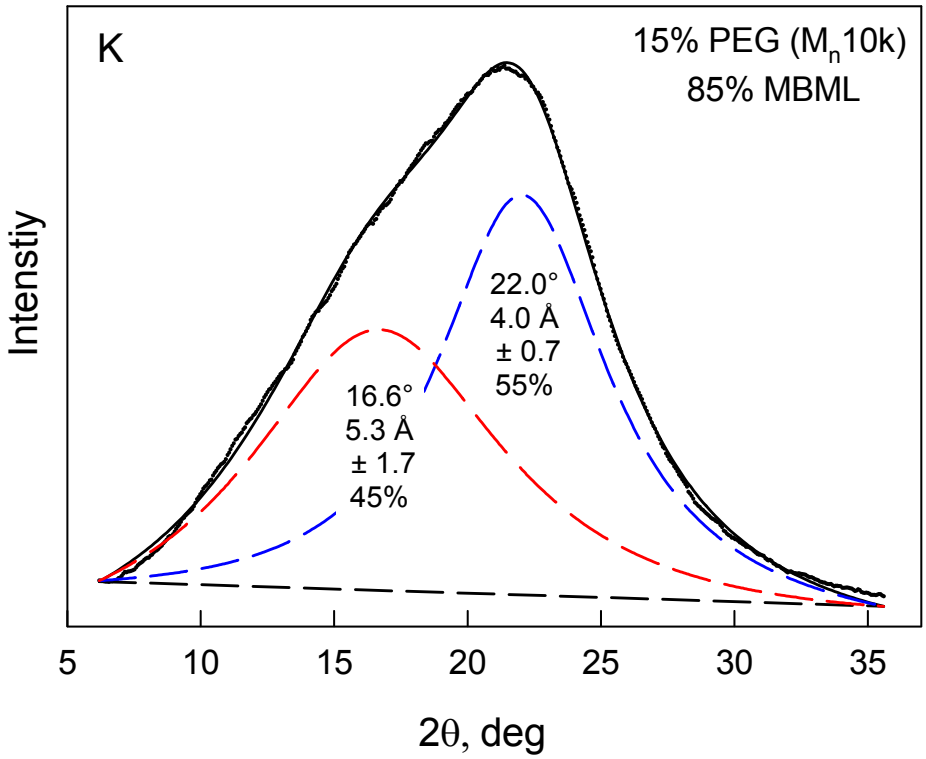

Figure 6.11 K Analysis of x-ray powder diffraction pattern of methylated ball-milled lignin (MBML)-based material using two Lorentzian functions $I(x) = I(0)/(1 + x^2/\text{hwhm}^2)$, $x = 2\theta - 2\theta_k$, where $I(x)$ is the scattered intensity at x from the Bragg angle $2\theta_k$ for the peak, 2θ is the scattering angle, and hwhm is the half-width at the half-maximum of the peak.

In the case of the MBML in blends with 5~15% PEG, the area of the lower-θ Lorentzian component peak increases monotonically with PEG content (Fig. 6.13), and the higher-θ Lorentzian component peak remains centered with little variation approximately around the same position (Fig. 6.11 D~K), even though the peak of pure amorphous PEG exhibits a maximium around $2\theta = 23^o$ (data not shown). Of course, PEG itself contributes very little to the x-ray diffraction patterns of MBML-based blends.

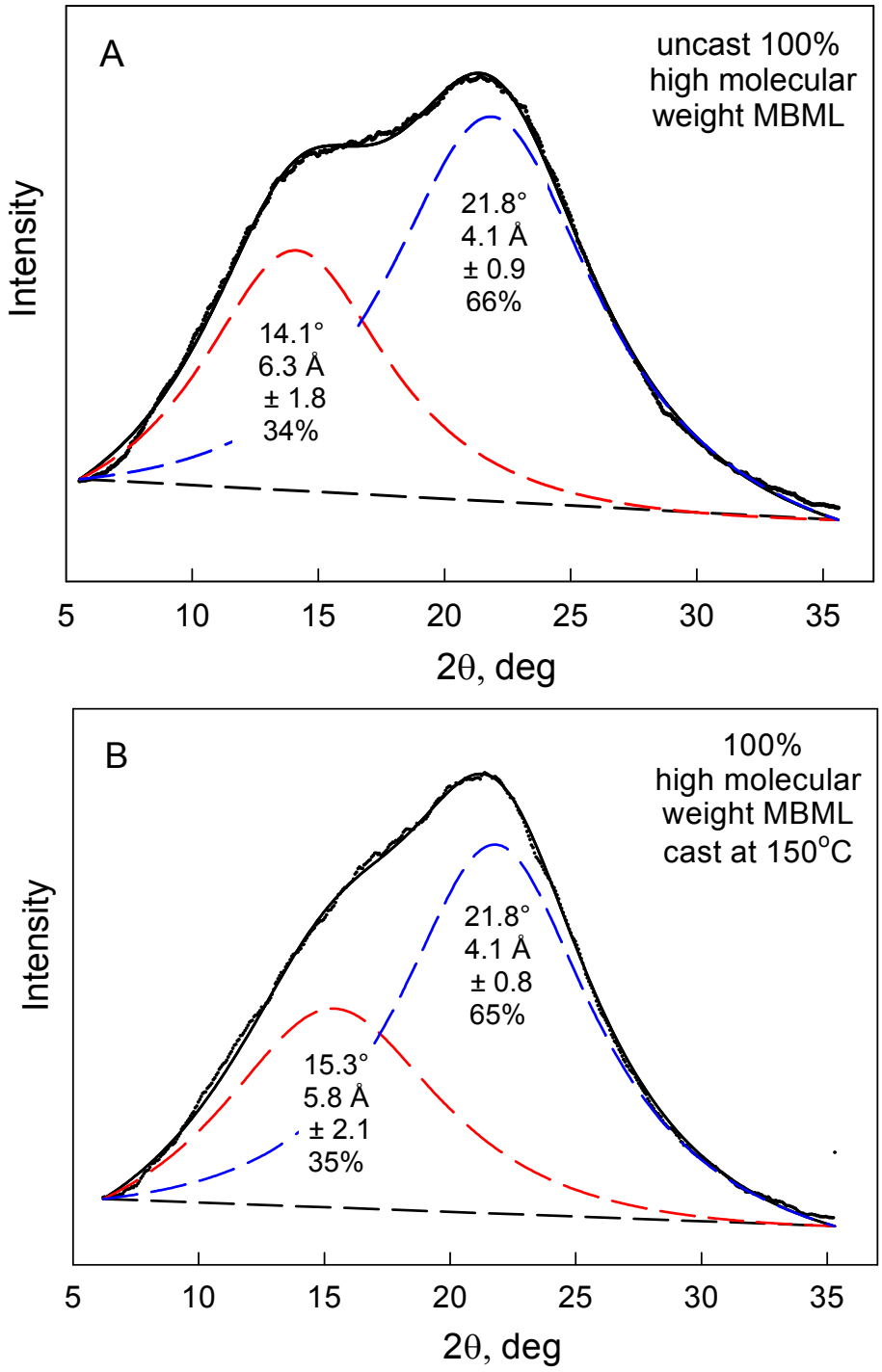

Figure 6.12 A&B Analysis of x-ray powder diffraction patterns of high molecular weight methylated ball-milled (MBML) lignin-based materials using two Lorentzian functions $I(x) = I(0)/(1 + x^2/\text{hwhm}^2)$, $x = 2\theta - 2\theta_k$, where $I(x)$ is the scattered intensity at x from the Bragg angle $2\theta_k$ for the peak, 2θ is the scattering angle, and hwhm is the half-width at the half-maximum of the peak.

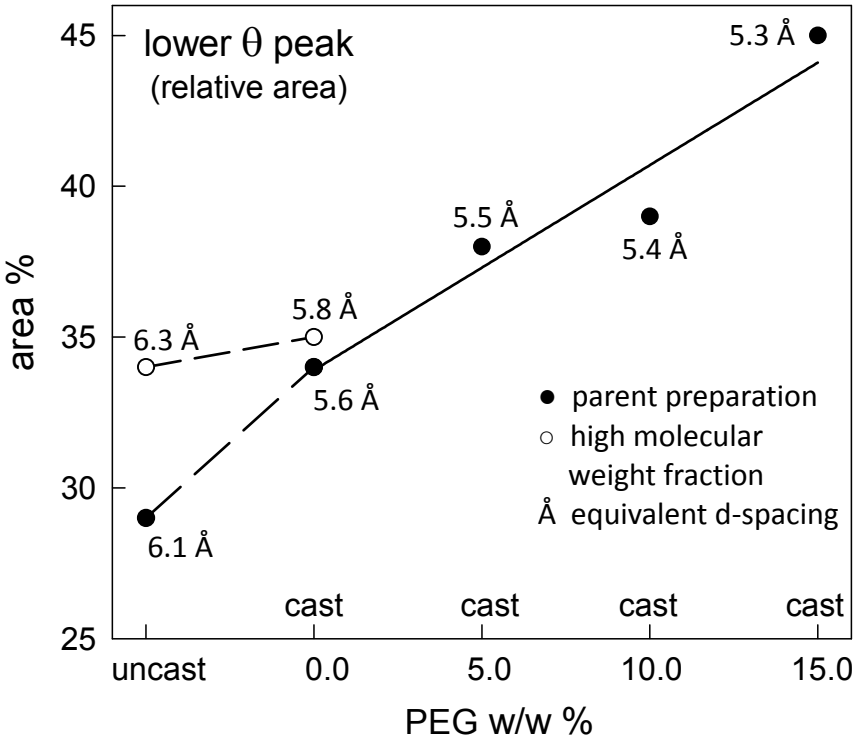

Figure 6.13 Relative areas of lower-θ Lorentzian component peaks in x-ray powder diffraction patterns of methylated ball-milled lignin-based material blends with increasing PEG content (av. area and equivalent d-spacing of blends containing same amount of PEG).

6.6 Differential Scanning Calorimetric (DSC) Analyses

Rearrangements of lignin chain segments have also been observed in thermal cycling studies carried out by DSC (Fig. 6.14 A&B): upon heating the material repeatedly through the same temperature range, the T_gs of the uncast parent preparation and high molecular weight fraction of methylated ball-milled lignin incrementally increased from 134 °C and 153 °C, respectively, to 150 °C and 167 °C. Thus, macromolecular chain

mobility in solid lignin domains is clearly influenced by the presence of lower molecular weight components, as was evident from x-ray powder diffraction studies (Fig. 6.13).

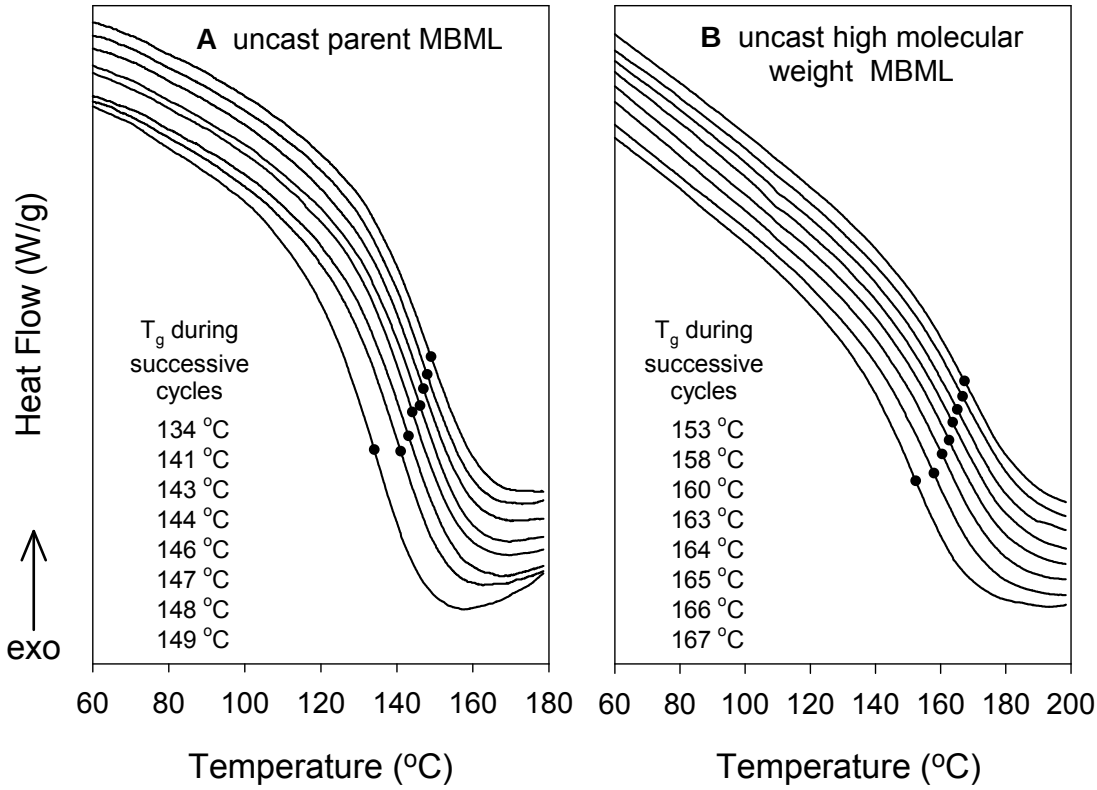

Figure 6.14 DSC thermograms (10 °C min^{-1}) characterizing T_g variation of **(A)** uncast 100% methylated ball-milled lignin (MBML) during successive thermal cycles between 40 and 180 °C, and **(B)** uncast high molecular weight MBML during successive thermal cycles between 40 and 200 °C The T_g's of the polymeric materials are denoted by symbol ●.

The mechanical properties of the MBML-PEG blends are sensitive to the molecular weight distribution of PEG (Fig. 6.10), but their glass transition temperatures (obtained by DSC) exhibit a stronger dependence on the blend composition than the molecular weight distribution of the PEG (Fig. 6.15).

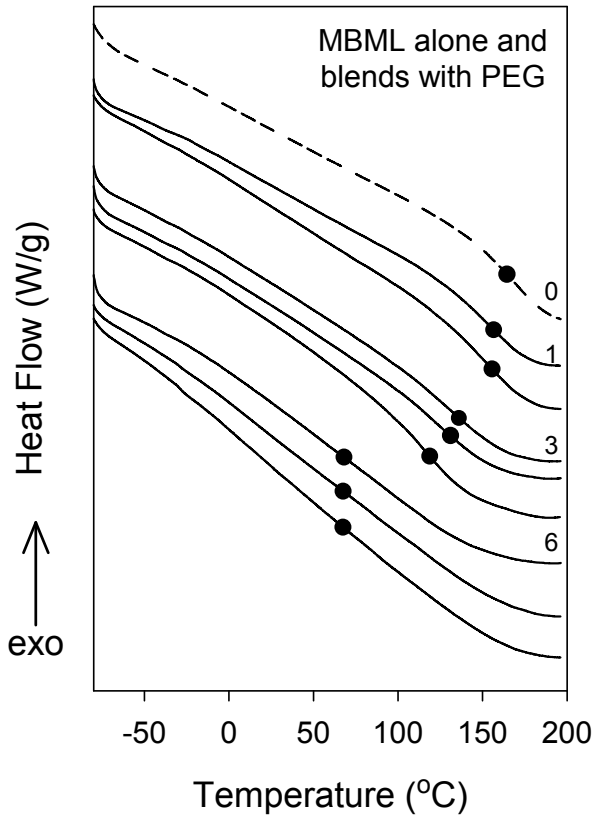

Figure 6.15 DSC thermograms (10 °C min^{-1}) of cast methylated ball-milled lignin (MBML) alone and blends with polyethlene glycol (PEG). [0] cast 100% MBML, T_g 166 °C; [1] 5% PEG M_n 400, T_g 157 °C; [2] 5% PEG M_n 1000, T_g 156 °C; [3] 5% PEG M_n 400 and 5% PEG M_n 10,000, T_g 136 °C; [4] 5% PEG M_n 400 and 5% PEG M_n 4600, T_g 131 °C; [5] 10% PEG M_n 400, T_g 119 °C; [6] 15% PEG M_n 2000, T_g 68 °C; [7] 15% PEG M_n 4600, T_g 67 °C; [8] 15% PEG M_n 10,000, T_g 68 °C.

It is not surprising that PEG is capable of disrupting the peripheral regions in the individual lignin complexes, and the relative proportion of the less stable edge-on configurations for the interacting aromatic rings increases owing to the entropy of mixing. However, the interactions between lignin chain segments and PEG molecules are so weak [Li and Sarkanen, 2005] that the glass transition temperatures for the MBML-based materials with 15% PEG contents are difficult to detect by DSC (Fig. 6.15). By

comparison, the glass transition regions are more readily distinguishable in the DSC thermograms of MBML blends with low T_g polyesters such as PTMG, PTMS and PES (Fig. 6.16). The equivalent Bragg spacing of the lower-θ Lorentzian component peak has been reported to increase when more PTMS is added to the methylated kraft lignin-based blends [Li and Sarkanen, 2005]. All of the above observations are consistent with the working hypothesis that T_gs traditionally ascribed to lignins arise from the molecular motions of lignin chain segments in the peripheral regions of the associated macromolecular lignin complexes. If this were not the case, it would be difficult to account for the (almost complete) disappearance of the glass transition in MBML blends with 15% PEG contents (Fig. 6.15).

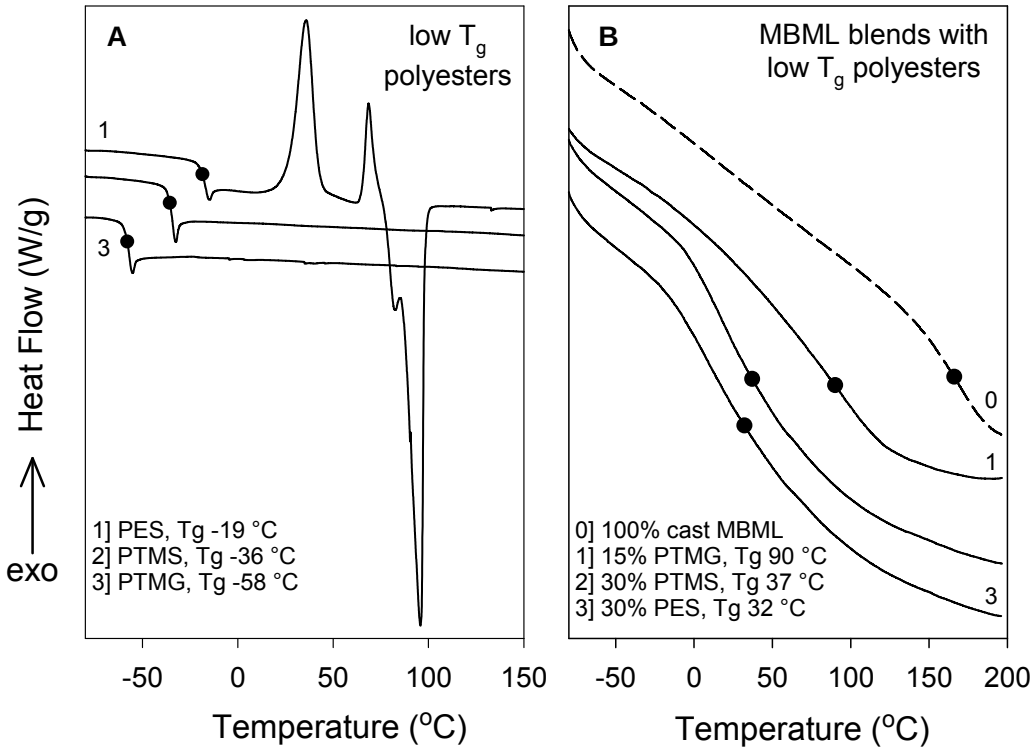

Figure 6.16 DSC thermograms (10 °C min^{-1}) of **(A)** poly(ethylene succinate) (PES), poly(trimethylene succinate) (PTMS) and poly(trimethylene glutarate) (PTMG), and **(B)** methylated ball-milled lignin (MBML)-based blends with PTMG, PTMS and PES, respectively.

6.7 Atomic Force Microscopy (AFM)

6.7.1 Experimental

The lignin-based plastics sample was sectioned and trimmed with a razor blade, and then mounted in an AFM specimen holder fitted with a double-D clamp (Mager Scientific Inc., Dexter, MI) for ultramicrotomy. The surface of the specimen was smoothed by ultramicrotome-cutting using a 45° glass blade on a Leica EM UC6 apparatus to produce successive layers with a step size of 1 μm. The mirror-like surface was burnished further using a step size of 300 nm several times, and the resulting new surface was subjected to AFM scanning immediately. The polystyrene pellets (Aldrich) were used as received for this purpose, while the lignin-based plastics were produced by solution-casting.

The AFM experiments were performed in air on a Bruker Nanoscope V multimode 8 scanning probe microscope employed in a tapping mode for generating a tip-oscillation-amplitude image (produced in response to interactions with the sample surface). The monolithic silicon probe (Arrow^{TM} NCR, NanoWorld AG, Switzerland) employed in this work features a 160-μm-long cantilever with a force constant of 42 N/m and resonance frequency of 285 kHz, and a tetrahedral tip with a height of 10-15 μm and a typical radius of curvature that is less than 10 nm.

AFM scans were collected by a Nanoscope 8.15 (Bruker) while online plane-fitting for images during scanning was turned off. Gwyddion 2.36 (developed by David Nečas *et al.*) was employed to process and analyze the output AFM images. Lines in the height image were corrected (i.e., eliminated) by matching the height median. Other reported images were not post-processed. The center-to-center distances between the adjacent

nodules in the amplitude image were collected manually. The quality of ultramicrotome-cutting was evaluated by the one-dimensional roughness average, R_a, as defined in Eq. 6.7.1-1, where N is the total number of pixels while z_j and $\bar{z}$ are the height of individual pixel j and the mean height of the image, respectively.

$$R_a = \frac{1}{N}\sum_{j}^{N}\left|z_j - \bar{z}\right| \qquad (6.7.1\text{-}1)$$

6.7.2 Results and discussion

The AFM images obtained from this research were scanned in a tapping mode where all forces applied are vertical to the sample surface, so that tip-induced surface deformation is significantly reduced. As shown in Fig. 6.17 A, the ultramicrotome-cut surface of the cast parent methylated ball-milled lignin-based material exhibits a nodular structure with an average diameter of 12.8 ± 3.3 nm (where the range refers to the root-mean-square variation in size). The lignin-based blend containing 15% poly(ethylene glycol) was ultramicrotome-cut at -40 °C (Fig. 6.18) and room temperature (for which the AFM images are not shown here) separately for comparative purposes. The shapes of the nodules observed in the two cases are quite similar, which may be largely a consequence of tip-convolution [Villarrubia, 1994]. Their sizes tend to be appreciably affected by the temperature at which the lignin-based plastic pieces were ultramicrotome-cut: larger nodules (with an average diameter of 16.3 ± 4.6 nm) were observed on the surface formed at room temperature, compared to the those (with an average diameter of 14.6 ± 4.2 nm)

obtained at -40 °C. Material deformability (resulting in partial coalescence) dependent on the processing temperature may account for the variation in nodule size.

The surface created by ultramicrotome-cutting represents a minimal energy fracture passing through non-covalent interactions between molecules or minimum-density profiles in the materials [Aspbury and Wake, 1979]. Here an interesting question arises as to whether the nano-scale nodules visualized with the AFM embody the supramolecular structure of the associated lignin complexes in condensed materials. In an AFM study on an ultramicrotome-cut epoxy surface, it was claimed that the sample surface with R_a less than 0.5 nm did not appear to be nodular [Haba *et al.*, 2014]. Nevertheless for lignin-based materials (Figs. 6.17 and 6.18) and polystyrenes with different molecular weight distributions (Figs. 6.20-22), the freshly ultramicrotome-cut surfaces were invariably nodular even in the areas with $R_a < 0.7$ nm.

However, the nodule contours on the ultramicrotome-cut surface of the solution-cast methylated parent ball-milled lignin visible in Fig. 6.17 became much more difficult to discern with AFM after 6 days at room temperature (Fig. 6.19). Although this lignin-based plastic itself is quite rigid at room temperature, associated lignin complexes that are partially exposed as a result of ultramicrotomy seem to undergo partial coalescence through relaxation of the peripheral components that had been previously immobilized by the surrounding complexes in the body of the amorphous material. Incidentally, it has been reported elsewhere that the nodule diameter of amorphous polycarbonate films increased from 4~6 nm to 25 nm after annealing at a temperature below T_g for 5 days [Neki and Geil, 1973].

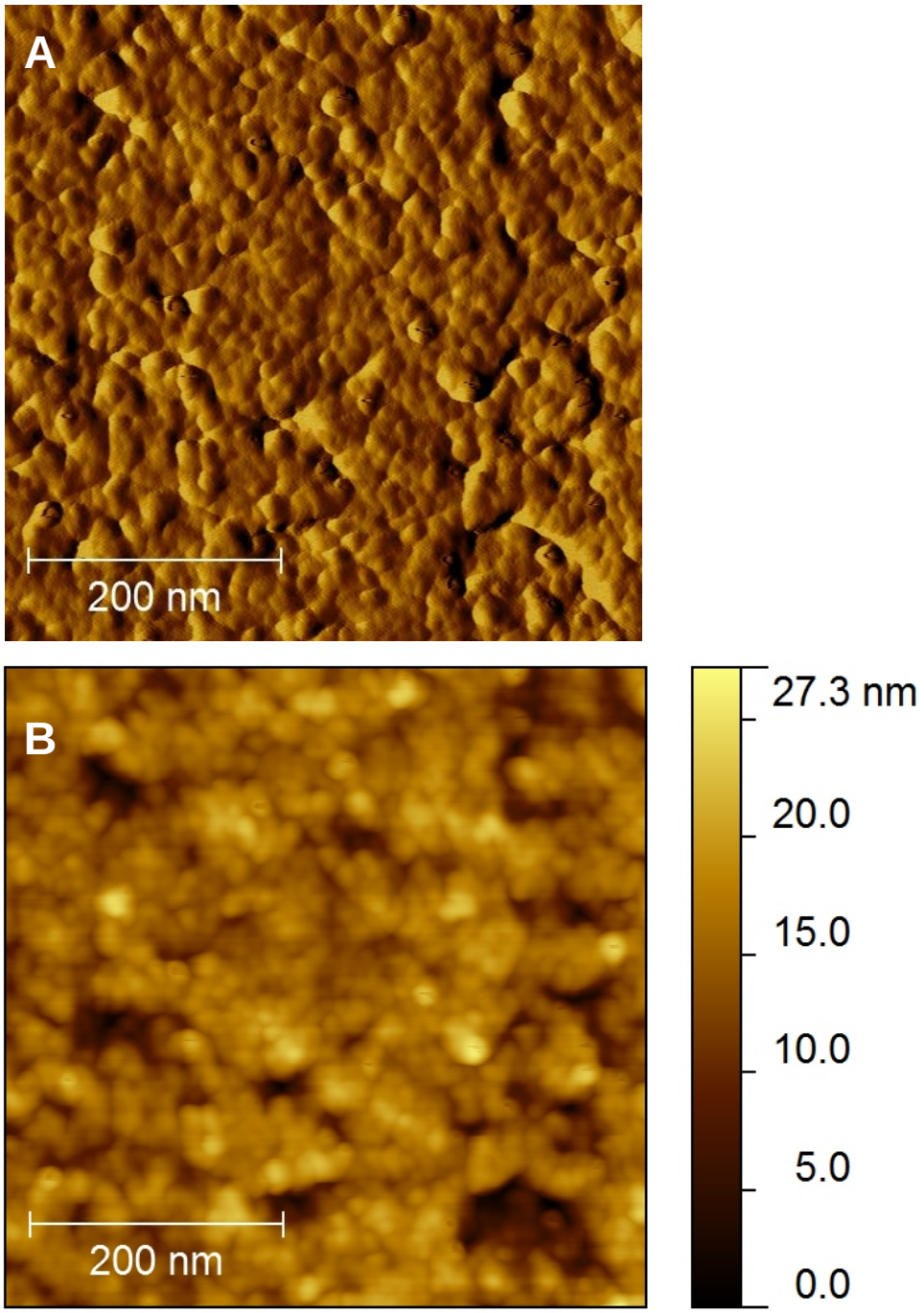

Figure 6.17 Tapping-mode AFM amplitude (**A**) and height (**B**) image (500 nm × 500 nm) of ultramicrotome-cut surface of 100% parent methylated ball-milled lignin (cast at 150 ºC for 23 h). Ultramicrotomy was performed at room termperature. The nodule diameter (12.8 ± 3.3 nm) represents the average of 892 center-to-center distances between adjacent nodules in image **A**. In image **B**, R_a < 0.9 nm.

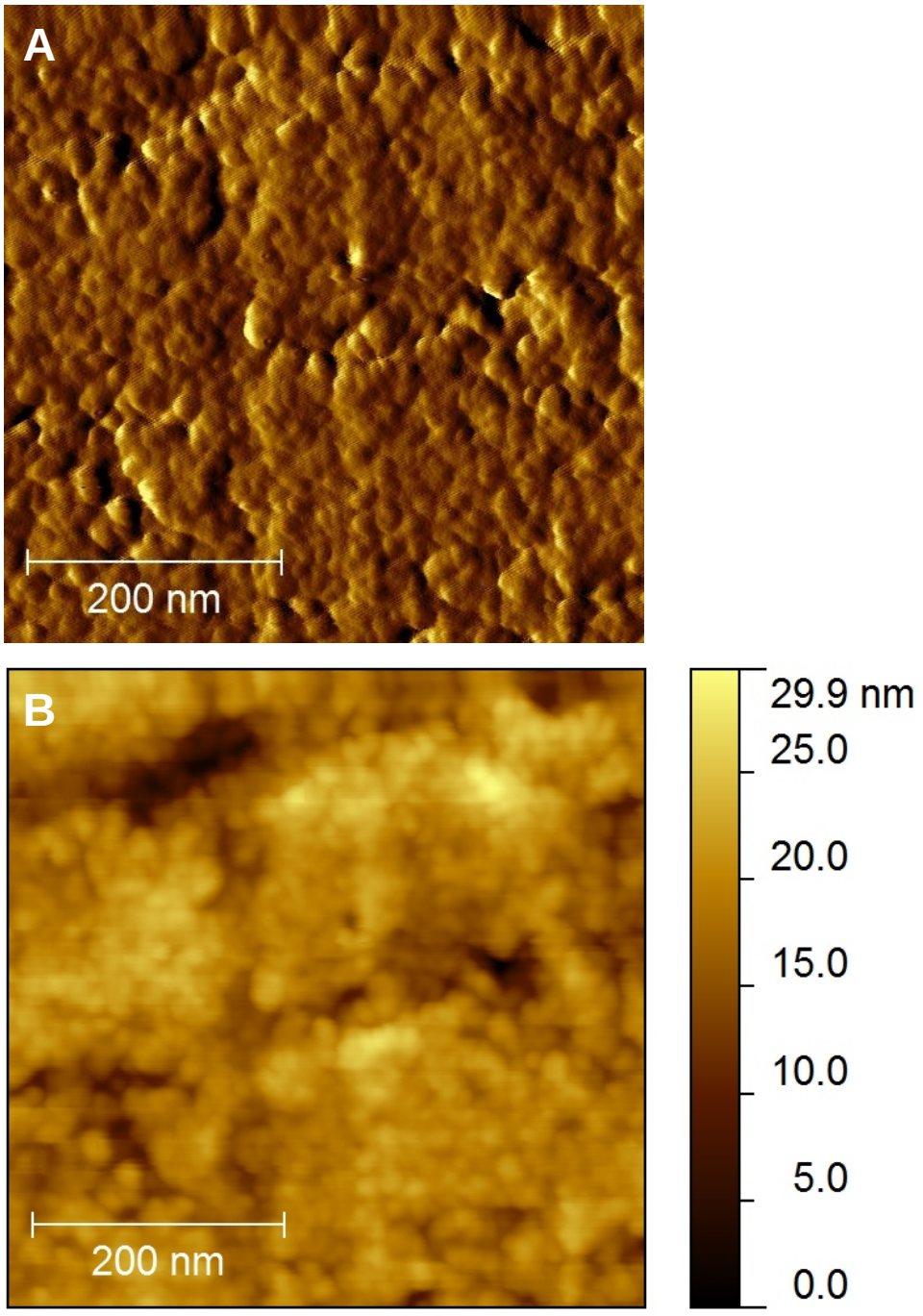

Figure 6.18 Tapping-mode AFM amplitude (**A**) and height (**B**) image (500 nm × 500 nm) of ultramicrotome-cut surface of methylated ball-milled lignin-based blend containing 15% poly(ethylene glycol) (M_w 10,000). Ultramicrotomy was performed at -40 °C. The nodule diameter (14.6 ± 4.2 nm) represents the average of 790 center-to-center distances between adjacent nodules in image **A**. In image **B**, R_a < 0.8 nm.

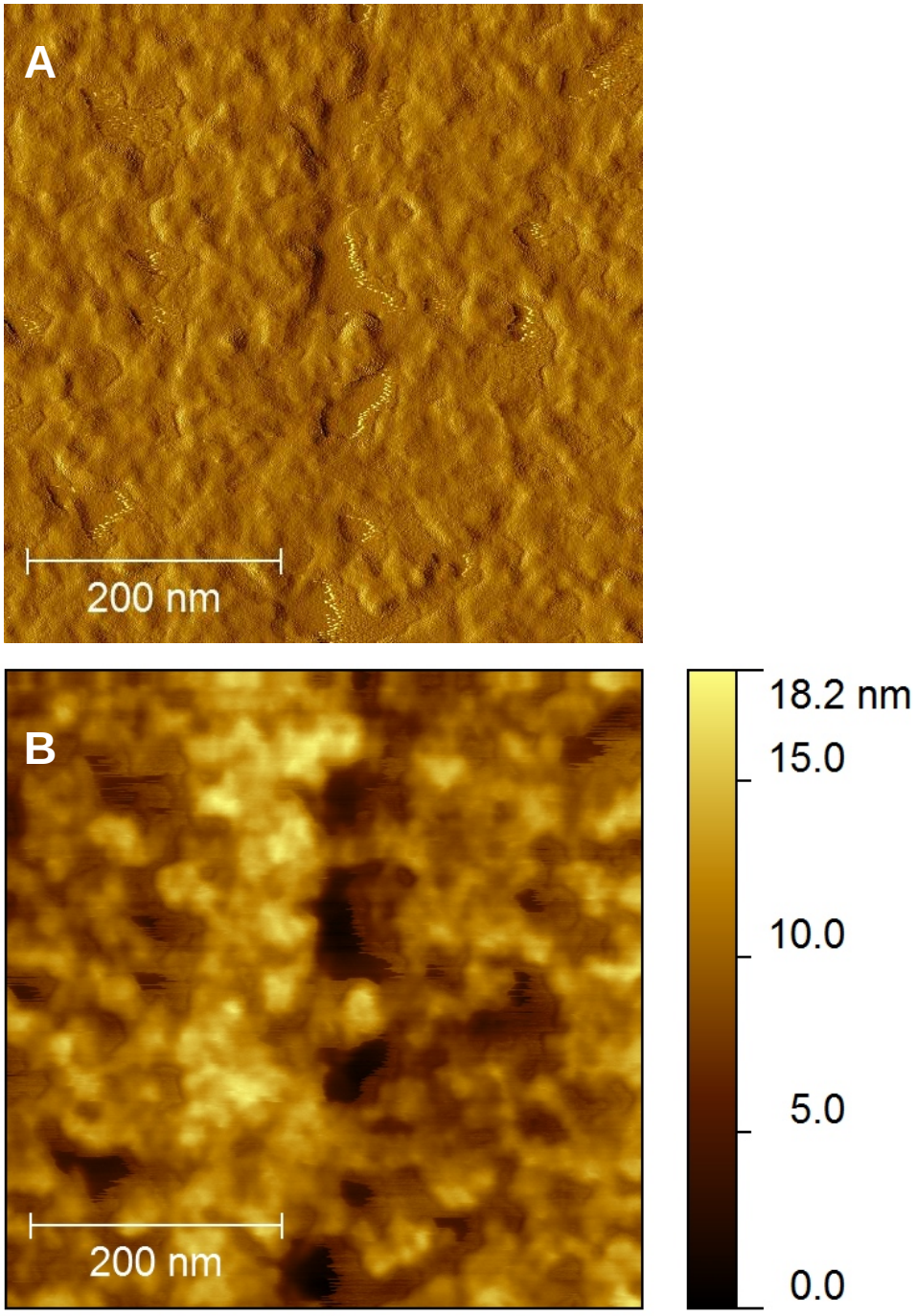

Figure 6.19 The re-scanned amplitude (**A**) and height (**B**) image (500 nm × 500 nm) of the surface presented in Fig. 6.17. The ultramicrotome-cut surface of 100% parent methylated ball-milled lignin (cast at 150 ºC for 23 h) had been kept at room temperature in a dust-free environment for 6 days. In image **B**, $R_a < 0.7$ nm.

Polystyrene pellets with different molecular weight distributions were employed as comparative references in these AFM studies of the surfaces of condensed lignin-based polymeric materials. Their ultramicrotome-cut surfaces exhibit uniform nodular topology (Figs. 6.20-22), and the diameters of the nodules tend to increase with the molecular weight of the polystyrene preparation. It was proposed in the random-coil model [Flory, 1976] that the flexible chain segments in amorphous polymers adopt the same conformations they possess in dilute solutions under θ conditions when the solute-solute and solvent-solute interactions cancel one another out. The measured nodule diameter (D) is approximately equal to (the extrapolated value of) $2R_g$, twice the radius of gyration of polystyrene in cyclohexane at the θ temperature (Table 6.2). Hereby, the R_g (Å) is estimated from the empirical Eq. 6.7.2-1 [Hiemenz and Lodge, 2007; Miyaki *et al.*, 1978] on the basis of the weight-average molecular weight (M_w) of the corresponding polystyrene sample.

$$R_g = 0.25 M_w^{0.51} \qquad (6.7.2\text{-}1)$$

In this context, the nodules observed on the ultramicrotome-cut polystyrene surfaces imaged with the AFM may embody random coils that pack to bulk densities. Similarly, it can be concluded that the nodular topology on the freshly cut surfaces of the lignin-based materials arises from partially coalesced associated lignin complexes.

Estimates for the average molecular weight of these macromolecular lignin species can be deduced from the differing relationships between R_g and M_w for polystyrene (Eq. 6.7.2-1, above) and the (unmethylated) lignin itself (Fig. 5.2), which together imply a possible range that tentatively falls between 54 kDa and 68 kDa.

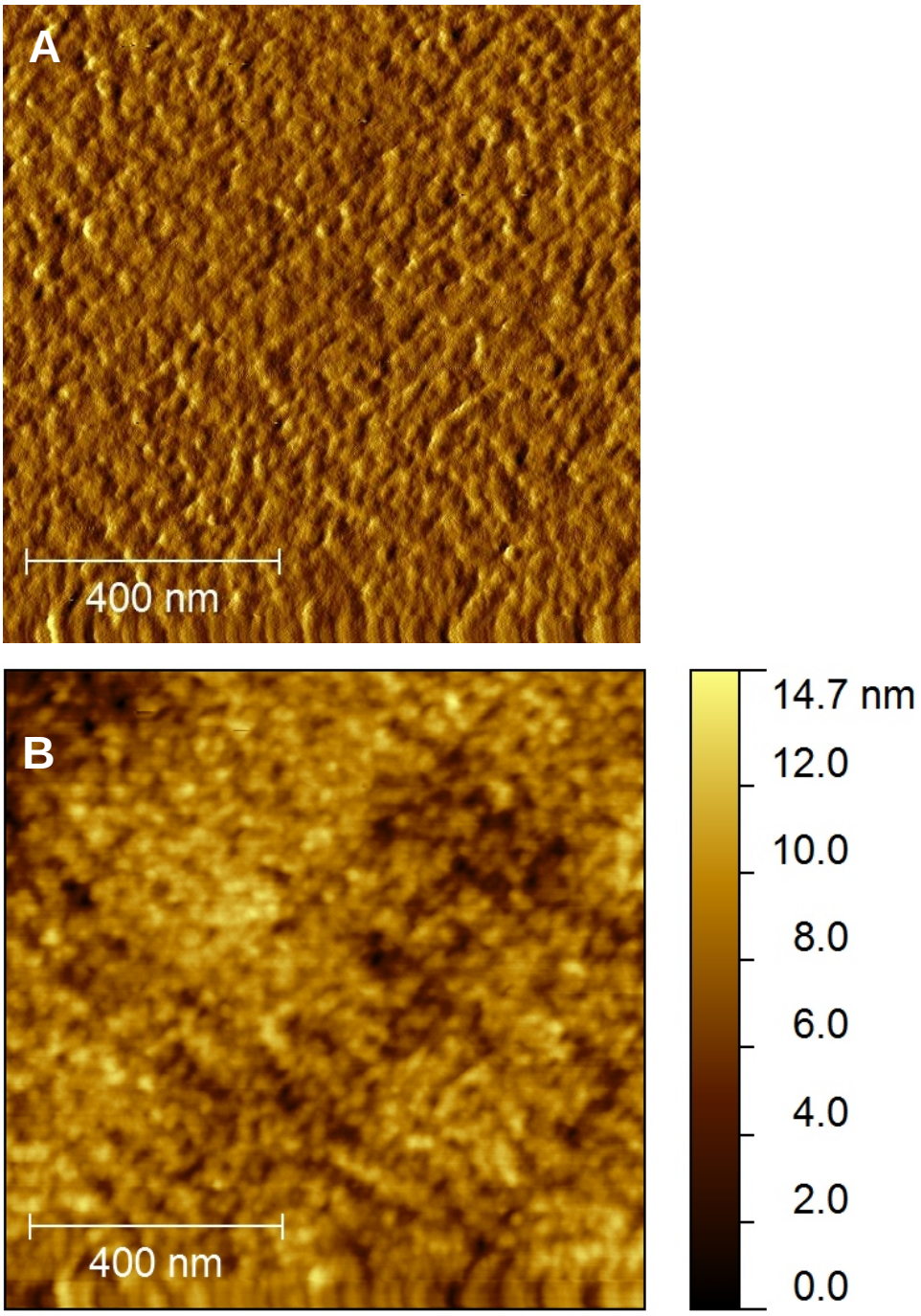

Figure 6.20 Tapping-mode AFM amplitude (**A**) and height (**B**) image (1 μm × 1 μm) of ultramicrotome-cut surface of polystyrene (M_w 190,000) pellet. Ultramicrotomy was performed at -60 °C. The nodule diameter (23.3 ± 6.1 nm) represents the average of 654 center-to-center distances between adjacent nodules in image **A**. In image **B**, Ra < 0.9 nm.

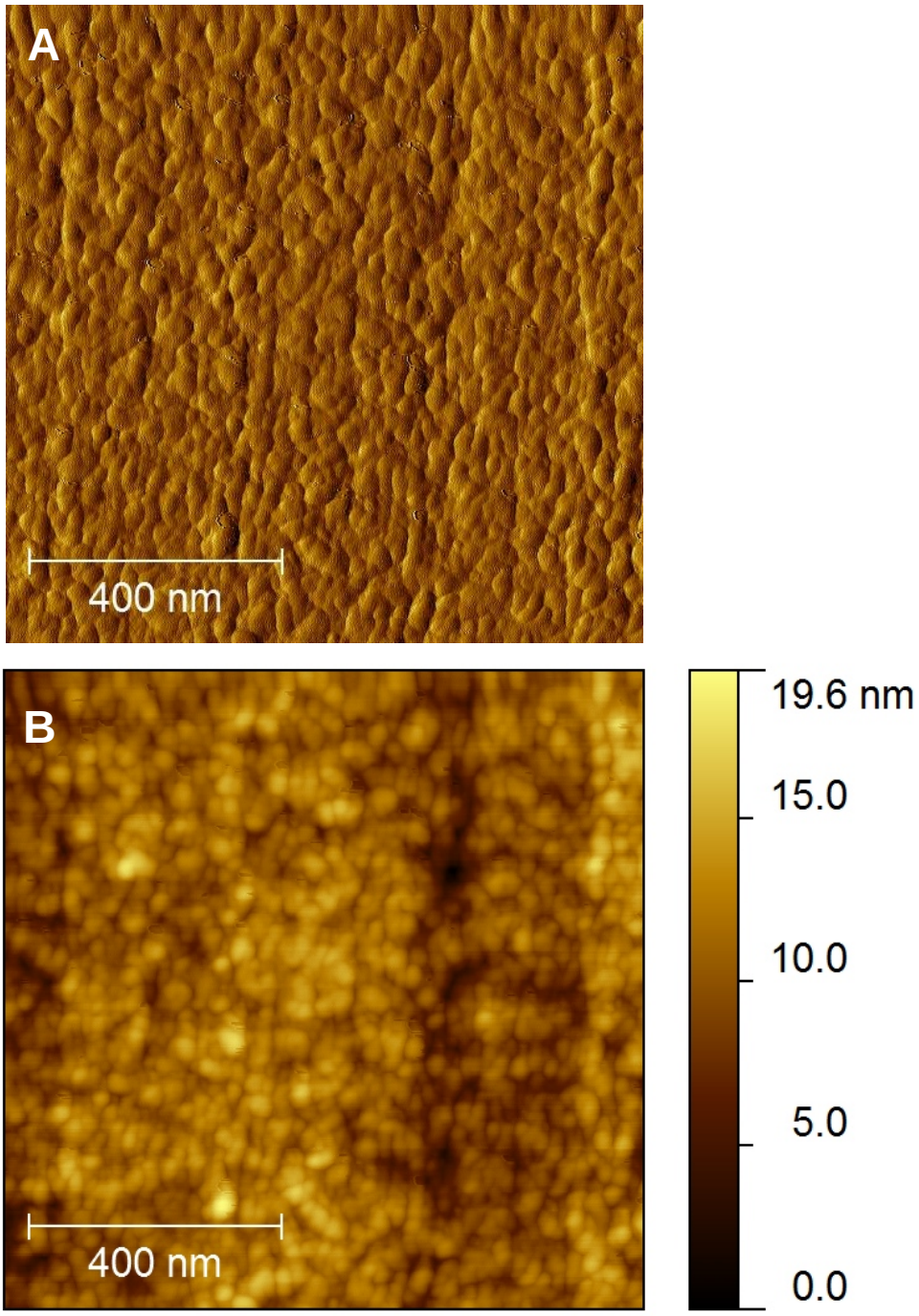

Figure 6.21 Tapping-mode AFM amplitude (**A**) and height (**B**) image (1 μm × 1 μm) of ultramicrotome-cut surface of polystyrene (M_w 280,000) pellet. Ultramicrotomy was performed at -60 °C. The nodule diameter (25.3 ± 6.6 nm) represents the average of 940 center-to-center distances between adjacent nodules in image **A**. In image **B**, R_a < 0.8 nm.

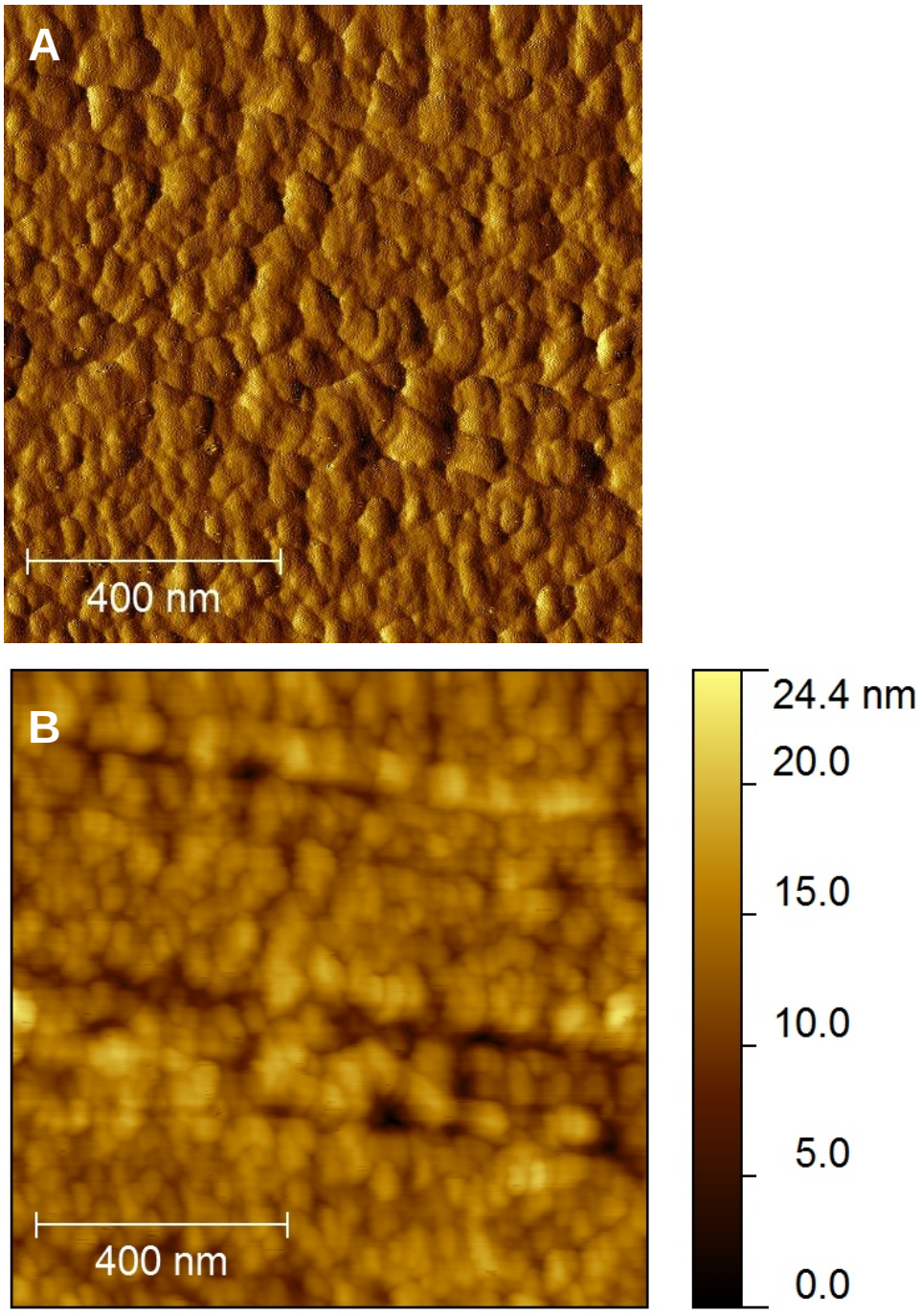

Figure 6.22 Tapping-mode AFM amplitude (**A**) and height (**B**) image (1 μm × 1 μm) of ultramicrotome-cut surface of polystyrene (M_w 350,000) pellet. Ultramicrotomy was performed at -60 °C. The nodule diameter (35.0 ± 10.4 nm) represents the average of 775 center-to-center distances between adjacent nodules in image **A**. In image **B**, $R_a < 0.8$ nm.

Table 6.2 Comparison between the predicted radius of gyration (R_g) of polystyrene in cyclohexane at the θ temperature [Hiemenz and Lodge, 2007; Miyaki *et al.*, 1978] and the measured diameter (D) of the nodules on ultramicrotome-cut polystyrene surfaces.

polystyrene M_w	predicted $2R_g$,nm[a]	measured D, nm[b]
190,000	24.6	23.3 ± 6.1
280,000	30.0	25.3 ± 6.6
350,000	33.6	35.0 ± 10.4

a. R_g was estimated by using Eq. 6.7.2-1
b. The values of D represent the averages of manually measured center-to-center distances between neighboring nodules in Figs. 6.20 A, 6.21 A and 6.22 A, respectively. The range of variation refers to the apparent size distribution, not errors in the measurements.

6.8 Conclusions

The feasibility of plasticizing methylated native softwood lignin with various plasticizers possessing different molecular weights and chemical properties has been examined in chapter. Among the candidate plasticizers tested, EBE, PEG and TBBP-A exhibit significant enhancements in ultimate tensile strength for the MBML-based polymeric materials at incorporation levels below 20%. Certain aliphatic diesters and PEG exhibit synergetic plasticization effects in tertiary blends with MBML. However monomeric plasticizers by themselves are not sufficient to improve lignin-based polymeric material ductility; in fact they may function as replacements for low-molecular weight lignin components that are lost during solution casting.

Through x-ray powder diffraction studies on parent and high-molecular-weight MBML preparations and their blends with PEGs, we found that two prominent Lorentzian

component peaks (the sums of which closely approximate to the overall diffraction pattern) can be correlated with the cofacial and edge-on configurations of non-covalently interacting aromatic rings in the lignin components. Their area ratios (cofacial to edge-on) in parent MBML preparations decrease after solution casting at elevated temperatures, and more of the cofacial configurations have been transformed into edge-on arrangements with increasing PEG content in the parent MBML-based blends. The intermolecular separations between the edge-on aromatic rings are appreciably sensitive to blend composition (decreasing somewhat with increasing PEG content, for example), while those between the cofacial aromatic rings are hardly affected. Based upon the preceding observations, we propose that in the condensed-phase MBML-based plastics, lignin macromolecules participate in the structures of partially coalesced associated complexes, where the cofacial aromatic rings occurs mainly within the inner regions, while the edge-on arrangements with much lower stabilization energies are found in the peripheral domains giving rise to continuity in the material as a whole.

The plasticization effects are governed by the interactions between the plasticizers and lignin components, or more specifically, the location of the plasticizer molecules in regard to the associated lignin complexes. When such interactions are powerful, monomeric plasticizers such as DEA or TBBP-A are incorporated more readily into the peripheral domains of the complexes, and they are able enhance the mobility of the surrounding lignin chain segments so that relative displacement between neighboring associated complexes may be more readily tolerated. On the other hand, when the lignin–plasticizer interactions are weaker and small molecules like DEG are excluded from

insertion between individual peripheral components in the lignin complexes, they may form a layer of lubricant located between neighboring associated macromolecular species. The mechanical strength of these lignin-based materials depends more on the interactions between complexes than chain entanglements involving individual lignin macromolecules, and therefore such materials can weaken rapidly as more monomeric plasticizer is introduced.

In the case of polymeric plasticizers, PEG macromolecules interact weakly with lignin components, but PEG preparations with molecular weight below 10,000 and above 400 are waxy materials which hardly possess any strength. Hence, an ideal plasticizer may be a low-T_g polymer that interacts as strongly as possible with associated lignin complexes without dismantling their inner structures. Concomitantly, this plasticizer should be capable of interposing viscoelastic domains between the more rigid lignin complexes so that the ductility of the blends as a whole will be enhanced.

BIBIOGRAPHY

Agosin, E., Jarpa, S., Rojas, E., Espejo, E., *Enzyme Microb Technol*, **1989**, 11, 511-7

Almanza, O. A., Rodríguez-Peréz, M. A., De Saja, J. A., *J Polym. Sci. B: Polym. Phys.*, **2000**, 38, 993-1004

Aspbury, P. J., Wake, W. C., *Br. Polym. J.*, **1979**, 11, 17-27

Baciocchi, E., Fabbri, C., Lanzalunga, O., *J. Org. Chem.*, **2003**, 68, 9061-9

Balakshin, M. Y., Capanema, E. A., Chang, H.-m., *Holzforschung*, **2007**, 61, 1-7

Björkman, A., *Svensk Papperstidn*, **1956**, 59, 477-85

Blanchette, R. A., Krueger, E. W., Haight, J. E., Akhtar, M., Akin, D. E., *J. Biotechnol*, **1997**, 53, 203-13

Bourbonnais, R., Leech, D., Paice, M. G., *Biochim. Biophys. Acta*, **1998**, 1379, 381-90

Bozell, J. J., Black, S. K., Myer, M., *Proc. 8th Internat. Symp. Wood Pulp. Chem.*, **1995**, I, 697-704

Brunow, G., Kilpeläinen, I., Sipilä, J., Syrjänen, K., Karhunen, P., Setälä, H., Rummakko, P., *ACS Symp. Ser.*, **1998**, 697, 131-47

BSEF, Bromine Science and Environmental Forum, TBBPA Factsheet, Brominated Flame Retardant, Oct. 2013 www.bsef.com/uploads/Documents/documents/BSEf%20factsheet%20TBBPA_web.pdf.

Camarero, S., Barrasa, J. M., Pelayo, M., Martínez, A. T., *J. Pulp Paper Sci.,* **1998**, 24, 197-203

Caramelo, L., Martínez, M. J., Martínez, A. T., *Appl. Environ. Microbiol.*, **1999**, 65, 916-22

Chen, F., Dixon, R. A., *Nat. Biotechnol.*, **2007**, 25, 759-61

Chen, Y.-r., Sarkanen, S., *Phytochem. Rev.*, **2003**, 2, 235-55

Chen, Y.-r., Sarkanen, S., *Phytochem.*, **2010**, 71, 453-62

Ciemniecki, S. L., Glasser, W. G., *Polymer*, **1988**, 29, 1021-29

Contreras, S., Gaspar, A. R., Guerra, A., Lucia, L. A., Argyropoulos, D. S., *Biomacromolecules*, **2008**, 9, 3362-9

Davis, J. R., *Tensile Testing* 2nd ed., ASM International, Materials Park, OH, 2004

de la Rubia, T., Linares, A., Pérez, J., Muñoz-Dorado, J., Romera, J., Martínez, J., *Res. Microbiol.*, **2002**, 153, 547-54

Dutta, S., Garver, T. M. Jr., Sarkanen, S., *ACS Symp. Ser.*, **1989**, 397,155-76

Every, A. E. Russu, I. M., *Biopolymers*, **2007**, 87, 165-73

Faison, B., Kirk, T. K., *Appl. Environ. Microbiol.*, **1983**, 46, 1140-5

Feldman, D., Banu, D., Luchian, C., Wang, J., *J. Appl. Polym. Sci.,* **1991**, 42, 1307-18

Forney, L. J., Reddy, C. A., Tien, M., Aust, S. D., *J. Biol. Chem.*, **1982**, 257, 11455-62

Garver, T. M. Jr., Iwen, M. L., Sarkanen, S., Fifth International Symposium on Wood and Pulping Chemistry, *TAPPI Proceeding*, TAPPI Press, Atlanta, GA, **1989**, Vol. I, 113-9

Gaskell, J., Marty A., Mozuch M., Kersten, P. J., BonDurant, S. S., Sabat, G., Azarpira, A., Ralph, J., Skyba, O., Mansfield, S. D., Blanchette, R. A., Cullen, D., *Appl. Environ. Microbiol.*, **2014**, 80, 5828-35

Gellerstedt, G., **2007**, http://rfparois.free.fr/LIG2G/Seminaire%20LIG2G-WEB-vs-tout-public.htm

Ghosh, I., Jain, R. K., Glasser, W. G., *J. Appl. Polym. Sci.,* **1999**, 74, 448-57

Giardina, P., Faraco, V., Pezzella, C., Piscitelli, A., Vanhulle, S., Sannia, G., *Cell. Mol. Life Sci.*, **2010**, 67, 369-85

Gilardi, G., Cass, A. E. G, *Langmuir*, **1993**, 9, 1721-6

Glasser, W. G., *ACS Symp. Ser.*, **1989**, 385, 43-54

Glasser, W. G., Wang, H.-X., *ACS Symp. Ser.*, **1989**, 397, 515-22

Glenn, J. K., Morgan, M. A., Mayfield, M. B., Kuwahara, M., Gold, M. H., *Biochem. Biophys. Res. Commun.* **1983**, 114, 1077-83

Gold, M. H., Kutsuki, H., Morgan, M. A., *Photochemistry Photobiology*, **1983**, 38, 647-51

Goring, D. A. I., In *Lignins – Occurrence, Formation, Structure and Reactions*, Sarkanen, K.V., Ludwig, C. H., Eds., Wiley-InterScience Publ, New York, **1971**, 695-768

Goring, D. A. I., Vuong, R., Gancet, C., Chanzy, H. J., *J. Appl. polym. Sci.*, **1979**, 24, 931-6

Guan, S. -Y., Mlynár, J., Sarkanen, S., *Phytochem.*, **1997**, 45, 911-8

Haba, D., Kaufmann, J., Brunner, A. J., Resch, K., Teichert, C., *Polymer*, **2014**, 55, 4032-40

Haemmerli, S. D., Leisola, M. S. A., Fiechter, A., *FEMS Microbiol. Lett.*, **1986**, 35, 33-6

Hall, P. L., *Enzyme Microb. Technol.*, **1980**, 2, 170-6

Hammel, K. E., Cullen, D., *Curr. Opin. Plant Biol.*, **2008**, 11, 349-55

Hammel, K. E., Jensen, K. A., Mozuch, M. D. Landucci, L. L., Tien, M., Dease E. A., *J. Biol. Chem.*, **1993**, 268, 12274-81

Hammel, K. E., Kapich, A. N., Jensen, K. A., Ryan, Z. C., *Enzyme Microb. Technol.*, **2002**, 30, 445-53

Hatakeyama, T., Hatakeyama, H., *Polymer*, **1982**, 23, 475-7

Heinfing, A., Martínez, M. J., Martínez, A. T., Bergbauer, M., Szewyk, U., *Appl. Environ. Microbiol.*, **1998**, 64, 2788-93

Hiemenz, P. C., Lodge, T. P., *Polymer Chemistry 2nd Ed.*, CRC Press, New York, **2007**; p 233

Higuchi, T., *Proc. Jpn. Acad., Ser. B*, **2004**, 80, 204-14

Hofmann, K., Glasser, W. G., *J. Wood Chem. Technol.*, **1993**, 13, 73-95

Hsu, O. H.-H., Glasser, W. G., *Appl. Polym. Symp.*, **1975**, 28, 297-307

Hsu, O. H.-H., Glasser, W. G., *Wood Sci.*, **1976**, 9, 97-103

Hu, Z., Yeh, T.-F., Chang, H.-m., Matsumoto, Y., Kadla, J. F., *Holzforschung*, **2006**, 60, 389-97

Karhunen, P., Rummakko, P., Sipilä, J, Brunow, G., Kipeläinen, I., *Tetrahedron Lett.,* **1995**, 36, 169-70

Katagiri, M., Maeno, H., Yamamoto, S., Hayaishi, O., Kitao, T., Oea, S., *J. Biol. Chem.*, **1965**, 240, 3414-7

Katz, J. R., *Trans. Faraday Soc.*, **1936**, 32, 77-94

Kawai, S., Ohashi, H., Hirai, T., Okuyama, H., Higuchi, T., *Mokuzai Gakkaishi*, **1993**, 39, 98-102

Kelly, S. S., Glasser, W. G., Ward, T. C., *Polymer*, **1989**, 30, 2265-8

Kelly, S. S., Ward, T. C., Glasser, W. G., *J. Appl. Polym. Sci.*, **1990**, 41, 2813-28

Kersten, P. J., Tien, M., Kalyanaraman, B., Kirk, T. K., *J. Biol. Chem.*, **1985**, 260, 2609-12

Kim, K. S., Tarakeshwar, P., Lee, J. Y., *Chem. Rev.*, **2000**, 100, 4145-85

Klapetek P., *Quantitative Data Processing in Scanning Probe Microscopy, SPM Applications for Nanometrology*, William Andrew (Elsevier), Oxford, UK, **2013**; p 93

Klug, H. P., Alexander, L. E., *X-ray Diffraction Procedures for Polycrystalline and Amorphous Materials*, Wiley, New York, **1954**, 716

Kutsuki, H., Gold, M. H., *Biochem. Biophys. Res. Commun.*, **1982**, 109, 320-7

Kuwahara, M. Glenn, J. K. Morgan, M. A. Gold, M. H., *FEBS Lett.*, **1984**, 169, 247-50

Lawoko, M., Henriksson, G., Gellerstedt, G., *Biomacromolecules*, **2005**, 6, 3467-73

Lawoko, M., Henriksson, G., Gellerstedt, G., *Holzforschung*, **2006**, 60, 162-5

Levasseur, A., Lomascolo, A., Chabrol. O., *et al.* (33 authors), *BMC Genomics*, **2014**, 15, 486

Li, K., Horanyi, P. S., Collins, R., Phillips, R. S., Eriksson, K.-E. L., *Enzyme Microb. Technol.*, **2001**, 28, 301-7

Li, Y., Mlynár, J., Sarkanen. S., *J. Polym. Sci. B: Polym. Phys.*, **1997**, 35, 1899-1910

Li, Y., Sarkanen, S., *ACS Symp. Ser.*, **1999**, 742, 351-66

Li, Y., Sarkanen, S., *Macromolecules*, **2002**, 35, 9707-15

Li, Y., Sarkanen, S., In *Biodegradation Polymers and Plastics*, Chiellini, E., Solaro, R., Eds, Kluwer Academic/Plenum Publishers, New York, **2003**, 121-39

Li, Y., Sarkanen, S., *Macromolecules*, **2005**, *38*, 2296-2306

Lundell, T., Schoemaker, H., Hatakka, A., Brunow, G., *Holzforschung*, **1993**, 47, 219-24

Lundquist, K., in "Methods in Lignin Chemistry", Lin, S. Y., Dence, C. W. (ed), Springer-Verlag, New York, **1992**, 65-70

Lundquist, K., Ohlsson, B., Simonson, R., *Sven Papperstidn*, **1977**, 80(5), 143-4

Lundquist, K., Stomberg, R. *Holzforschung*, **1988**, 42, 375-84

Martinez, D., Challacombe, J., Morgenstern, I., *et al*. (53 authors), *Proc Natl Acad Sci USA,* **2009**, 106, 1954-9

Meier, H., *Acta Chem. Scand.* **1982**, 12, 144-6

Mester, T., Ambert-Balay, K., Ciofi-Baffoni, S., Banci, L., Jones, A. D., Tien, M., *J. Biol. Chem*., **2001**, 276, 22985-90

Miller, R. L., Boyer, R. F., *J. Polym. Sci.: Polym Phys.*, **1984**, 22, 2021-41

Miyaki, Y., Einaga, Y., Fujita, H., *Macromolecules*, **1978**, 11, 1180-6

Morokuma, K., *Acc. Chem. Res.*, **1977**, 10, 294-300

Mosier, N., Wyman, C., Dale, B., Elander, R., Lee, Y. Y., Holtzapple, M., Ladisch, M., *Bioresource Technology*, **2005**, 96, 673-86

Muller, P. C., Kelley, S. S., Glasser, W.G., *J. Adhesion*, **1984**, 17, 185-206

Murthy, N. S., Minor, H., *Polymer*, **1990**, 31, 996-1002

Murthy, N. S., Minor, H., Bednarczyk, C., Krimm, S., *Macromolecules*, **1993**, 26, 1712-21

Neki, K., Geil, P. H., *J. Macromol. Sci. Phys*, **1973**, 8, 313-59

Nicole, M., Chamberland, H., Rioux, D., Xixuan, X. Blanchette, R. A., Geiger, T. P., Ouellette, G. B., *Can. J. Microbiol.*, **1995**, 41, 253-65

Ortuño, N., Moltó, J., Conesa, J. A., Font, R., *Environmental Pollution*, **2014**, 191, 31-7

Otsuka, Y., Sonoki, T., Ikeda, S., Kajita, S., Nakamura, M., Katayama, Y., *Eur. J. Biochem*., **2003**, 270, 2353-62

Ralph, J., Lundquist, K., Brunow, G., Lu, F., Kim, H., Schatz, P. F., Marita., J. M., Hatfield, R. D., Ralph, S. A., Christensen, J. H. *et al.*, *Phytochem. Rev*., **2004**, 3, 29-60

Rials, T. G., Glasser, W. G., *J. Appl. Polym. Sci.*, **1989**, 37, 2399-2415

Riley, R., Salamov, A. A., Brown, D. W., *et al.*(25 authors), *Proc Natl Acad Sci USA*, **2014**, 111, 9923-8

Roblin, J.-P., Duran, H., Duran, E., Gorrichon, L., Donnadieu, B., *Chem. –Eur. J.*, **2000**, 6, 1229-35

Ruland, W., *Pure Appl. Chem.*, **1969**, 18, 489-515

Sakakibara, A. A., *Wood Sci. Technol.*, **1980,** 14, 89

Saraf, V. P., Glasser, W. G., *J. Appl. Polym. Sci.*, **1984**, 29, 1831-41

Saraf, V. P., Glasser, W. G., Wilkes, G. L., McGrath, J. E., *Appl. Polym. Sci.*, **1985**, 30, 2207-24

Sarkanen, S., *ACS Symp. Ser*. **1991**, 460, 247-69

Sarkanen, S., Chen, Y.-r., *59th Appita Proceedings incorporating 13th Internat. Symp. Wood Fibre Pulp. Chem.*, Carlton, Victoria, Australia, **2005**, 2, 407-14

Sarkanen, S., Razal, R. A., Piccariello, T., Yamamoto, E., Lewis, N. G., *J. Biol. Chem*., **1991**, 266, 3636-43

Sarkanen, S., Teller, D. C., Stevens, C. R., McCarthy, J. L., *Macromolecules*, **1984**, 17, 2588-97

Shadle, G., Chen, F., Reddy, M. S. S., Jackson, L., Nakashima, J., Dixon, R. A., *Phytochem*., **2007**, 68, 1521-29

Skyba., O., Douglas, C. J., Mansfield, S. D., *Appl. Environ. Microbiol.*, **2013**, 79, 2560-71

Srebotnik, E., Messner, K., Foisner, R., *Appl. Environ. Microbiol*., **1988**, 54, 2608-14

Stomberg, R., Lundquist, K. *Acta Chem. Scand. A*, **1986**, 40, 705-10

Stomberg, R., Lundquist, K. *Acta Chem. Scand. B*, **1987**, 41, 304-9

Suzuki, K., Gomi, T., Kaidoh, T., Itagaki, E., *J. Biochem.*, **1991**, 109, 348-53

Tien, M., Kirk, T. K., *Science*, **1983**, 221, 661-3

Tuor, U., Wariishi, H., Schoemaker, H. E., Gold, H. M., *Biochemistry*, **1992**, 31, 4986-95

Vanden Wymelenberg, A., Minges, P., Sabat, G., *et al.*, *Fungal Genet. Biol.*, **2006**, 43, 343-56

Villarrubia, J. S., *Surf. Sci*, **1994**, 321, 287-300

Wariishi, H., Valli, K., Gold, M. H., *Biochem. Biophys. Res. Commun.*, **1991**, 176, 269-75

Wei, D., Houtman, C. J., Kapich, A. N., Hunt, C. G., Cullen, D., Hammel, K. E., *Appl. Environ. Microbiol.*, **2010**, 76, 2091-7

White-Stevens, R. H., Kamin, H., *J. Biol. Chem.*, **1972**, 247, 2358-70

White-Stevens, R. H., Kamin, H., Gibson, Q. H., *J. Biol. Chem.*, **1972**, 247, 2371-81

Wyatt, P. J., *Anal. Chim. Acta*, **1993**, 272, 1-40

Yelle, D. J., Wei, D., Ralph, J., Hammel, K. E., *Environ. Microbiol.*, **2011**, 13, 1091-1100

Yokota, S., Umezawa, T., Higuchi, T., *Mokuzai Gakkaishi*, **1991**, 37, 535-41

Yoshida, H., Mörck, R., Kringstad, K. P., Hatakeyama, H., *J. Appl. Polym. Sci.*, **1987**, 34, 1187-98

Yoshida, H., Mörck, R., Kringstad, K. P., Hatakeyama, H., *J. Appl. Polym. Sci.*, **1990**, 40, 1819-32

Zhang, L., Gellerstedt, G., *6th European Workshop on Lignocellulosics and Pulp*, Bordeaux, France, **2000**, 7-10

Zhao, H., Brown, P. H., Schuck, P., *Biophys. J.*, **2011**, 100, 2309-17

Zhao, Y., Schultz, N. E., Truhlar, D. G., *J. Chem. Theory Comput*. **2006**, 2, 364-382

Zimm, B. H., *J. Chem. Phys.*, **1948**, 16, 1093-9

APPENDIX

A.1 Correlations between Tensile Parameters for Lignin-based Plastics

Significant correlations were found between toughness and elongation-at-break as well as between tensile strength and modulus for the lignin-based plastics described in Chapter 6 (Table A1). However, the correlations between elongation-at-break and tensile strength and between toughness and tensile strength for these materials were very weak. Virtually no correlation between toughness and modulus or between elongation-at-break and modulus was observed. As shown in Fig. A1, the correlation between toughness and elongation-at-break was appreciable providing that plastic deformation did not contribute substantially to tensile behavior. On the other hand, the somewhat weaker correlation between tensile strength and modulus in Fig. A2 was little affected by the ductility of the lignin-based plastics described. A strong relationship between toughness and tensile strength would have been advantageous for improving lignin-based plastics formulations, but as shown in Fig. A3, the correlation was very weak.

Table A1 Tensile strength (σ_{max}), modulus, elongation at break (ε_b) and toughness for the lignin-based plastics presented in Figs. 6.1–6.7 and 6.9–6.10.

Blend Composition	σ_{max} MPa	Modulus GPa	ε_b %	Toughness MJ·m^{-3}
Figure 6.1				
15% PCL(M_n 6.1 kDa), 85% MBML	61	1.07	7.2	2.4
15% PCL(M_n 2.9 kDa), 85% MBML	52	1.06	6.8	1.9
15% PTMG, 85% MBML	39	0.96	5.7	1.2
25% PBA, 75% MBML	41	1.02	6.9	1.6
30% PBA, 70% MBML	31	0.76	13.3	2.9
30% PTMS, 70% MBML	24	0.79	8.0	1.3
30% PES, 70% MBML	25	0.72	10.5	1.8
Figure 6.2				
15% EBE, 85% MBML	69	1.28	7.0	2.7
20% EBE, 80% MBML	63	1.11	9.0	3.4
15% EBE, 85% 10k MBML	43	1.04	5.1	1.2
20% EBE, 80% 10k MBML	41	0.77	7.8	1.9
25% EBE, 75% MBML	30	0.81	11.9	2.8
25% EBE, 75% 10k MBML	30	0.67	16.8	4.0
30%EBE, 70% 10k MBML	18	0.60	20.6	3.3
30%EBE, 70% MBML	16	0.56	17.4	2.4
Figure 6.3				
15% EBE, 85% MBML	69	1.28	7.0	2.7
20% EBE, 80% MBML	63	1.11	9.0	3.4
15% PEO, 85% MBML	52	1.19	6.3	1.8
15% EB,(1,2) 85% MBML	33	0.95	4.1	0.7
22% EB (1,2), 78% MBML	45	0.83	7.3	1.8
20% PEO, 80% MBML	47	0.94	8.2	2.2
Figure 6.4				
15% PEO, 85% MBML	52	1.19	6.3	1.8
2% DEG, 13% PEO, 85% MBML	64	0.95	10.6	3.7
2% DEA, 13% PEO, 85% MBML	54	0.95	10.7	3.4
2% DES, 13% PEO, 85% MBML	48	0.83	9.0	2.4

Table A1 Contiune

Blend Composition	σ_{max} MPa	Modulus GPa	ε_b %	Toughness $MJ \cdot m^{-3}$
Figure 6.5				
100% MBML, 1.8% loss of lignin	51	1.05	7.4	2.1
100% MBML, 1.1% loss of lignin	50	0.93	8.4	2.3
100% MBML, 3% loss of lignin	29	0.85	4.6	0.7
100% MBML, 8% loss of lignin	17	0.89	2.7	0.2
Figure 6.6				
100% MBML, 2.1 % loss of lignin	29	0.92	4.3	0.7
1.7% DEA, 2.1% lignin loss	47	0.71	11.7	3.5
2.1% DEA, 4.9% lignin loss	44	0.97	9.6	2.6
4.2% DEA, 5.2% lignin loss	42	0.73	8.3	2.0
Figure 6.7				
3.6% DES, 6.9% lignin loss	34	0.97	4.9	0.9
3.8% DEG, 8% lignin loss	37	0.89	7.7	1.8
4.6% DEG, 6.2% lignin loss	30	0.79	7.8	1.6
10% DEG, 4.8% lignin loss	18	0.31	8.4	0.8
Figure 6.9				
10% TBBP-A, 90% MBML, 140°C	66	1.34	9.0	3.7
10% TBBP-A, 90% MBML, 150°C	63	1.25	8.2	3.0
10% DBAP, 90% MBML	52	1.12	8.0	2.5
20% DBAP, 80% MBML	49	1.11	9.3	3.0
10% DBBP, 90% MBML	46	1.04	7.0	1.9
100% MMWL	43	1.25	5.4	1.3
Figure 6.10				
5% PEG M_n 0.4 kDa	65	1.08	9.6	3.7
5% PEG M_n 0.4 kDa, 5% PEG M_n 10 kDa	63	1.14	11.2	4.4
15% PEG M_n 4.6 kDa	55	1.05	9.4	3.2
5% PEG M_n 0.4 kDa, 5% PEG M_n 4.6 kDa	52	0.97	13.5	5.2
10% PEG M_n 0.4 kDa	50	0.99	10.9	3.8
5% PEG M_n 1 kDa	47	1.22	9.1	3.0
15% PEG M_n 2 kDa	46	1.05	11.4	3.7
15% PEG M_n 10 kDa	39	0.86	12.4	3.6
15% PEGM M_n 5 kDa	37	0.81	8.8	2.2

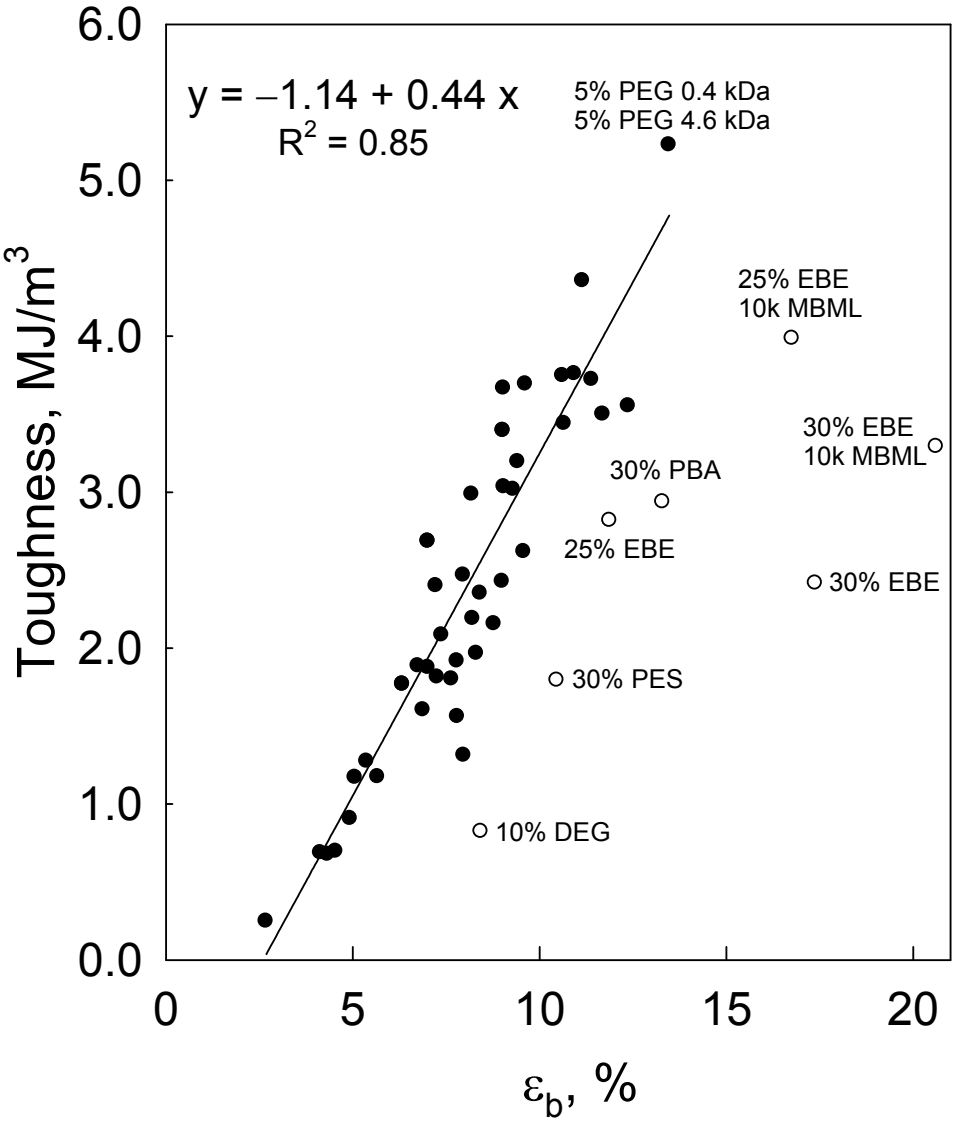

Figure A1 Correlation between toughness and elongation-at-break (ε_b) for the lignin-based plastics listed in Table A1 (data from Chapter 6). The symbols ○ denote data points that are not included in the linear regression analysis: they represent tensile behavior that embodies substantial plastic deformation.

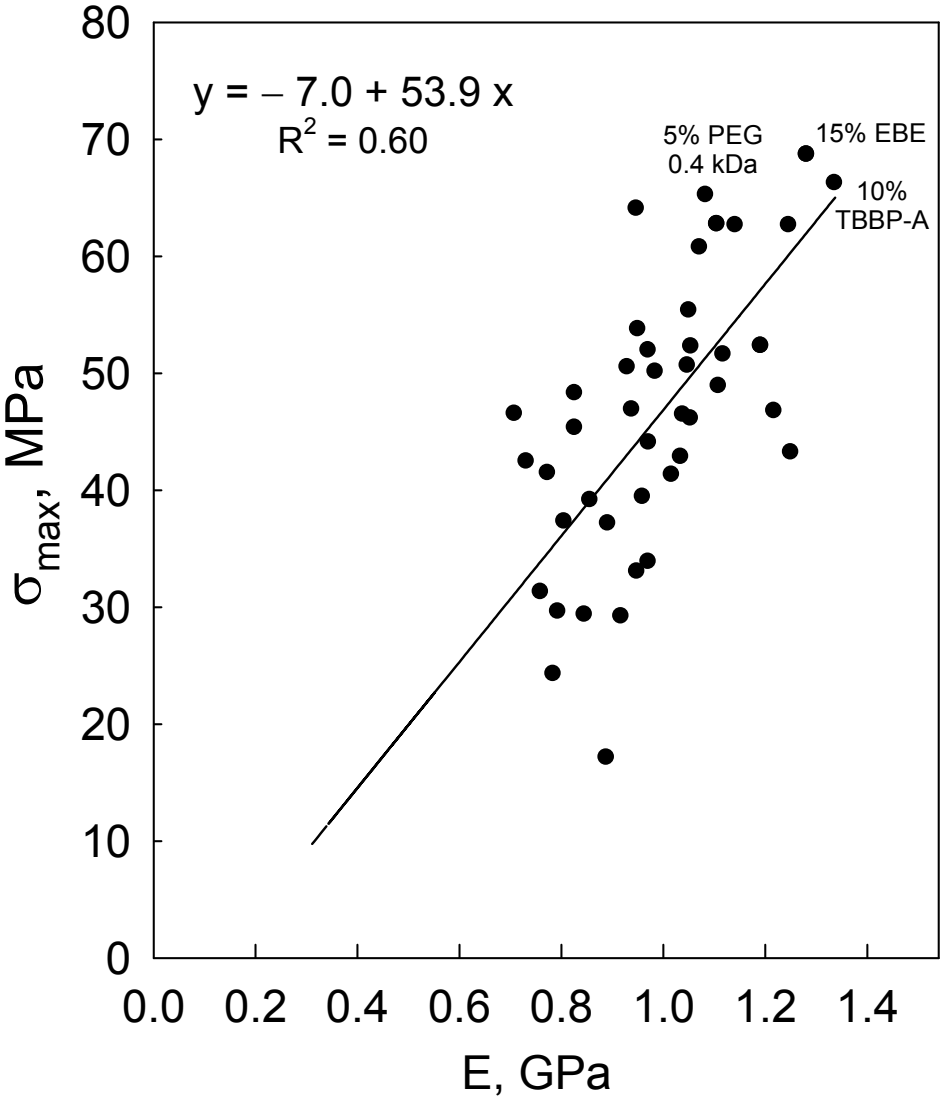

Figure A2 Correlation between tensile strength (σ_{max}) and modulus (E) of the lignin-based plastics listed in Table A1 (data from Chapter 6).

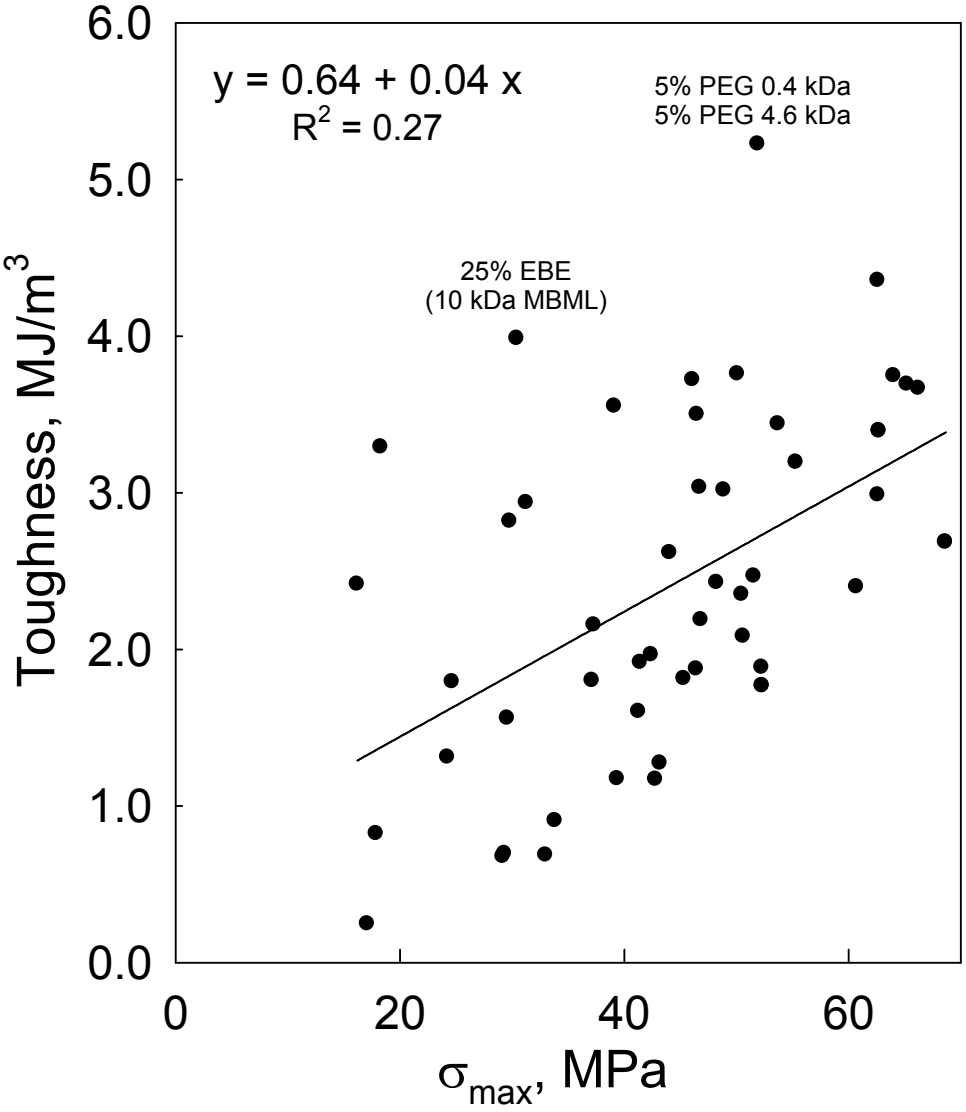

Figure A3 Weak correlation between toughness and tensile strength (σ_{max}) for the lignin-based plastics listed in Table A1 (data from Chapter 6).

A.2 Estimated Separation Distances between Nodules in AFM Images

Separation distances between nearest-neighbor peak maxima in the tapping-mode AFM amplitude images were determined both manually and through one-dimensional height-height correlation functions (Eq. A.2-1) along the fast-scanning axis [Klapetek, 2013]. The height-height correlation functions were evaluated in regions that were not marked by cliffs or ravines between features. As expected, the separation distances estimated from one-dimensional height-height correlation functions were shorter than the corresponding average diameters measured manually in two dimensions (Table A.2).

$$H_x(\tau_x) = \frac{1}{N(M-m)} \sum_{l=1}^{N} \sum_{n=1}^{M-m} \left(z_{n+m,l} - z_{n,l}\right)^2 \qquad \text{(A.2-1)}$$

where $\tau_x = x_1 - x_2$ and $m = \tau_x/\Delta x$.

Table A.2 Comparison between manually measured distances between peak maxima (D) of neighboring nodules and the corresponding parameters (τ_x) determined from one-dimensional height-height correlation functions in AFM-image regions unmarked by cliffs or ravines between features: freshly ultramicrotome-cut surfaces of methylated ball-milled lignin (MBML)-based materials and polystyrene (PS) samples produced as described in section 6.7.

Sample	measured D, nm[a]	τ_x, nm[a]	mol weight
MBML (Fig. 6.17)	12.8 ± 3.3	11.5 ± 3.1	68 kDa[b]
15% PEG, 85% MBML (Fig. 6.18)	14.6 ± 4.2	14.7 ± 2.3	not applicable
PS M_n 190 kDa (Fig. 6.20)	23.3 ± 6.1	21.1 ± 1.6	170 kDa[c]
PS M_n 280 kDa (Fig. 6.21)	25.3 ± 6.6	22.5 ± 3.8	200 kDa[c]
PS M_n 350 kDa (Fig. 6.22)	35.0 ± 10.4	31.4 ± 6.1	380 kDa[c]

[a] Ranges of dimensions should not be construed as standard errors.
[b] Estimated from Fig. 5.2.
[c] Estimated from Eq. 6.7.2-1 [Hiemenz and Lodge, 2007].